Dissertation

submitted to the

Combined Faculties for the Natural Sciences and for Mathematics

of the Ruperto-Carola University of Heidelberg, Germany

for the degree of

Doctor of Natural Sciences

presented by

Master of Science: Ling Zhang

Born in: Anhui, China

Oral-examination: 22.01.2014

CKAMP44 interacts with AMPARs via different protein domains and modulates neuronal morphogenesis

Erklärung gemäß §8 (3) b) und c) der Promotionsordnung

Hiermit erkläre ich, dass ich die vorliegende Dissertation selbst verfasst und mich dabei keiner anderen als der von mir ausdrücklich bezeichneten Quellen und Hilfen bedient habe. Des Weiteren erkläre ich, dass ich an keiner anderen Stelle ein Prüfungsverfahren beantragt oder die Dissertation in dieser oder einer anderen Form bereits anderweitig als Prüfungsarbeit verwendet oder einer anderen Fakultät als Dissertation vorgelegt habe.

Heidelberg, den 05.11.2013

⎯⎯⎯⎯⎯⎯⎯⎯⎯⎯⎯⎯⎯⎯⎯⎯

Dedicated to my parents
and to my husband

Acknowledgement

This research project was performed in the laboratory of Dr. Rolf Sprengel in the Department of Molecular Neurobiology headed by Prof. Dr. Peter H Seeburg, Max Planck Institute for Medical Research, Heidelberg, Germany. I would like to take this opportunity to make a grateful acknowledgement to the people without whose support I never could accomplish this thesis.

First of all, I would like to give me deepest appreciation to my direct supervisor **Dr. Rolf Sprengel**, for offering me this precious opportunity to pursue my doctoral research in his lab, and for his intellectual and constant guidance throughout my whole PhD study. I especially thank him for his kind encouragement and inspiring discussion during hard times when the project went wrong, for providing me chances to travel to Shanghai, Oslo and United States for joint projects and brainstorming conferences, and for being such a good friend to introduce me the history of Western civilization and to drive me home in cold winter.

In particular, I would like to sincerely thank **Prof. Dr. Peter H Seeburg** for providing me a working place in his excellent department, for his insightful discussion in the institute seminar, for his kind supervision as my first thesis advisory committee member, and for his effort in my thesis revision.

Furthermore, I would like to deeply thank **Dr. Anton Meinhart** for being one member of my thesis advisory committee, for his critical discussions, and especially for his constructive suggestion to focus on one project but not "go to two parties at the same time".

Moreover, I would like to show my greatest appreciation to **Prof. Dr. Stephan Frings** and **Prof. Dr. Ana Martin-Villalba** for their participation in my dissertation committee and for the evaluation of this thesis work.

I deeply thank my excellent collaborators **Dr. Jakob von Engelhardt** and **Dr. Paul Farrow** in Deutsches Zentrum für Neurodegenerative Erkrankungen e.V. (DZNE) & Deutsches Krebsforschungszentrum (DKFZ) for their vigorous efforts in the electrophysiological recordings presented and discussed in this thesis. I am also very grateful for the financial support from PPP (project number: 56444379), SFB636/A4 and BMFT NGFN_SP10 program.

I wish to show my heartfelt appreciation to my past and present labmates for

Abstract

The L-α-amino-3-hydroxy-5-methyl-4-isoxazolepropionic acid receptors (AMPARs) are glutamate-gated ion channels that are important for fast synaptic transmission and synaptic plasticity in the central nervous system. The AMPARs' gating properties are tightly regulated by receptor number, subunit composition, co-transcriptional as well as post-translational subunit modifications and by their interactions with auxiliary proteins. Recently, a novel endogenous auxiliary protein of AMPARs, CKAMP44, was identified. CKAMP44 modulates the gating kinetics of AMPARs, such as deactivation, desensitization and recovery from desensitization. However, the detailed molecular mechanisms for the CKAMP44/AMPAR interaction and CKAMP44 regulation of AMPAR gating remain to be resolved. This dissertation unravels different CKAMP44 domains involved in AMPAR interaction and modulation, and investigates new roles of CKAMP44 in neuronal morphogenesis of primary neurons.

In order to identify CKAMP44 protein domains that are essential for CKAMP44/AMPAR interaction, AMPAR-mediated current modulation, and CKAMP44 spine delivery, a series of CKAMP44 deletion mutants were generated, expressed in HEK293 cells, primary hippocampal neurons and in neonatal mouse brains, and analyzed by co-immunoprecipitation, immunostaining and electrophysiological recordings. Our results show that the extracellular CKAMP44 domain triggers the modulation of AMPARs' gating properties. The intracellular C-terminal domain of CKAMP44 is required for postsynaptic localization of CKAMP44, and the R/K domain is needed for the physical CKAMP44/AMPAR interaction as well as for the efficient spine targeting of CKAMP44. The requirement of the R/K domain in CKAMP44/AMPAR binding might explain why the recombinantly expressed CKAMP44 extracellular domain failed to modulate AMPAR activity.

In addition to the regulatory function of CKAMP44 on AMPAR-mediated currents, our bidirectional manipulation of CKAMP44 expression in primary hippocampal neurons of *Ckamp44*$^{-/-}$ and wild-type mice provided evidence that neuronal morphogenesis is modulated by CKAMP44. Primary neurons derived from *Ckamp44*$^{-/-}$ mice exhibited increased dendritic arborization and spine volume, but decreased spine density when compared to CKAMP44 expressing neurons.

CKAMP44 overexpression in neurons leads to the opposite results. In addition, CKAMP44 overexpression induced irregular spine morphology and multiple synapses generated at single spines. Therefore, we suggest that, in addition to the modulation of the AMPAR gating, CKAMP44 can tune dendritic arborization and spine formation during neuron maturation.

Zusammenfassung

Bei L-α-Amino-3-hydroxy-5-methyl-4-isoxazol-propionsäure-Rezeptoren (AMPARs) handelt es sich um Glutamat-gesteuerte Ionenkanäle, die eine wichtige Rolle bei der schnellen synaptischen Transmission und bei der synaptischen Plastizität im Zentralnervensystem spielen. Die Ionendurchlässigkeit von AMPARs wird durch Rezeptoranzahl, Zusammen-setzung der Rezeptoruntereinheiten, co-transkriptionale sowie posttranslationale Modifikationen der Rezeptoruntereinheiten und durch die Wechselwirkung mit eng assoziierten Proteinen streng reguliert. Vor kurzem wurde ein neues endogenes, mit AMPA-Rezeptoren wechselwirkendes Membranprotein, CKAMP44, von unserer Arbeitsgruppe beschrieben. CKAMP44 verändert die Deaktivierung, die Desensitisierung und die Aktivierungskinetik nach der Desensitisierung von AMPA-Rezeptoren. Die genauen molekularen Mechanismen der CKAMP44/AMPAR-Wechselwirkung sowie die Regulation der Ionenkanal-Steuerung durch CKAMP44 waren jedoch bislang unklar. In dieser Dissertation werden verschiedene CKAMP44-Domänen charakterisiert, die an der Wechselwirkung und der Modulation von AMPA-Rezeptoren beteiligt sind, und es werden neue Einflüsse auf die neuronale Morphogenese primärer Neuronen durch CKAMP44 untersucht.

Um CKAMP44-Proteindomänen zu identifizieren, die essentiell für die CKAMP44/AMPAR-Wechselwirkung, die Modulation AMPAR-vermittelter Ionenströme und möglicherweise für die neuronale Morphogenese sind, wurde eine Auswahl an verkürzten CKAMP44-Proteinen hergestellt, welche in HEK293-Zellen, primären hippocampalen Neuronen und neonatalen Mäusegehirnen exprimiert und mittels Co-Immunopräzipitation, Immunfärbung und elektrophysiologischer Aufzeichnung analysiert wurden. Die Ergebnisse zeigen, dass die extrazelluläre Domäne von CKAMP44 für die Modulation der Ionenkanal-Durchlässigkeit von AMPA-Rezeptoren verantwortlich ist. Die intrazelluläre, C-terminale Domäne von CKAMP44 ist für die postsynaptische Lokalisation verantwortlich, während die R/K-Domäne für die CKAMP44/AMPAR-Wechselwirkung und für eine effiziente Translokation von CKAMP44 in die dendritischen Dornen unabdingbar ist. Die Notwendigkeit der R/K-Domäne für die Bindung von CKAMP44 an den AMPA-

Rezeptor könnte erklären, weshalb die rekombinant exprimierte, extrazelluläre CKAMP44-Domäne nicht in der Lage ist, die AMPAR-Aktivität zu verändern.

Zusätzlich zu der regulatorischen Wirkung von CKAMP44 auf AMPAR-gesteuerte Ionenströme zeigte die bidirektionale Manipulation der CKAMP44-Expression in primären hippocampalen Neuronen von *Ckamp44*$^{-/-}$ und Wildtyp-Mäusen, dass auch die neuronale Morphogenese durch CKAMP44 beeinflusst wird. Primäre Neuronen aus *Ckamp44*$^{-/-}$ Mäusen zeigten eine stärkere dendritische Verzweigung und ein größeres Volumen der dendritischen Dornen, jedoch eine niedrigere Dornendichte im Vergleich zu Wildtyp-Neuronen. Eine Überexpression von CKAMP44 in primären Neuronen führte zum entgegengesetzten Effekt. Darüber hinaus besaßen die dendritischen Dornen in diesem Fall eine unregelmäßige Form sowie multiple Synapsen am selben Dorn. Daher sollten zukünftige Analysen berücksichtigen, dass CKAMP44 nicht nur die Modulation der AMPAR-gesteuerten Ionenströme, sondern auch die Verzweigung der Dendriten und die Ausbildung dendritischer Dornfortsätze während der neuronalen Morphogenese beeinflussen kann.

Abbreviations

AAV, adeno-associated virus; AMPAR, L-α-amino-3-hydroxy-5-methyl-4-isoxazolepropionic acid receptors; ANOVA, analysis of variance; β-gal, β-galactosidase; bp, base pair; CA, cornu ammonis; CAG, CMV chicken early enhancer/chicken beta actin; CaMKII, Ca^{2+} /calmodulin-dependent protein kinase II; CKAMP, cystine-knot AMPAR modulating protein; CMV, cytomegalovirus; CNIH, cornichon; CNS, central nervous system; Co-IP, co-immunoprecipitation; CT, C-terminal domain; CTZ, cyclothiazide; Cys-knot, cystine-rich domain; DG, dentate gyrus; DIV, days *in vitro*; E, elution; *E. coli*, *Escherichia coli*; EDTA, ethylene diamine tetraacetic acid; EGFR, epidermal growth factor receptor; EM, electron microscopy; Endo H, Endoglycosidase H; EPSC, excitatory postsynaptic current; ER, endoplasmatic reticulum; Ex, extracellular domain; f, flag tag; FCS, fetal calf serum; FITC, fluorescein isothiocyanate; FP, fluorescent protein; FT, flowthrough; GC, genome copy; GFAP, glial fibrillary acidic protein; GFP, green fluorescent protein; Glu, glutamate; GluA1-4, glutamate-gated AMPAR unit 1-4; GluN1, glutamate-gated NMDAR unit 1; GOI, gene of interest; H, His tag; HEK, human embryonic kidney; HP, hippocampus; HTNCre, His-tag, TAT-tag and Nuclear localization signal fused Cre recombinase; ICC, immunocytochemistry; IHC, immunohistochemistry; IPTG, isopropyl β-D-1-Thiogalactopyranoside; IRES, internal ribosomal entry site; ITR, inverted terminal repeat; JNK, c-Jun N-terminal kinase; Kal7, Kalirin-7; KO, knockout; L, lysate; L, linker domain; LBD, ligand-binding domain; LTP, long-term potentiation; M, membrane-spanning segment; MEM, minimum essential medium; mEPSC, miniature excitatory postsynaptic current; NeuN, neuronal nuclear antigen; NGS, normal goat serum; NLS, nuclear localization signal; NMDAR, N-methyl-D-aspartate receptor; NT, N-terminal Amino-terminal; OB, olfactory bulb; ORF, open reading frame; P, postnatal day; P, pellet; pA, polyadenylation signal; PAGE, polyacrylamide gel electrophoresis; PBS, phosphate buffer saline; PFA, paraformaldehyde; PKC, protein kinase C; PNGase F, peptide-N-Glycosidase F; PSD, postsynaptic density; PDZ, post synaptic density protein (PSD95), Drosophila disc large tumor suppressor (Dlg1) and zonula occludens-1 protein (zo-1); R/K, arginine (R) and lysine (K) rich domain; rpm, rounds per minute; RT, room temperature; S, supernatant; S1/2, serotype 1/2; SD, standard deviation; SDS, sodium dodecyl sulfate;

SEM, standard error of the mean; SFGFP, superfolded GFP; SP, signal peptide; Syn/Tx, TritonX-100 solubilized extrasynaptic fraction; T, thrombin recognition site; TARP, transmembrane AMPAR regulatory proteins; Trx, thioredoxin tag; VDCC, voltage-dependent calcium channel; WPRE, woodchuck posttranscriptional regulatory element; WT, wildtype.

Table of Contents

1. Introduction

The L-α-amino-3-hydroxy-5-methyl-4-isoxazole propionic acid receptors (AMPARs) are glutamate-gated ion channels that play a critical role in fast excitatory synaptic transmission. Upon glutamate binding, AMPAR ion channels are permeable for extracellular sodium ion influx, which results in membrane depolarization, and can lead to the firing of an action potential. In addition, AMPARs are also of vital importance in activity dependent synaptic plasticity – a potential molecular mechanism for learning and memory.

AMPARs are heterotetramers assembled from four different subunits, GluA1-4 (Hollmann *et al.*, 1990; Keinanen *et al.*, 1990; Rosenmund *et al.*, 1998). AMPARs with different subunit compositions exhibit diverse functional features (Hollmann and Heinemann, 1994; Rosenmund *et al.*, 1998). The expression of different AMPAR subunits is brain region specific (Keinanen *et al.*, 1990) and their distribution is developmentally regulated (Monyer *et al.*, 1991). All four AMPAR subunits are expressed in different isoforms by alternative RNA splicing (Monyer *et al.*, 1991; Sommer *et al.*, 1990) and site-selective RNA editing (Lomeli *et al.*, 1994; Sommer *et al.*, 1991), making the diversity of AMPARs even more complex. Thus, the heterogeneity of AMPAR subunits is a major factor that regulates AMPAR-mediated synaptic transmission.

In heterologous expression system, AMPAR subunits can assemble and form functional AMPARs with glutamate-gated ion channel activity (Boulter *et al.*, 1990; Keinanen *et al.*, 1990). However, the kinetics of recombinantly expressed AMPARs and native AMPARs do not match perfectly, e.g. the deactivation and desensitization of recombinant AMPARs expressed *Xenopus* oocytes (Mosbacher *et al.*, 1994) are always faster than those of native AMPARs (Colquhoun *et al.*, 1992; Geiger *et al.*, 1995). Additionally, the single particle analysis obtained by EM imaging suggests that native AMPARs are significantly bigger than postulated AMPAR 3D structure by computer modeling (Nakagawa *et al.*, 2005).

The discrepancy between recombinant and native AMPARs was resolved with the discovery of stargazin as a type of AMPAR auxiliary proteins, which is mutated in stargazer mice (Letts *et al.*, 1998; Noebels *et al.*, 1990). Stargazin, also named as TARP γ2 (transmembrane AMPAR modulatory protein) was found to be able to

shape diverse aspects of AMPAR functions, including ion channel gating kinetics (Milstein *et al.*, 2007; Tomita *et al.*, 2005a), single channel conductance (Soto *et al.*, 2007; Tomita *et al.*, 2005a), as well as activity dependent trafficking (Chen *et al.*, 2000) and synaptic plasticity (Rouach *et al.*, 2005; Tomita *et al.*, 2005b). The discovery of TARP γ2 opened the view that AMPARs function as a big complex with auxiliary proteins, and the latter ones constitute another type of major determinants for native AMPAR behavior.

After the description of TARP γ-2 as an AMPAR auxiliary protein, several other TARP family members (TARP γ-3, -4, -5, -7, -8) were subsequently found to differentially regulate AMPAR functions (Kato *et al.*, 2008; Kato *et al.*, 2007; Tomita *et al.*, 2003). In addition to TARPs, further proteomic research of native AMPARs also identified additional AMPAR auxiliary proteins, among which cornichon 2/3 (CNIH-2/3) (Schober *et al.*, 2011; Schwenk *et al.*, 2009; Shi *et al.*, 2010) and CKAMP44 were most intensively studied (von Engelhardt *et al.*, 2010). This chapter gives an introduction of the molecular biology and functionality of AMPARs, and their auxiliary proteins including TARPs, CHINs and CKAMP44.

1.1. AMPARs

1.1.1. AMPARs subunit composition

AMPARs are heterotetramers composed of four closely related subunits GluA1-4 encoded by four separate genes. The predominant AMPARs in adult hippocampal excitatory neurons are GluA1/2 and GluA2/3 heterodimers (Wenthold *et al.*, 1996). All four subunits exhibit similar functional domain organization, starting with an extracellular N-terminal domain (NTD) important for subunit dimerization, followed by a ligand binding domain (LBD) composed of S1 and S2 segments, three membrane-spanning domains (M1, M3 and M4), a pore-forming membrane re-entry loop (P-loop) determining Ca^{2+} permeability and a C-terminal intracellular domain required for partner binding and receptor trafficking (Sobolevsky *et al.*, 2009) (Fig. 1).
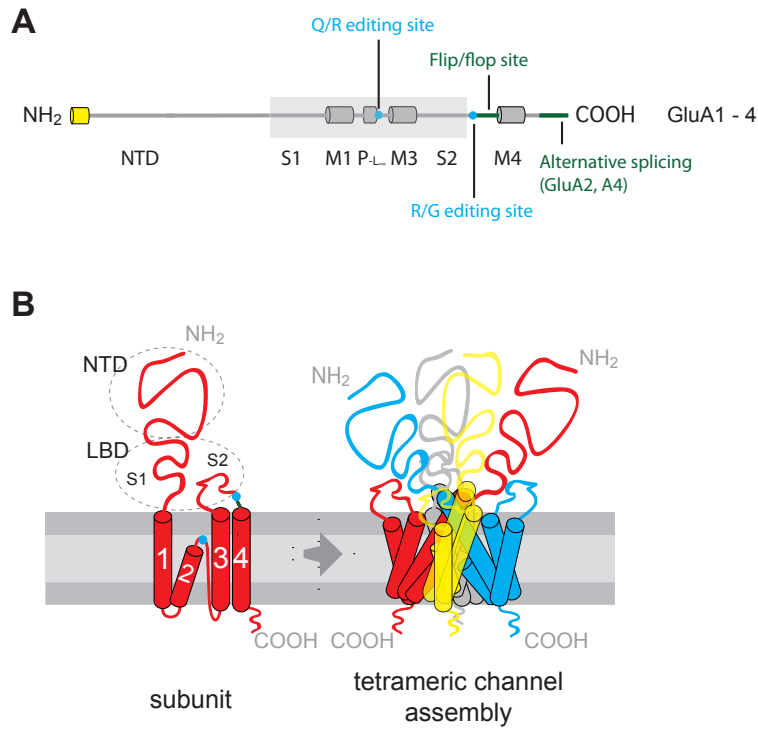
Fig. 1. Structure and composition of AMPARs. (A) Primary structure of AMPAR subunits (GluA1-4) with identical functional domains. NTD, N-terminal domain; S1, ligand binding domain 1; M1, membrane spanning α-helix 1; P, pore loop α-helix; M3, membrane spanning α-helix 3; S2, ligand binding domain S2, and M4, membrane spanning α-helix 4; NH_2, N-terminus; COOH, C-terminus. In yellow represents the hydrophobic signal peptide which is cleaved off during the membrane insertion of the subunit. Post-transcriptional alternative spliced protein segments are outlined in green lines and RNA editing sites are given in blue filled circles. Hydrophobic segments are depicted in barrels. **(B)** Postulated secondary structure of a single AMPAR subunit in the membrane before (left) and after channel assembly (right). Subunits are given in different colors. Lettering is as in (a), except that 'M' is missing in M1, M3 and M4 [figure and legend are adapted from (Sprengel, 2006)].

GluA1-4 share high degree of homology in the LBD, M and P-loop domain, but are variable in their C-terminal cytoplasmic domains, which determine specific partner interactions for each subunit. Besides the heterogeneity of the different AMPAR subunit sequences, each subunit also has variable isoforms due to alternative RNA splicing and RNA editing.

1.1.1.1. Alternative splicing

Commonly found in eukaryotes, alternative splicing allows the expression of several proteins from a single coding gene, thus greatly increasing the complexity of the genome encoded genetic information. GluA2 and GluA4 occur in two different spliced isoforms with long or short C-terminal tails, namely GluA2L, GluA2S,

GluA4L and GluA4S. All four AMPAR subunit genes contain two alternative spliced exons 14 and 15 (Sommer *et al.*, 1990), "flip" and "flop (Fig. 1). The "flip" and "flop" isoforms have distinct pharmacological and channel properties. For example, compared to the "flip" form, the "flop" variant desensitizes more rapidly, and is less responsive to cyclothiazide, a pharmacological reagent which blocks desensitization (Mosbacher *et al.*, 1994). The alternative splicing event is developmentally controlled (Monyer *et al.*, 1991), for example, the "flip" forms of AMAPR subunits are prominent in early development, while the expression of "flop" forms is increasing during postnatal development. In adult rodent brains the "flip" and "flop" isoforms are expressed at similar levels.

1.1.1.2. RNA editing

In addition to RNA splicing, further AMPAR subunit complexity is introduced by RNA editing, resulting in single nucleotide conversion (adenosine to inosine) mediated by dsRNA adenosine deaminase during RNA maturation (Higuchi *et al.*, 2000). Two different RNA editing sites are found in AMPAR subunit genes (Sommer *et al.*, 1991) (Fig. 1). The most prominent one occurs exclusively in the GluA2 subunit, converting the codon for glutamine (Q) to an arginine (R) codon (CAA to CGA) with 100% efficiency during pre-mRNA maturation (Higuchi *et al.*, 1993). The functional consequence of this Q/R-site editing for GluA2 containing AMPARs is a decreased permeability for divalent cations, in particular Ca^{2+} ions, making GluA2 subunit distinct from three other subunits (Burnashev *et al.*, 1992). Thus GluA2 containing AMPARs exhibit low channel conductance and impermeability to Ca^{2+} due to the positively charged arginine in the channel pore (Burnashev *et al.*, 1992), and genetically modified mice deficient for GluA2 Q/R editing die at early phase of postnatal development (Brusa *et al.*, 1995). In addition to the role in controlling Ca^{2+} permeability, Q/R editing in GluA2 also regulates AMPAR assembly (Greger *et al.*, 2003) and AMPAR exit from the endoplasmic reticulum (Greger *et al.*, 2002). Due to this Q/R editing, the presence of GluA2 shape AMPARs with linear current-voltage relationships (I-V), while AMPAR lacking GluA2 exhibit rectifying I-V relationships (Burnashev *et al.*, 1992; Hayashi *et al.*, 2000; Hollmann *et al.*, 1991).

Another RNA editing site, termed as R/G editing site, is localized in the S2 segment encoding exons of GluA2-4 subunit genes (*Gria* 2-4). Within the *Gria* 2-4 pre-mRNAs, the codon for arginine can be converted to a glycine codon (AGA to

GGA). The edited AMPARs show higher recovery from desensitization compared to unedited receptors (Lomeli *et al.*, 1994).

1.1.2. AMPARs function in synaptic transmission, synaptic plasticity as well as learning and memory

Fast excitatory synaptic transmission involves presynaptic glutamate release, and postsynaptic receptor binding and activation (Fig. 2). During synaptic transmission, glutamate released from presynaptic neurons binds to AMPAR ligand binding domain, inducing conformational changes and the opening of the ion channel gate. Due to the Q/R editing, GluA2 containing AMPARs are selectively permeable to monovalent Na^+ ions, and the strong Na^+ ions influx depolarizes the local postsynaptic membrane, enabling the release of Mg^{2+} block in co-localized N-Methyl-D-aspartate receptors (NMDARs). Once the Mg^{2+} block is removed, NMDARs are ready to be activated, and another pulse of glutamate release from the same presynapse can activate both postsynaptic AMPA- and NMDARs. Different from AMPARs, NMDARs are Ca^{2+} permeable. Therefore, now the signal transmission via Na^+ is accompanied by strong Ca^{2+} influx into dendritic spines. Ca^{2+} binds to Calmodulin which activates Ca^{2+}/calmodulin-dependent protein kinase II (CaMKII). CaMKII phosphorylates AMPARs to increase single channel conductance, and activates a number of postsynaptic cellular processes including the translocation of AMPARs from perisynaptic to postsynaptic sites, resulting in an increased synaptic transmission. The increased excitatory transmission can last for hours, days or months, and was described as long-term potentiation (LTP). Experimental data showed that GluA1 deficient mice failed to show any induced field LTP at the hippocampal CA3-CA1 synapses (Zamanillo *et al.*, 1999). Therefore, AMPARs are not only important for mediating fast excitatory transmission, but also for induction of some forms of LTP.

It is commonly believed that learning and memory are both based on a change of the synaptic strength. LTP, as one phenomenon of synaptic plasticity, is thus thought to be an important molecular mechanism underlying learning and memory (Morris *et al.*, 1986; Tsien *et al.*, 1996). Indeed, previous reports showed that GluA1 knock-out mice which fail to have the expression of the early LTP component and field LTP at hippocampal synapses are impaired in spatial working but not in spatial

reference memory (Reisel *et al.*, 2002; Zamanillo *et al.*, 1999), indicating that AMPARs participate in certain form but not all of the learning and memory.
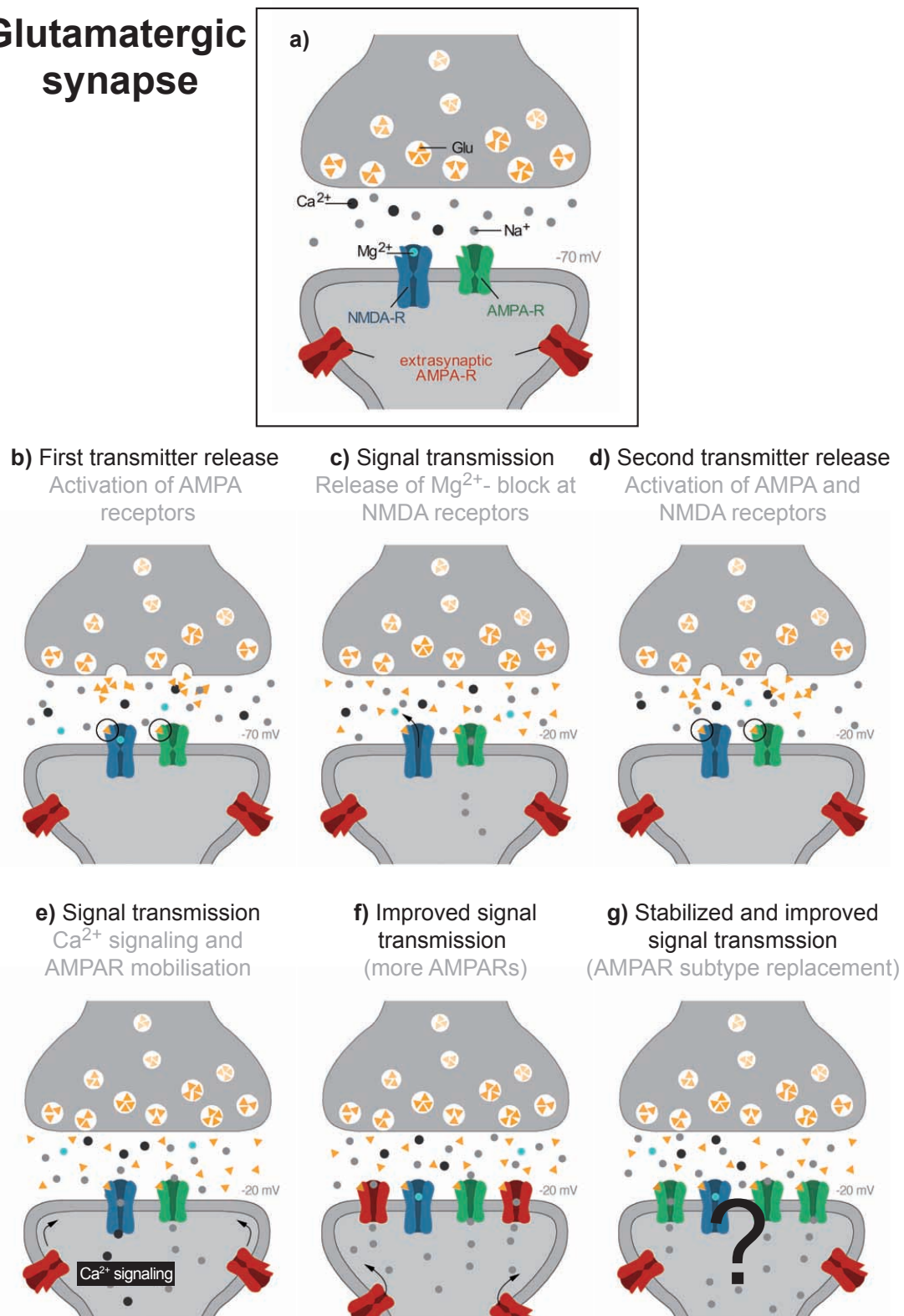
Fig. 2. Six scenarios of synaptic transmission at glutamatergic synapses. (a) Glutamatergic synapses with opposed pre- and post-synaptic component. Presynapse contains

synaptic vesicles filled with signal transmitter glutamate (Glu, orange filled triangle), which once is released into synaptic cleft, will bind to AMPARs (green) and NMDARs (blue) on the postsynaptic membrane. In the absence of Glu, all receptors are in closed state, and the postsynaptic membrane lies at resting potential (indicated by -70 mV). Free ions including Na^+ and Ca^{2+} ions in the synaptic cleft are depicted in grey and black filled circles. **(b)** The first step of fast synaptic transmission mediated by AMPARs, starting from the presynaptic Glu release triggered by the action potential in the presynaptic neuron. Released Glu binds to AMPA- and NMDAR ligand binding sites. The AMPAR ion channel pores are open while NMDAR ion pores are closed due to the Mg^{2+} ion block at the channel pore. **(c)** Mg^{2+} block release from NMDARs after the signal transmission. The postsynaptic membrane is depolarized (indicated by -20 mV), triggering the removal of Mg^{2+} ion from the NMDAR ion pore. **(d)** Activation of both AMPA- and NMDARs by another round of Glu release. **(e)** Further signal transmission by activated NMDARs as well as AMPARs. At this time point, the participation of NMDARs introduces Ca^{2+} in addition to Na^+ ion influx, and Ca^{2+} ion as an important second messenger induces downstream signal pathways, which translocate AMPARs from the perisynaptic to the postsynaptic membrane, resulting in increased number of postsynaptic AMPARs. **(f)** To this end, the postsynapse will exhibit a stronger response to glutamate, which can be recorded as an improved chemical signal transmission. **(g)** The long-lasting changes of this improved transmission are stabilized over time. This process is dependent on protein synthesis and might be mediated by an exchange of newly incorporated AMPARs by AMPARs with a different subunit combination. However, the long lasting changes are very complex and need more investigation [Figure and figure legend adapted from (Sprengel, 2013)].

1.2. AMPAR auxiliary proteins

Accumulating evidences indicate that native AMPARs are big complexes composed not only of AMPAR subunit tetramers but also of a number of auxiliary proteins, which regulate the trafficking and gating kinetics of AMPAR ion channels. Among them, TARPs, CNIHs and CKAMP44 are most intensively studied (Fig. 3).
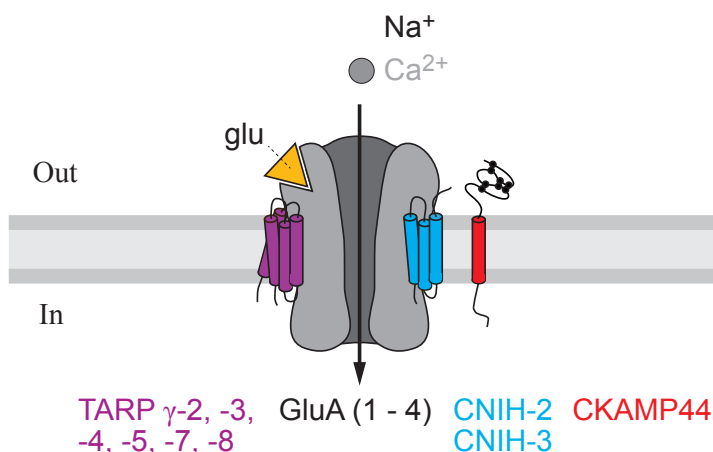
Fig. 3. Schematic illustration of a membrane localized AMPAR. An AMPAR with permeability for sodium (Na^+) but limited permeability for calcium (Ca^{2+}) ions is depicted in grey. The AMPAR ligand binding site is occupied with glutamate (yellow). Three auxiliary subunits (TARP, CNIH, and CKAMP44) are drawn in different colored structural barrel cartons next to AMPAR.

1.2.1. TARPs

1.2.1.1. Discovery of the prototypical TARP stargazin/γ-2

The first identified AMPAR auxiliary protein was stargazin/γ-2 discovered in *STARGAZER* mice, which show characteristic ataxia and seizure behavior (Letts *et al.*, 1998; Noebels *et al.*, 1990). Detailed analysis showed that in stargazer mice a single gene was disrupted in both alleles, and the disruption of this gene was responsible for the "star-gazing" phenotype. The translated protein from this disrupted gene was therefore named after the mutant mouse model as stargazin, or as γ-2 due to its sequence similarity to the gamma subunit of skeletal muscle voltage-dependent calcium channel (VDCC) γ-1 (Letts *et al.*, 1998). Stargazin/γ-2 was thought to be a subunit for VDCC, and neurological disorder in *STARGAZER* mice might be the consequence of neuronal VDCC dysfunction (Letts *et al.*, 1998). But further molecular and physiological analysis proved that stargazin/γ-2 contributed only a minor effect on calcium channel properties (Green *et al.*, 2001; Klugbauer *et al.*, 2000; Osten and Stern-Bach, 2006; Rousset *et al.*, 2001). On the contrary, AMPAR component mEPSC in the cerebellum mossy fiber to granule cell synapse was greatly impaired in *STARGAZER* mice (Chen *et al.*, 1999; Hashimoto *et al.*, 1999), indicating the loss of functional AMPARs on the surface of cerebellar granule cells. The rescue experiment by overexpressing wild-type stargazin in *STARGAZER* mice could restore AMPAR mEPSC (Chen *et al.*, 2000), providing evidence that stargazin/γ-2 is indispensible to facilitate AMPAR trafficking to postsynaptic membrane.

1.2.1.2. TARP family members, structure and distribution

The discovery of stargazin/γ-2 triggered a new round of molecular cloning experiments, and in total eight stargazin-related proteins could be identified (γ-1 to γ-8) (Tomita *et al.*, 2003), among which four (γ-2, γ-3, γ-4 and γ-8) were collectively named as TARPs (transmembrane AMPAR regulatory proteins) due to their very similar influence on the trafficking and gating kinetics of AMPARs in distinct cell types (Tomita *et al.*, 2003). Later studies further confirmed that γ-5 and γ-7 also selectively modulate certain subgroups of AMPARs (Kato *et al.*, 2008; Kato *et al.*, 2007), and thus γ-5 and γ-7 were classified as type II TARPs (Kato *et al.*, 2008), while γ-2, γ-3, γ-4 and γ-8 were grouped as type I TARPs. All type I TARPs have a PDZ binding motif (-RR/KTTPV) at the carboxyl terminus for associating with

PSD95 at the synapse (Bats *et al.*, 2007). Type II TARPs contain an atypical C-terminal PDZ-binding motif (–S/TTPC) at the COOH terminus, which might also be associated with AMPARs at the synases (Kato *et al.*, 2007).

All TARPs share similar secondary structure, with four membrane-spanning domains, a short cytosolic N-terminal domain, two extracelluar domains, one of which is involved in modulating AMPAR channel properties and a C-terminal intracellular domain with typical (–TTPV) or atypical (–S/TTPC) PDZ binding motif at the carboxyl terminus.

TARPs exhibit an overlapping distribution in the mouse brain as demonstrated by *in situ* hybridizations and western-blots (Fukaya *et al.*, 2005; Tomita *et al.*, 2003). Thus, one cell type might exhibit the expression of multiple TARPs. However, each TARP gene has preferable expression in distinct brain areas, e.g. TARP γ-2 shows high expression in cerebellum (Tomita *et al.*, 2003), TARP γ-3 in cerebral cortex (Tomita *et al.*, 2003), TARP γ-4 in neonatal forebrain (Tomita *et al.*, 2003), TARP γ-5 in Bergman glia cells of the cerebellum (Fukaya *et al.*, 2005), TARP γ-7 in cerebellum (Fukaya *et al.*, 2005; Kato *et al.*, 2007; Tomita *et al.*, 2003), and TARPs γ-8 in hippocampus (Fukaya *et al.*, 2005; Tomita *et al.*, 2003). The redundancy of TARPs expression is crucial for maintaining AMPAR function as most of single TARP knock-out mice don't show behavioral impairments, possibly due to the compensation by other TARPs (Menuz *et al.*, 2009; Menuz *et al.*, 2008).

1.2.1.3. TARPs regulate AMPAR trafficking

As described above TARP γ-2 is of great importance in facilitating AMPAR trafficking, which is best documented by *STARGAZER* mice and by stargazin/γ-2 rescue experiments (Chen *et al.*, 1999; Chen *et al.*, 2000; Hashimoto *et al.*, 1999). The current model suggests that in the ER TARP γ-2 associates with tetrameric AMPARs to facilitate efficient transportation from ER to Golgi (Vandenberghe *et al.*, 2005a, b). In Golgi, the neuronal isoform of protein-interacting specifically with TC10 (nPIST) binds to the C-terminal domain of TARP γ-2, and chaperone the TARP-AMPAR complex to the cell surface (Cuadra *et al.*, 2004).

The surface delivery of AMPARs is independent of C-terminal PDZ binding domain of TARP γ-2 (Chen *et al.*, 2000). However, the postsynaptic delivery of AMPARs, as the second mechanism of AMPAR trafficking, requires the TARP PDZ

domain (Chen *et al.*, 2000), which directly binds to PSD95 (Chen *et al.*, 2000; Schnell *et al.*, 2002) and other membrane-associated guanylate kinases (MAGUKs) (Dakoji *et al.*, 2003; Elias *et al.*, 2006) to anchor the AMPAR complex on the postsynaptic membrane. Indeed, removal of the four C-terminal residues of stargazin (stargazinΔC) failed to rescue AMPAR EPSCs in *STARGAZER* granule cells (Chen et al., 2000). Similar results were obtained in hippocampal slice cultures, which showed that AMPARs are localized to synapses through direct binding of the first two PDZ domains of synaptic PSD-95 to stargazin. When PSD95 expression level was not increased, only extrasynaptic AMPAR but not synaptic AMPAR current could be enhanced by stargazin overexpression (Chen *et al.*, 2000; Schnell *et al.*, 2002).

1.2.1.4. TARPs regulate the physiological properties of AMPARs

TARPs modulate not only AMPAR trafficking, but also AMPAR gating properties. In heterologous system, coexpression of GluA1 and TARP γ-2 could increase glutamate-evoked AMPAR currents by facilitating single channel conductance as well as surface AMPAR expression (Chen *et al.*, 2003; Tomita *et al.*, 2005a; Tomita *et al.*, 2004; Yamazaki *et al.*, 2004). TARPs prolong channel opening and enhance the recovery from desensitization of AMPARs (Cho *et al.*, 2007; Korber *et al.*, 2007; Priel *et al.*, 2005; Tomita *et al.*, 2005a). The overall output of TARP modulation is an enhanced charge transfer through TARP-associated AMPARs.

Despite of the consensus in AMPAR regulation of different TARPs, subtle differences can be observed between different TARP subtypes. For example, TARP γ-4 and γ-8 exhibited slower AMPAR deactivation and desensitization compared to γ-2 and γ-3 due to the amino acid variability in the first extracellular loop of TARPs (Cho *et al.*, 2007; Kott *et al.*, 2007; Milstein *et al.*, 2007). Consistently, rescue experiments in stargazer granule cell culture by different TARPs also showed that γ-4 induced dramatically slower decay of AMPAR mEPSC than other TARPs, and knocking out endogenous γ-4 resulted in faster decay and rise time of mEPSC (Milstein *et al.*, 2007). Thus, the heterogeneity of TARPs has a strong impact on the kinetics of native AMPARs in central synapses.

In addition, TARPs modulate the pharmacological properties of AMPARs. Native AMPARs respond better to kainate than to glutamate, while AMPARs expressed in heterologous system behave in the opposite way, which can be converted

by overexpressing TARPs (Tomita *et al.*, 2005a; Tomita *et al.*, 2007; Turetsky *et al.*, 2005). These results demonstrate that native AMPARs complex contain TARPs, and also prove that TARPs could shape the pharmacology of AMPARs in an TARP subtype dependent manner. TARPs also increase the affinity and efficacy of AMPAR potentiators including cyclothiazide, PEPA and CX546, which increase signaling by blocking channel closure (Tomita *et al.*, 2006).

1.2.2. CNIHs

Following the discovery of TARPs, another type of AMPAR auxiliary proteins, cornichons (CNIH2 and 3), was identified by proteomics (Schwenk *et al.*, 2009). CNINs are trimembrane spanning proteins that modulate channel properties of AMPARs and promote AMPAR surface expression in heterologous cells.

1.2.2.1. Roles of CNIHs in AMPAR trafficking

Before CNIHs were identified as AMPAR auxiliary proteins, their homologs in *Drosophila melanogaster* (Bokel *et al.*, 2006)*, Saccharomyces cerevisiae* (Castillon *et al.*, 2009) and *Gallus domesticus* (Hoshino *et al.*, 2007)*, were reported as chaperon like endoplasmic reticulum (ER) cargo exporters for epidermal growth factor receptor (EGFR) ligands. In 2009, Schwenk *et al.* found that CNIH2/3 were associated with native AMPAR auxiliary proteins in rat neurons (Schwenk *et al.*, 2009). The authors described that CNIH2/3 increased surface expression of AMPARs in cultured rat primary neurons and in *Xenopus laevis* oocytes, most likely by using their conserved role as a cargo exporter from the ER as suggested by later studies of CNIH-2 functions in AMPAR processing in heterologous cells and primary rat neurons (Harmel *et al.*, 2012; Shi *et al.*, 2010).

1.2.2.2. Roles of CNIHs in modulating AMPAR gating

In addition to AMPAR trafficking, CNIHs are involved in modulating AMPAR gating similar as TARPs. In heterologous system, CNIH2 slows AMPAR decay kinetics and alters the pharmacology of kainate and AMPAR potentiators (Schober *et al.*, 2011; Schwenk *et al.*, 2009; Shi *et al.*, 2010).

It seems that CNIH2/3 differentially modulate channel properties of AMPARs associated with different TARPs, as CNIH2 overexpression slowed AMPAR mEPSC kinetics of neurons expressing γ-8, but did not alter mEPSC from neurons expressing

γ-2/stargazin (Shi et al., 2010). The interaction between CNIH-2 and specific TARPs within the AMPAR complex was first suggested by Kato *et al*. (Kato *et al.*, 2010). The authors showed that in heterologous system, the overexpression of TARP γ-4, γ-7, or γ-8 caused resensitization which is not present in γ-8 containing hippocampal neurons, and co-expression of CNIH-2 with γ-8 abolished this phenomenon (Kato *et al.*, 2010). Further more, genetic disruption of γ-8 markedly and selectively reduced CNIH-2 and GluA protein levels. From those data, Kato *et al.* suggested that CNIH-2, TARP γ-8 and AMPARs form a tripartite protein complex in native neurons (Kato *et al.*, 2010). The interplay between AMPAR subunits, CNIHs and TARPs was further validated by using CNIH-2 and CNIH-3 conditional knock-out mice (Herring *et al.*, 2013). CNIHs knock-out in hippocampus selectively reduced AMPAR-mediated synaptic transmission, mostly by removing GluA1/A2 AMPARs, leaving fast GluA2/A3 γ-8 AMPAR complexes, whose interaction with CNIHs is prevented by the presence of γ-8. Therefore, the interplay among CNIHs, AMPARs, and TARPs determines the trafficking and gating properties of individual AMPARs.

1.2.3. CKAMP44

After the discovery of TARPs and CNIHs as AMPAR auxiliary proteins, immunoprecipitation combined with mass spectrometry identified the cystine-knot AMPAR modulating protein with predicted molecular weight of 44 kDa (CKAMP44) as an additional AMPAR auxiliary protein in the native AMPAR complexes (von Engelhardt *et al.*, 2010).

1.2.3.1. Primary structure and CKAMP or Shisa protein family

CKAMP44 is a type I transmembrane protein. The CKAMP44 precursor protein is 424 amino acid residues in length and contains an N-terminal signal peptide, an extracellular domain with eight cysteines, followed by a single membrane spanning segment and C-terminal intracellular domain terminated by a PDZ binding motif.

The primary amino acid sequence of CKAMP44 identifies CKAMP44 as a member of the endogenous Shisa protein family. Therefore CKAMP44 is also called Shisa9 according to the numbering of the 9 proteins of the Shisa family (Shisa1-9) (Fig. 4) (Pei and Grishin, 2012). Notably, CKAMP44 and other members of Shisa family exhibit the same cysteine pattern ('C*C*CC*C*CC*C', * represents a stretch

The figure is a multiple sequence alignment (rotated 90°) of Shisa protein families, grouped as follows:

Shisa1:
- NW_001471681.1 — Gg
- NP_001085264.1 — Xl — 22 ... 128 [269]
- NP_001003631.1 — Dr — 26 ... 132 [258]
- CA354146.1 — Om

Shisa2:
- NP_001007539.1 — Hs — 36 ... 147 [295]
- NP_989832.1 — Gg — 26 ... 136 [284]
- NP_001086445.1 — Xl — 29 ... 140 [288]
- XP_003201351.1 — Dr — 28 ... 137 [294]

Shisa3:
- NP_001073974.1 — Hs — 26 ... 128 [238]
- NW_001471686.1 — Gg
- NP_001079833.1 — Xl — 22 ... 123 [232]
- CD754252.1 — Dr

Shisa4:
- NP_937792.2 — Hs — 29 ... 121 [197]
- NP_001089674.1 — Xl — 24 ... 116 [218]
- NP_001017869.1 — Dr — 24 ... 118 [193]

Shisa5:
- NP_057563.3 — Hs — 29 ... 144 [240]
- NP_001038335.1 — Dr — 23 ... 118 [261]
- XP_705094.1 — Dr — 23 ... 132 [231]
- NP_001122168.1 — Dr — 25 ... 109 [209]

Shisa_Bf:
- XP_002597311.1 — Bf — 16 ... 108 [197]

Shisa6:
- NP_997269.2 — Hs — 92 ... 207 [551]
- XP_002941768.1 — Xt — 72 ... 182 [433]
- XP_002667337.1 — Dr — 65 ... 176 [264]

Shisa7:
- NP_001138648.1 — Hs — 80 ... 215 [538]
- XP_002940010.1 — Xt — 65 ... 178 [504]
- XP_001332022.1 — Dr — 105 ... 219 [632]

Shisa8:
- XP_003121062.1 — Hs — 58 ... 171 [547]
- XP_001508883.1 — Oa — 94 ... 206 [281]

Shisa9:
- NP_001138676.2 — Hs — 72 ... 183 [424]
- XP_414733.2 — Gg — 59 ... 170 [218]
- A7MC48.2 — Xt — 57 ... 168 [390]
- NP_001129447.2 — Dr — 95 ... 205 [433]
- NP_001013527.1 — Dr — 55 ... 166 [382]

The alignment includes a C-terminal transmembrane region marked =====TM=====.

Fig. 4. Multiple sequence alignment of Shisa proteins. The cysteine-rich domains and transmembrane regions of representative Shisa proteins (with a 'C*C*CC*C*CC*C' pattern) from nine vertebrate Shisa subfamilies (Shisa1–9) and one sequence from *Branchiostoma floridae* (Shisa_Bf) are included in this alignment. NCBI accession numbers are shown. A few proteins were derived from genome or EST sequences (accession numbers in italic and underlined). Starting and ending residues numbers for sequences with protein accession numbers are shown before and after the sequences, respectively. Protein lengths are shown in brackets. Conserved cysteines are shaded in yellow or red (the additional two cysteine positions compared to Shisa-like proteins). Non-charged residues in positions with mainly hydrophobic residues were shaded in cyan. Prolines and glycines are shown in red letters. Cysteines within and after the predicted transmembrane segments are shaded in gray. Arginines and lysines, occurring frequently C-terminal to the predicted transmembrane segments (TM), are shown in blue letters. Species name abbreviations shown after the accession numbers are as follows: Bf, *Branchiostoma floridae*; Dr, *Danio rerio*; Gg, *Gallus gallus*; Hs, *Homo sapiens*; Om, *Oncorhynchus mykiss*; Oa, *Ornithorhynchus anatinus*; Xt: *Xenopus tropicalis*; and Xl, *Xenopus laevis* [Figure and figure legend are from (Pei and Grishin, 2012)].

of 2 to 15 amino acids) in the N-terminal extracellular domain, but with different number of residues between two neighboring cysteines (Fig. 4).

Within the family of Shisa proteins CKAMP44 shows the highest similarity to Shisa-6, -7 and -8, which Sprengel *et al.* described in 2009 as CKAMP59, 52 and 39, respectively, according to their predicted molecular weight (Pei and Grishin, 2012; Sprengel *et al.*, 2009). Compared to Shisa1-5, the CKAMPs don't have multiple cysteines after the TM region in the cytoplasmic domain (Fig. 4). Thus, in this thesis, we consider only Shisa-6, -7 and -8 as CKAMP44 homologs.

1.2.3.2. CKAMP44 expression and subcellular distribution

The expression of CKAMP44 is brain specific, and can be detected during embryonic and postnatal development as indicated by tissue-specific Northern blot and *in situ* hybridization. CKAMP44 is enriched in Triton X-100–insoluble postsynaptic density and colocalized with AMPARs at spine heads as demonstrated by subcellular fractionation and immunocytochemistry (von Engelhardt *et al.*, 2010).

1.2.3.3. CKAMP44 modulation on AMPARs

When expressed in *Xenopus laevis* oocytes, CKAMP44 could reduce GluA1- and GluA2-mediated steady-state currents, as well as the potency of cyclothiazide (CTZ) in preventing AMPAR desensitization. In hippocampal CA1 pyramidal neurons, overexpression of CKAMP44 resulted in a faster desensitization and slower recovery from desensitization. In dentate gyrus granule neurons with high CKAMP44

expression, CKAMP44 knock-out caused an increase in the paired-pulse ratio of AMPA currents in lateral and medial perforant path–granule cell synapses (von Engelhardt *et al.*, 2010), indicating that CKAMP44 modulates short-term plasticity at specific synapses.

1.3 Objectives of this study

1.3.1 Why do we study CKAMP44? – CKAMP44 is unique in many aspects

Compared to other AMPAR auxiliary proteins CKAMP44 has unique structural features and has very specific effect on the function of AMPARs. First, CKAMP44 has only one TM segment while CNIHs and TARPs have three and four TM segments, respectively. Most remarkable, in the extracellular domain, CKAMP44 has multiple cysteines presumably forming a Cystine-knot, similar to many cysteine-rich neurotoxins that interact with ion channels. Second, the modulation of AMPAR desensitization is different between CKAMP44 and TARPs or CNIHs, e.g. CKAMP44 increases desensitization time constant and slows the recovery from desensitization, opposite to what TARPs and CNIHs do.

1.3.2 Scientific questions that need to be addressed

The novel structural and AMPAR modulatory functions of CKAMP44 and its relation to Shisa1-8 proteins raises the questions whether the cysteine-rich extracellular domain of CKAMP44 functions like neurotoxins and whether CKAMP44 has additional functions on neuronal morphogenesis, similar to the regulation of morphogenic features (head formation and segmental patterning) of Shisa 1 and 2 in *Xenopus laevis* larvae. Therefore, CKAMP44 deletion mutants were expressed and functionally analyzed in several systems, starting from *E. coli* up to *Mus musculus*.

2. Result

2.1. Expression of CKAMP44-Ex in *E. coli*, and functional analysis

2.1.1. Setting up *E. coli* expression system

To express the CKAMP44 extracellular domain (CKAMP44-Ex) in *E. coli*, we first started out to setup the *E. coli* expression system by expressing a cell-permeable Cre protein and a series fluorescent proteins (FPs).

2.1.1.1. Cre recombinase expression

Expressed from pTriex-HTNC in BL21(DE3)placI *E. coli* strain, the Cre recombinase (Cre) was fused with a His tag for affinity purification, a TAT transduction domain derived from HIV for cell permeability and a nuclear localization signal (NLS), and thus was named as HTNCre (Fig. 5A) (Peitz *et al.*, 2002). HTNCre was over-expressed after IPTG induction, and was successfully purified by immobilized-metal affinity chromatography (Ni^{2+} column), as shown by SDS-PAGE (Fig. 5B). Purified HTNCre was able to exert efficient recombination activity as commercial Cre (NEB) did, as shown by the releasing of an additional 3136 bp DNA fragment after HTNCre incubation with a linearized 4996 bp DNA containing two parallel loxP sites (Fig. 5C) (Shimshek *et al.*, 2002). The functionality of HTNCre was further validated in CV1/lacZ indicator cells (Ludwig and Stringer, 1994). HTNCre recombination in cells results in the removal of floxed transcriptional stop insert and the expression of β-galactosidase (β-gal), which could later be detected by lacZ staining. Our results showed that after lacZ staining, HTNCre treated CV1/lacZ cells had some populations of recombination-positive cells with blue color, while CV1/lacZ cells treated by normal Cre recombinase lacking TAT and NLS tags didn't show β-gal expression (Fig. 5D).
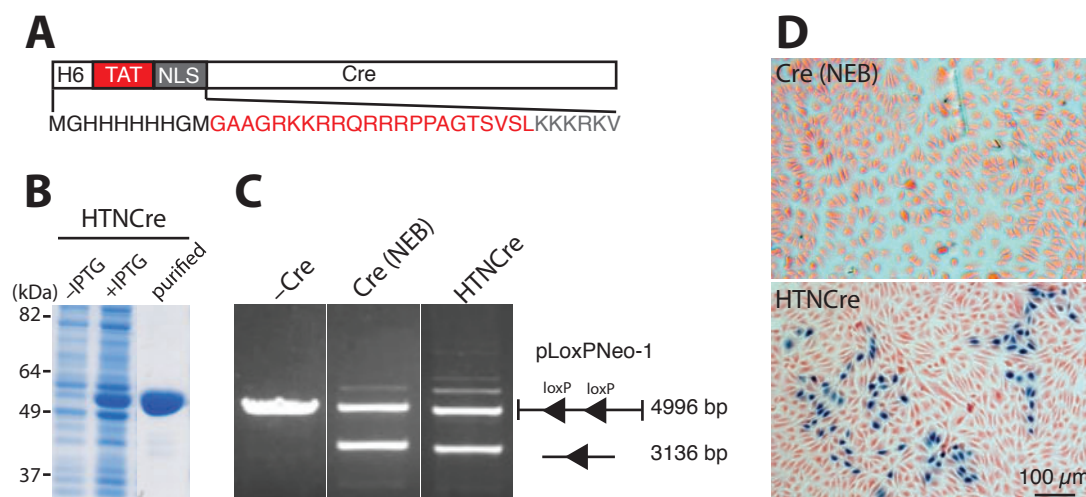
Fig. 5. Functional prokaryotic expression of HTNCre in *E. coli*. (A) Schematic diagram representing recombinant cell permeable HTNCre with His tag, TAT tag and nuclear localization signal (NLS) at the N-terminal. Protein sequence of the amino terminus is depicted with TAT in red and NLS in grey (adapted from (Nolden *et al.*, 2006)). **(B)** *E. coli* expression and purification of HTNCre. Total cell lysate in the first two lanes shows induced HTNCre expression by IPTG, and the last lane indicates purified HTNCre by Ni^{2+} column. **(C)** *In vitro* recombination activity of HTNCre with commercial NEB Cre as a positive control. Linearized 4996 bp dsDNA with two parallel loxP sites is subjected to Cre recombination, generating an additional DNA band with 3136 bp. **(D)** *In vivo* recombination activity of HTNCre, with commercial NEB Cre as a negative control. Cre reporter cell line CV1/lacZ showed blue positive cells two days after HTNCre transduction and lacZ staining, but not after cell impermeable NEB Cre treatment. Cells were counterstained by Eosin Y.

2.1.1.2. Fluorescent protein expression

Genes of fluorescent proteins (FPs) were sub-cloned into pET expression vector with six repeated histidines (H6) at the C-terminus of FPs (Fig. 6A). Expression trails were carried out in XL-Blue, BL21 and Tuner(DE3)pLysS *E. coli* strains for superfolded GFP (SFGFP), and finally Tuner(DE3)pLysS strain which gave the highest expression yield for SFGFP was chosen for the following expression including CKAMP44-Ex (Fig. 6B).

The expression of various FPs after IPTG induction could be detected by SDS-PAGE (Fig. 7A), and the expressed FPs were able to emit corresponding color after UV light excitation (Fig. 7B). The expressed FPs were later used for screening stable FPs that could preserve maximum fluorescence during the optical clearing process of mouse brain for light-sheet fluorescence microscope imaging (Niedworok *et al.*, 2012).
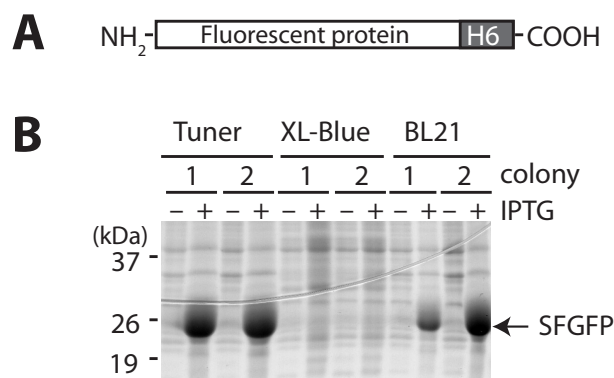
Fig. 6. Expressing conditions for high yield protein production in *E. coli*. (A) Schematic diagram for FP expression with six repeated histidines at the C-terminus. **(B)** SDS-PAGE analysis of different *E. coli* strains used for SFGPF expression. In total, three *E. coli* strains were tested, including Tuner(DE3)pLysS (Tuner), XL-Blue and BL21, with two colonies for each strain. Under the same conditions, Tuner(DE3)pLysS strain gave the highest yield of SFGFP expression (arrow) after IPTG induction. + and – represent total protein lysate before and after IPTG induction.
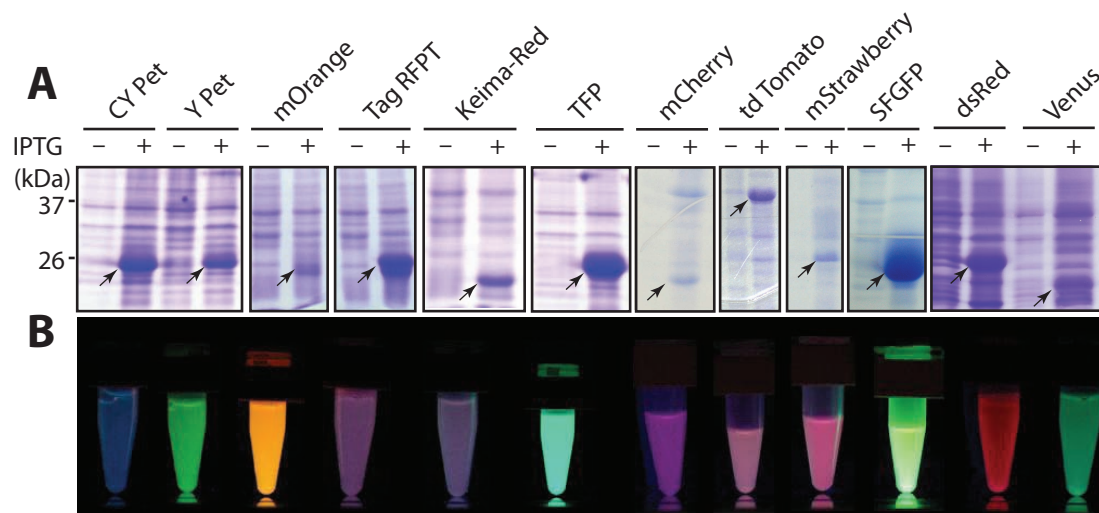
Fig. 7. Functional prokaryotic expression of FPs in *E. coli*. (A) SDS-PAGE analysis of FP expressions in *E. coli* after IPTG induction. Arrows indicate the expressed FPs. **(B)** Fluorescence emitted by *E. coli* culture overexpressing different FPs under the UV light (260 nm) stimulation, with the same order as presented in A.

In short, we were able to establish an *E. coli* expression system that successfully expresses active FPs and functional HTNCre, paving path for following CKAMP44-Ex expression *in vitro*.

2.1.2. Soluble expression of CKAMP44-Ex in *E. coli*

After successfully expressing twelve different FPs and recombinant HTNCre protein, we expressed the extracellular domains (Ex) from all four mouse CKAMPs in *E. coli*.

Ex gene fragments from four CKAMP proteins CKAMP44, 39, 52 and 59 were subcloned into the same pET vector used for FPs in Fig. 6 and 7, and the proteins were expressed in *E. coli* Tuner(DE3)pLysS strain at 37 °C for 3 h after IPTG induction (Fig. 8). The results showed that only CKAMP44-Ex showed a clear IPTG-induced protein expression, and most of the expressed CKAMP44-Ex was in inclusion bodies (Fig. 8B pellet fraction). CKAMP39-, 52- and 59-Ex were expressed only at low levels. The soluble supernatant of the CKAMP44-Ex expressing total cell lysate was subjected to Ni^{2+} column, and the soluble CKAMP44-Ex was concentrated and purified by Ni^{2+} column (Fig. 8B). The purified CKAMP44-Ex was used for functional tests in electrophysiological recordings, and was proven to be dysfunctional (Fig. 10), which might be simply due to too little CKAMP44-Ex protein.
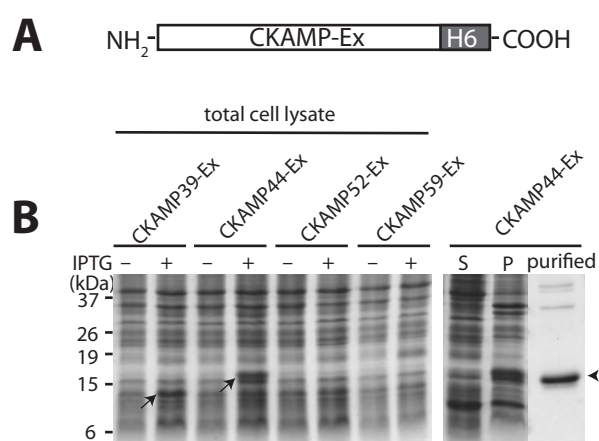
Fig. 8. *E. coli* expression and purification of soluble CKAMP44-Ex. (A) Schematic representation of four different CKAMP extracellular domain (CKAMP-Ex) expressions in *E. coli*, with His tag at the C-terminus. **(B)** SDS-PAGE analysis of CKAMP-Ex expression in *E. coli* after IPTG induction, and CKAMP44-Ex purification by immobilized metal affinity chromatography (Ni^{2+} column). Induced proteins in total cell lysate and purified CKAMP44-Ex are indicated by arrows and an arrowhead, respectively. S and P: supernatant and pellet after cell lysis.

Therefore, to improve the expression and solubility level, pET32a vector and Rosseta-gamiB(DE3)pLysS *E. coli* strain was used. The pET32a vector expresses target proteins with thioredoxin tag (Trx-tag) to facilitate protein folding (Fig. 9A), and the Rosseta-gamiB(DE3)pLysS *E. coli* strain could enhance both the expression yield of eukaryotic proteins and the disulfide bond formation of target proteins. Since only CKAMP44 has known function, we focused on CKAMP44-Ex in the following experiments.

The expression level of recombinant Trx-CKAMP44-Ex was much higher than CKAMP44-Ex expression in Tuner(DE3)pLysS, and the purification from Ni^{2+} column using gradient imidazole elution resulted in high protein yields with satisfying purity (Fig. 9C).
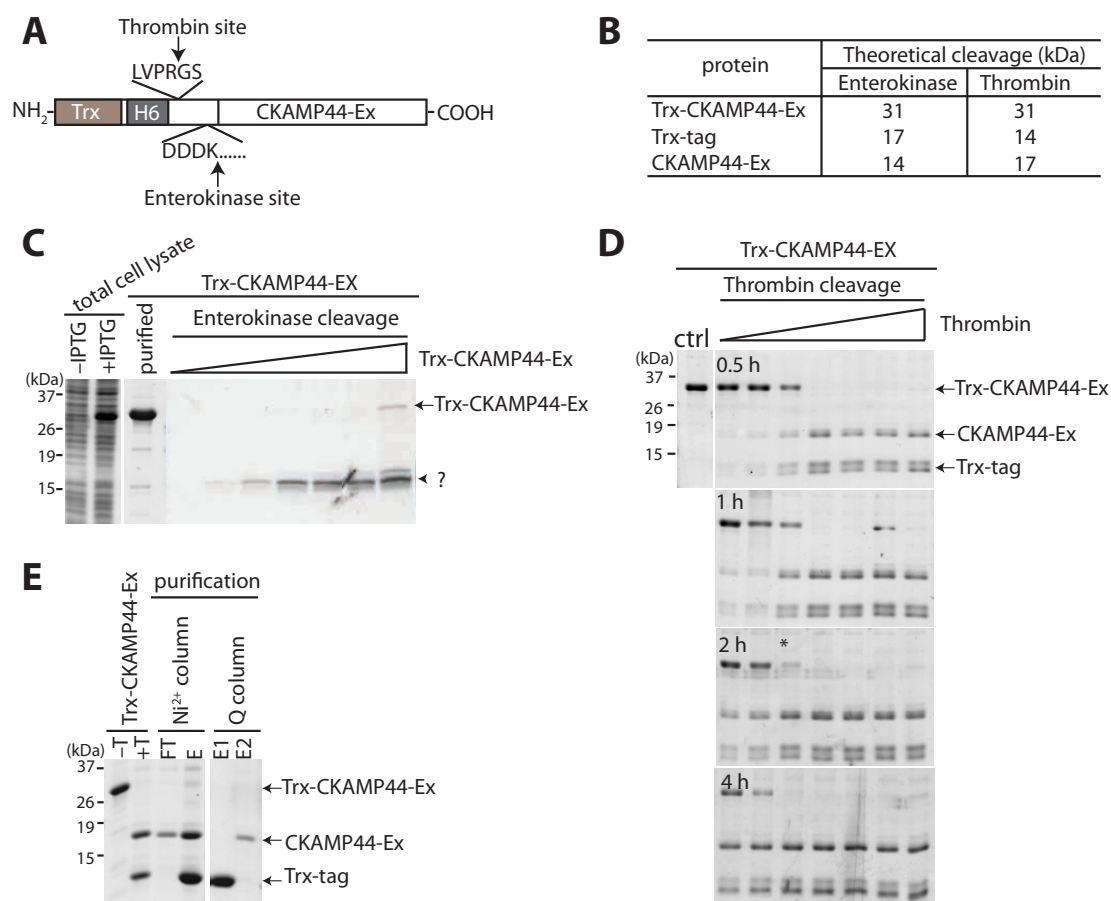
Fig. 9. Recombinant *E. coli* Trx-CKAMP44-Ex expression, enzymatic digestion and further purification of CKAMP44-Ex *in vitro*. (A) Schematic representation of recombinant Trx-CKAMP44-Ex, with thioredoxin (Trx) and His tag (H6) at the N-terminal to facilitate protein folding and subsequent protein purification. In between tags and CKAMP44-Ex are Thrombin and Enterokinase cleavage sites with indicated recognition sequence. **(B)** Summary of the theoretical protein size after two different protease digestions. **(C)** SDS-PAGE showing that Trx-CKAMP44-Ex (arrow) was expressed after IPTG induction, purified by immobilized metal affinity chromatography (Ni^{2+} column), and digested by Enterokinase with increasing amount of Trx-CKAMP44-Ex. Arrowhead and question mark (?) indicate protein product that does not match the theoretical digestion. **(D)** SDS-PAGE showing different conditions tested for Thrombin digestion, with increasing Thrombin amount (but fixed Trx-CKAMP44-Ex amount) and incubation time of 0.5, 1, 2, and 4 h. Asterisk (*) points out the chosen condition. **(E)** SDS-PAGE analysis of CKAMP44-Ex purification after thrombin digestion, including Ni^{2+} column reloading and an anion exchange Q column. −T and +T indicate before and after thrombin digestion; FT: flowthrough; E: elution; E1 and E2: Elution fraction 1 and 2.

Further protease digestion was applied to obtain CKAMP44-Ex protein. Enterokinase was first selected for the protease digestion, but the digestion resulted in one major protein band with two other smear bands (Fig. 9C), which could not match with the theoretical protein size of CKAMP44-Ex (Fig. 9B). Therefore, Thrombin digestion was used as an alternative approach (Fig. 9D). Different parameters were optimized for the thrombin digestion, including sample/enzyme ratio and incubation time. Finally, 50 µg Trx-CKAMP44-Ex/unit thrombin for 2 h digestion at RT was used.

To separate CKAMP44-Ex from Trx-tag, two different separation methods were tried, Ni^{2+} column reloading and anion Q column exchange (Fig. 9E). Ni^{2+} column reloading could not efficiently separate CKAMP44-Ex protein from Trx-tag, since except in flowthough, CKAMP44-Ex was also coeluted with Trx-tag in elution. In Q column exchange experiment, CKAMP44-Ex can be completely separated from Trx-tag, but thioredoxin was present in higher amounts than the CKAMP44-Ex protein, indicating that most of the CKAMP44-Ex protein aggregated during Q anion exchange preparation (probably because of the buffer change), and was clogged in column. Finally, 20 ml of 0.2 µg /µl CKAMP44-Ex (about 10 µM) was prepared and used for functional analysis in electrophysiological recordings (described in 2.1.3 and Fig. 10).

2.1.3. Functional assay of CKAMP44-Ex in hippocampal dentate gyrus neurons by patch-clamp

The function of purified proteins was investigated by applying purified proteins onto outside-out patches of hippocampal dentate gyrus neurons while recording glutamate evoked AMPAR-mediated currents (carried out by Dr. J. von Engelhardt, DKFZ, Heidelberg). With the exception of Trx-CKAMP44-Ex influence on 20-80% rise time and deactivation time constant which was thought to be unspecific (Fig. 10), no obvious modulation on AMPAR-mediated currents, including peak amplitude, desensitization time constant, and recovery from desensitization, was observed for any of proteins that were prepared.
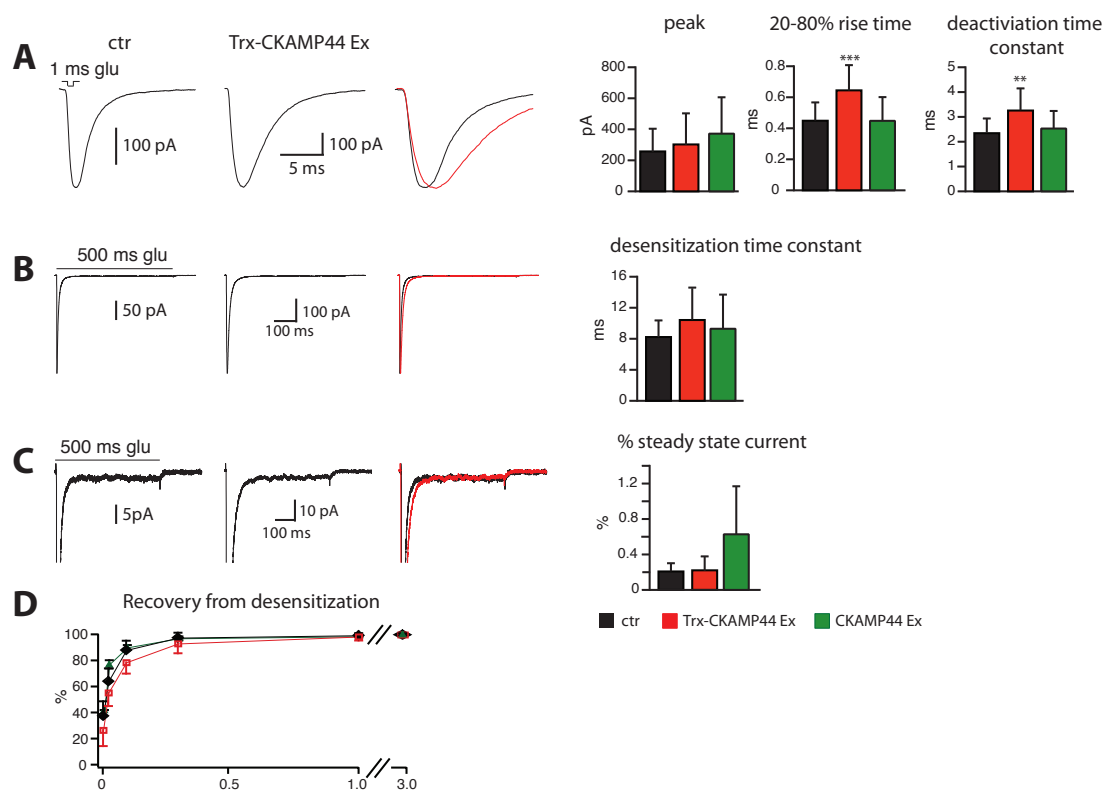
Fig. 10. *E. coli* expressed CKAMP44-Ex failed to modulate AMPAR-mediated current measured by outside-out patches in dentate gyrus granule cells of acute mouse brain slices. The AMPAR responses in current tracings in A, B, and C are shown on the left, and the bar graph statistics is on the right. Control condition without the presence of *E. coli* expressed proteins is given in black, while the addition of Trx-CKAMP44-Ex and CKAMP44-Ex are in green and red, respectively. **(A)** Analysis of AMPAR deactivation. Short pulse of glutamate (1 ms Glu) triggers the opening of AMPARs, which afterwards undergo deactivation. The peak amplitude, 20-80% rise time and deactivation time constant were analyzed on the right. The continuous presence of Trx-CKAMP44-Ex significantly increased 20-80% rise time and deactivation time constant. However, this might be due to the side effect of the high viscosity of the protein sample, since no other kinetics was altered (see B, C and D) which should also be changed by functional CKAMP44. Thus, CKAMP44-Ex had no obvious impact on AMPAR deactivation. **(B, C)** Analysis of AMPAR desensitization and steady state current. Continuous exposure to glutamate (500 ms Glu) induced AMPAR desensitization. Statistics shows that none of the recombinant proteins has any effect on AMPAR desensitization or steady state current. **(D)** Analysis of AMPAR recovery from desensitization. The recovery from desensitization makes AMPARs sensitive to glutamate again, and is tested by several subsequent waves of glutamate stimuli. No modification of the AMPAR recovery from desensitization was observed for any of the *E. coli* expressed protein. The data was kindly provided by Dr. J. von Engelhardt.

In conclusion, the prokaryotic *E. coli* expression system successfully expressed biologically functional FPs and recombinant Cre recombinase, but failed to express functional CKAMP44-Ex. Although it cannot be excluded that the amount of CKAMP44-Ex that was used in the electrophysiological recording was below the

threshold, it is more likely that CKAMP44-Ex was misfolded in *E. coli,* which is the limitation for the prokaryotic protein expression system. Due to the unknown cystine pattern of CKAMP44-Ex and that of native CKAMP44, it is difficult to evaluate if the CKAMP44-Ex was expressed in the correct conformation. Therefore, the eukaryotic Baculovirus expression system might be more suitable to achieve the expression of functional CKAMP44-Ex.

2.2. CKAMP44 domain mapping

CKAMP44 belongs to a small vertebrate and brain specific protein family comprising three other members CKAMP39, 52 and 59, whose functions remain to be explored. In the literature, CKAMPs are also classified as Shisa protein family members, and are named as Shisa6, 7, 8 and 9 for CKAMP59, CKAMP52, CKAMP39 and CKAMP44, respectively (Pei and Grishin, 2012). All CKAMPs share similar protein domains (Fig. 11A), including an N-terminal signal peptide (SP), an extracellular domain, a single alpha helical membrane-spanning segment (M) that is followed by a short hydrophilic region rich in positively charged residues (R/K) and the C-terminal intracellular domain (CT) (Fig. 11C). The extracellular domain is further divided into an N-terminal domain (NT), a highly conserved cysteine-rich domain (Cys-knot) and a linker domain (L) (Fig. 11B). The CT domain is highly variable between CKAMPs, and it is encoded by different exons which can be alternatively spliced. The C-terminal domain is terminated by a PDZ type II ligand motif that might be important for postsynaptic localization (Fig. 11D).

For the analysis of CKAMP44 domain functions, a series of pAAV expressing EGFP or Venus tagged CKAMP44 deletion mutants were generated (Fig. 11E). Subsequently, the CKAMP44 mutant expression vectors were used to investigate the CKAMP44/AMPARs interaction in HEK293 cells, the CKAMP44 subcellular localization in transfected primary neurons, and the AMPAR modulation activity in acute brain slices of infected mouse brains.
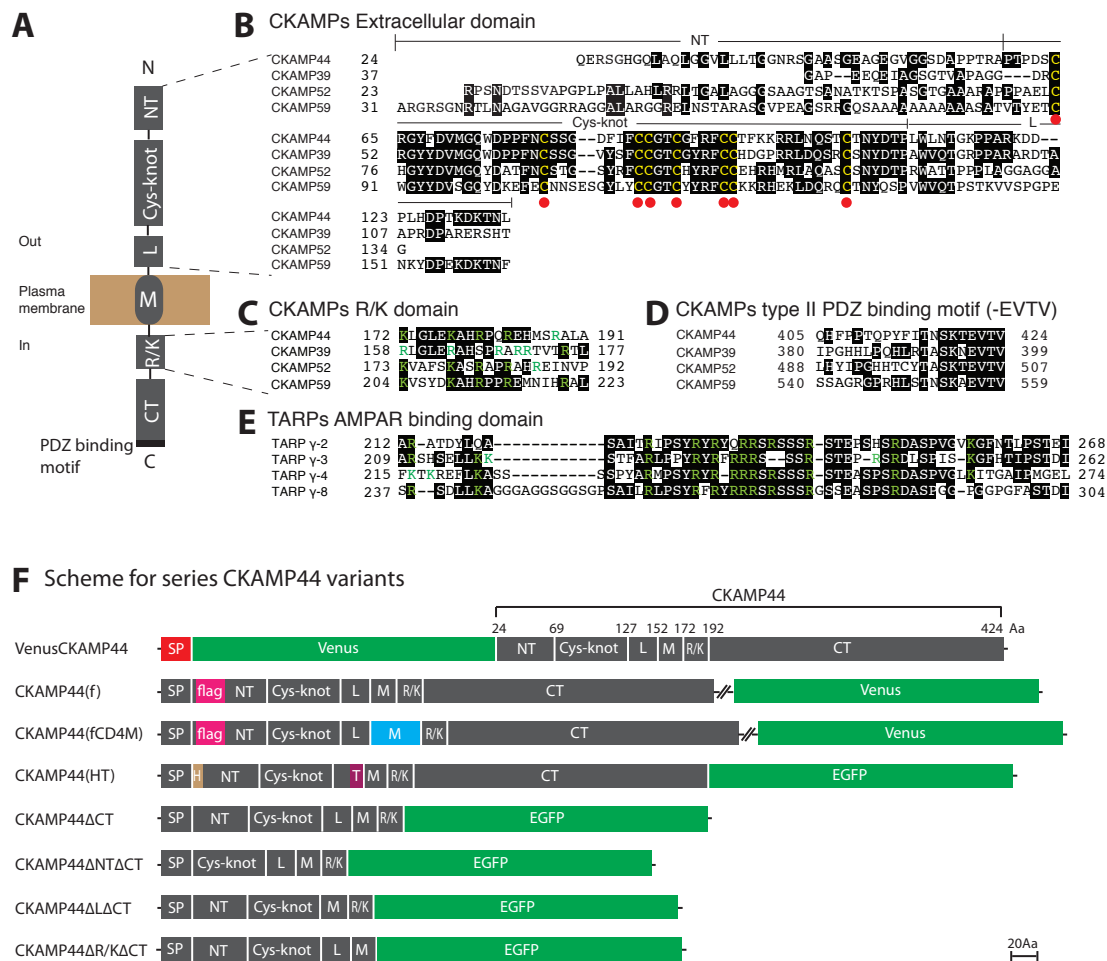
Fig. 11. CKAMP family domain arrangement and domain mapping scheme for CKAMP44. (A) Schematic drawing of CKAMP44 as a single membrane-spanning protein with an N-terminal extracellular domain and a C-terminal intracellular domain. According to the sequence alignment within CKAMP protein family in B, C and D, the extracellular domain is divided into an N-terminal domain (NT) with less similarity within CKAMP family, a highly conserved cysteine rich domain (Cys-knot) and a linker domain (L) linking Cys-knot and membrane spanning region. Shortly after the membrane-spanning region (M), there is a short region (20 amino acids) rich in hydrophilic basic residues arginine R and lysine K (5 out of 20 for CKAMP44, 52 and 59 or 6 out of 20 for CKAMP39), and is therefore named as R/K domain. The remaining intracellular C-terminal domain is terminated with type II PDZ binding motif. **(B)** Sequence alignment of the extracellular domain within CKAMP protein family, with residue numbers on the left side. Conserved residues (2 out of 4 proteins) are shaded in black background, and conserved cysteines are highlighted in yellow. Divided subdomains including N-terminal domain (NT), cysteine rich domain (Cys-knot) and linker domain (L) are indicated on top of the alignment. The conserved eight cysteines in Cys-knot domain are highlighted by red filled circles underneath. **(C)** Sequence alignment of the R/K domain. Basic residues R and K are highlighted in green. **(D)** Conserved C-terminal type II PDZ binding motif (-EVTV). **(E)** Sequence alignment of AMPAR interacting domains in the C-terminal intracellular domain of TARP γ2, 3, 4 and 8, which are also rich in R and K highlighted in green. **(F)** Domain mapping scheme for CKAMP44. Full-length CKAMP44 with GluA1 signal peptide and Venus at the N-terminal (VenusCKAMP44) and flag-tagged CKAMP44 coexpressed with Venus using IRES as a linkage (CKAMP44(f)) were used as

positive controls. Each domain is marked with the number for the starting amino acid on the top of the diagram. For both CKAMP44(f) and CKAMP44(fCD4M), the flag tag is inserted between amino acid (Aa) 29 (histidine) and 30 (glycine). CKAMP44 mutants are named according to the deleted domains. In CKAMP44(HT), a his-tag with six histidine repeat was inserted after the SP and a thrombin recognition site (LVPRGS) was placed in front of M domain by sequence replacement. SP: GluA1 signal peptide; M: TM domain from CD4 protein; flag: Flag tag; H: his-tag; T: thrombin recognition site.

2.2.1. CKAMP44 and AMPAR association in HEK 293 cells

First, we analyzed the molecular interaction between CKAMP44 variants and homomeric GluA1 AMPARs after transient transfections in HEK293 cells by co-immunoprecipitation (Co-IP). As expected, Venus-tagged full length CKAMP44 (VenusCKAMP44), but not Venus, was found to be associated with GluA1, indicating that the interaction between CKAMP44 and GluA1 can be traced by Venus and is independent of other AMPAR associating proteins that are absent in HEK293 cells (Fig. 12). Similarly, CKAMP44 deleted mutants CKAMP44ΔCT, CKAMP44ΔNTΔCT and CKAMP44ΔLΔCT could co-precipitate GluA1 in Co-IPs, suggesting that the C-terminal domain and two non-cysteine containing regions in the extracellular domain, namely NT and L domain, are not important for the CKAMP44/AMPAR interaction.

To further identify the function of the R/K and M domain of CKAMP44 in AMPAR interaction, we truncated the R/K domain (CKAMP44ΔR/KΔCT) and generated M domain replacement by the transmembrane region of the membrane protein CD4 (CKAMP44(fCD4M)). In CKAMP44(fCD4M), Venus was co-expressed by an IRES containing bicistronic mRNA. The very inefficient co-precipitation of CKAMP44ΔR/KΔCT and AMPARs showed that the deletion of the R/K domain diminished the tight association between CKAMP44 and AMPARs. The strong reduction of CKAMPΔR/KΔCT/GluA1 binding could be restored by introducing the R/K domain in CKAMP44(fCD4M), since GluA1 was efficiently co-immunoprecipitated with CKAMP44(fCD4M). This result indicates that the CKAMP44 R/K rather than the M domain is important for a strong CKAMP44/AMPAR interaction. This finding is reminiscent with previous report showing that AMPAR auxiliary protein TARP γ2 associates with AMPARs using part of an intracellular C-terminal domain localized shortly after the fourth TM of TARP (Tomita *et al.*, 2004). Interestingly, the AMPAR binding domain in TARP γ2 is also

rich in R and K (10 out of 57 Amino acids), and like CKAMP family, this domain is also conserved within TARP family, including TARP γ3, γ4, and γ8 (Fig. 11D). This data suggests that CKAMP44 and TARPs interact with AMPARs using a similar mechanism.

In short, our Co-IP studies in HEK293 cells demonstrate that the R/K domain is critically involved in CKAMP44/AMAPR interaction (Fig. 13).
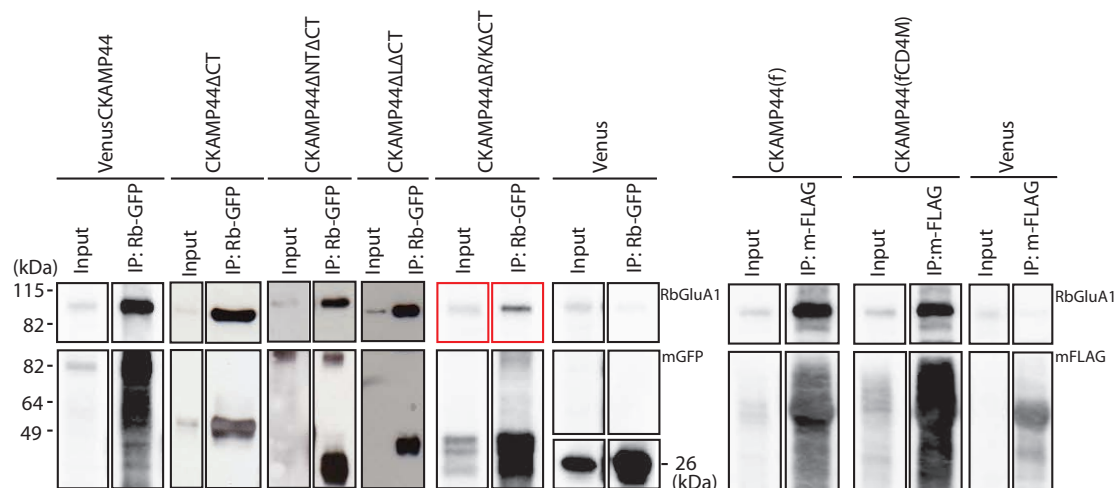
Fig. 12. Co-immunoprecipitation for different CKAMP44 mutants with GluA1 subunit in HEK 293 cells. CKAMP44 mutants were co-transfected with GluA1 in HEK293 cells and the total cell lysate was used for following Co-IPs. Co-IP experiments were done by rabbit α-GFP or mouse α-Flag, and detected by rabbit α-GluA1 antibody (upper panels), mouse α-GFP and mouse α-Flag antibody (lower panels). The inefficient enrichment of GluA1 in α-GFP Co-IP is boxed in red.
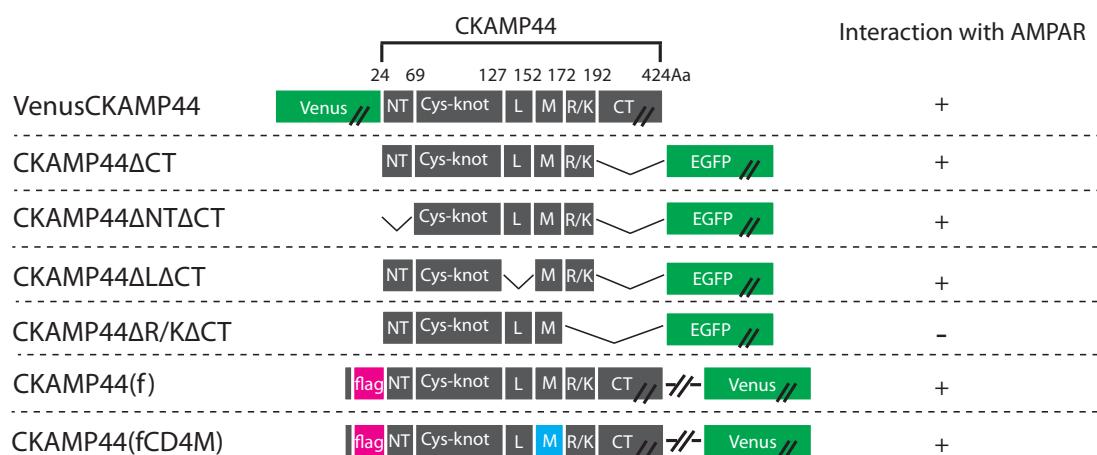
Fig. 13. Summary of CKAMP44 variant interaction with AMPARs based on the Co-IP shown in Fig. 12. '+' and '–' represent positive and negative interaction with AMPARs, respectively, as demonstrated in Co-IP experiments in HEK293 cells. Symbols and constructs are given as in Fig. 11.

2.2.2. Subcellular localization of CKAMP44 variants in primary neurons

The domain mapping of CKAMP44 by Co-IPs unraveled the domain important for CKAMP44/AMPAR association. To analyze the different domain functions in CKAMP44 spine targeting, we analyzed the subcellular distribution of the CKAMP44 variants in transfected rat hippocampus primary neurons by immunocytochemistry (Fig. 14). Given that CKAMP44 is primarily localized in synaptic spines (von Engelhardt *et al.*, 2010), the subcellular distribution studies were focused on dendritic expression.

The spine head localization of different CKAMP44 variants was evaluated by the colocalization of Venus or EGFP with GluA1 (Fig. 14A). The spine targeting was quantified by the ratio of green fluorescence intensity in spines to that in dendritic shaft (Fig. 14B). Cytosolic Venus as a negative control was not able to be targeted to spine head as indicated by the non-overlapping red GluA1 signal at the tip of the spines (arrows in Fig. 14A). But as a commonly used spine-labeling tool, Venus could be expressed in spines with a mean spine/dendritic shaft ratio of 1.26 ± 0.03. The N-terminal Venus-tagged full length CKAMP44 (VenusCKAMP44), instead, could be targeted to spine head, as depicted by the perfect overlapping with GluA1 signal in spines (arrowheads in Fig. 14A), and showed a privileged localization in spines over dendritic shafts (spine/dendritic shaft ratio 2.5 ± 0.05, Fig. 14C).

Similar to the N-terminal Venus fused CKAMP44 (VenusCKAMP44), the C-terminal Venus fused CKAMP44 mutant CKAMP44(HT), as well as flag-tagged CKAMP44(f) and CKAMP44(fCD4M) stained by flag-tag antibody could also co-localize with GluA1 at spine heads (Fig. 14A) and showed stronger expressions in spines than in dendritic shafts (spine/dendritic shaft ratio 1.82 ± 0.1, 2.4 ± 0.02, 3.0 ± 0.27, respectively) (Fig. 14C). These data implies that Venus fusion, regardless of N- or C-terminal fusion, different tag insertions in the extracellular domain and transmembrane domain replacement does not inhibit the postsynaptic localization nature of CKAMP44.
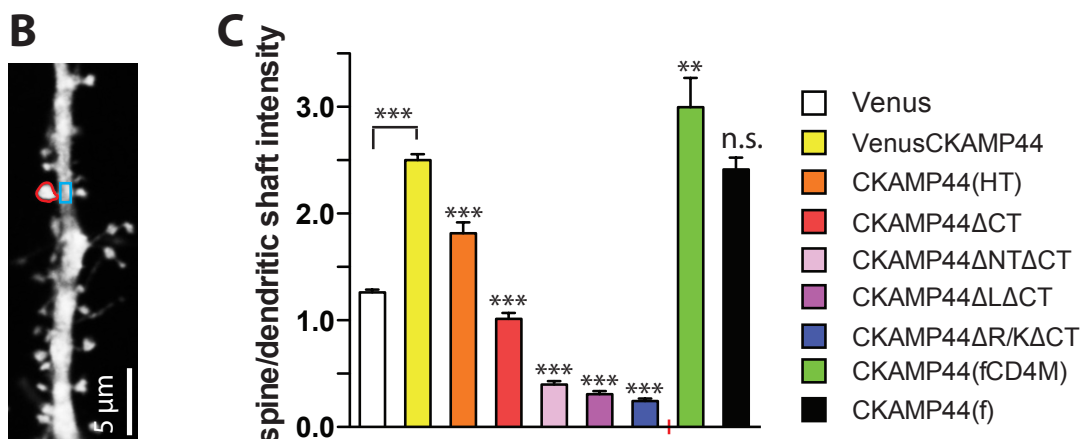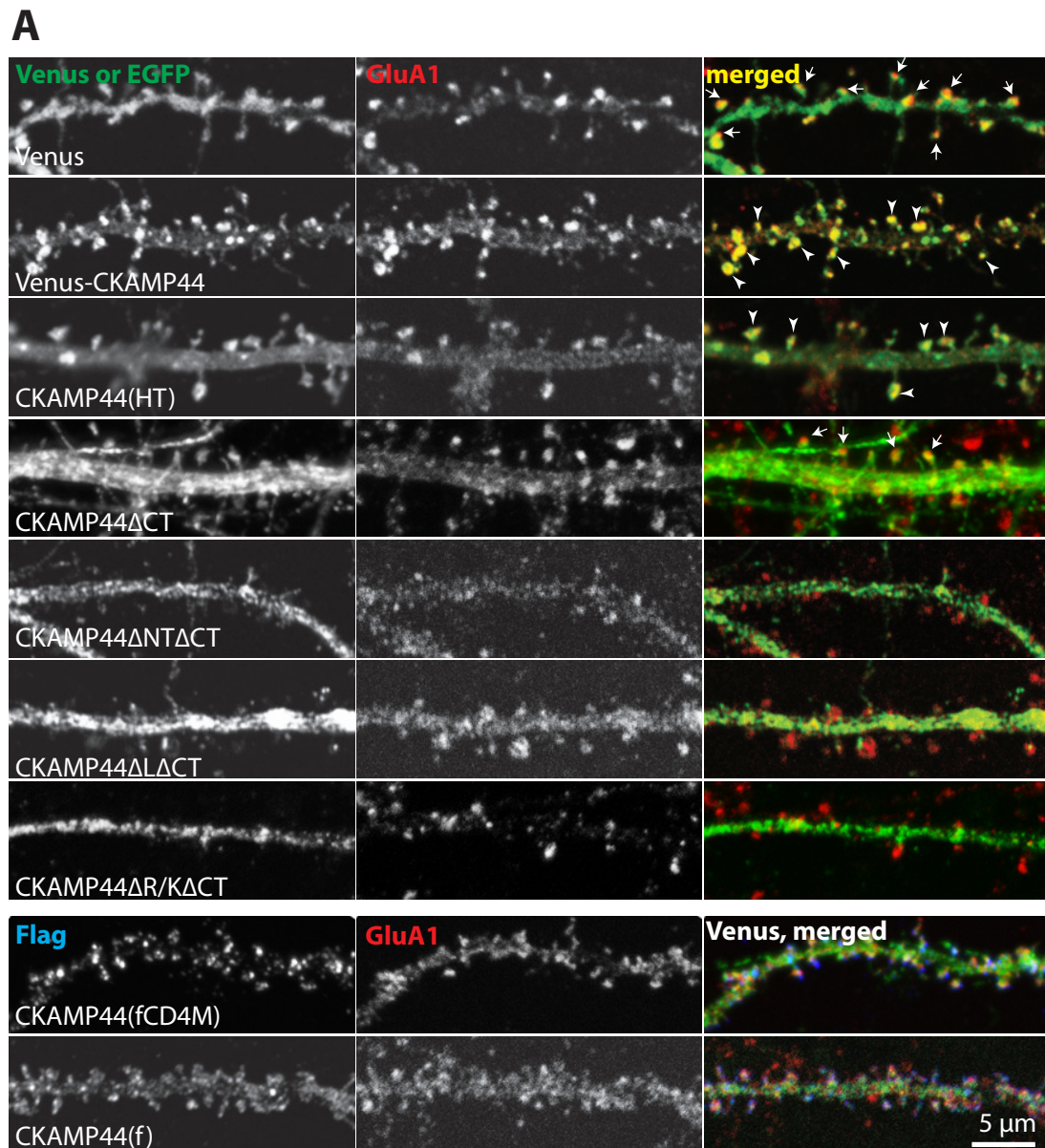
Fig. 14. Spine targeting of CKAMP44 variants and their colocalization with GluA1 in rat primary hippocampal neurons. **(A)** Dendrites from primary hippocampal neurons transfected with indicated CKAMP44 variants, and double immuno-stained for GFP-fused

CKAMP44 variants (green) and endogenous GluA1 (red) or triple stained with additional flag antibody (blue) for neurons transfected with CKAMP44 (fCD4M)-IRES-Venus and CKAMP44(f)-IRES-Venus. In triple stained images, blue flag signal stands CKAMP44 variants, green signal for cytosolic Venus expression, and red signal for endogenous GluA1 signal. Arrows indicate spines that lack Venus or EGFP signal at spine heads, and arrowheads point spines with perfectly overlapping Venus or EGFP and GluA1 signals. **(B)** Example image of a dendritic segment showing the measurement of spine (manually drawn red line)/dendritic shaft (blue rectangle) intensity done in ImageJ. **(C)** Quantification of fluorescence intensity in spines versus that in dendritic shafts of each CKAMP44 variant as an index of spine targeting. VenusCKAMP44 was compared with Venus control. All other CKAMP44 variants were compared with VenusCKAMP44. Analysis was done by one-way ANOVA followed by Bonferroni's post-hoc comparison test. All values are shown in mean ± SEM. **$P<0.01$, ***$P<0.001$, n.s: not significant.

However, the C-terminal domain truncated CKAMP44 (CKAMP44ΔCT), which could still interact with GluA1 homomers in HEK293 cells, was not co-localized with AMPARs at spine heads (Fig. 14A), and showed an even distribution in spines and dendritic shafts like the Venus control (spine/dendritic shaft ratio 1.01 ± 0.05) (Fig. 14C). This finding suggests that the intracellular C-terminal CKAMP44 domain is required for postsynaptic spine head localization and enriched spine expression, and that the correct subcellular localization is independent of AMPAR receptor interaction.

Partial extracellular domain deleted CKAMP44, including CKAMP44ΔNTΔCT and CKAMP44ΔLΔCT, as well as conserved intracellular R/K domain deleted CKAMP44 (CKAMP44ΔR/KΔCT) could not be localized at spine heads (Fig. 14A), consistent with the result of CKAMP44ΔCT. Different from CKAMP44ΔCT, they all showed impaired spine expressions with spine/dendritic shaft ratio of 0.40 ± 0.03, 0.308 ± 0.03 and 0.243 ± 0.02, respectively (Fig. 14C). These findings suggest that the extracellular domain and the R/K domain is important for spine expression. However, we could not rule out the possibility that double domain deletions, which are ΔNTΔCT, ΔLΔCT and ΔR/KΔCT, lead to protein dysfunction. Therefore, further experiments with single domain truncation should be carried out to verify the function of the extracellular and the R/K domain in CKAMP44 spine expression.
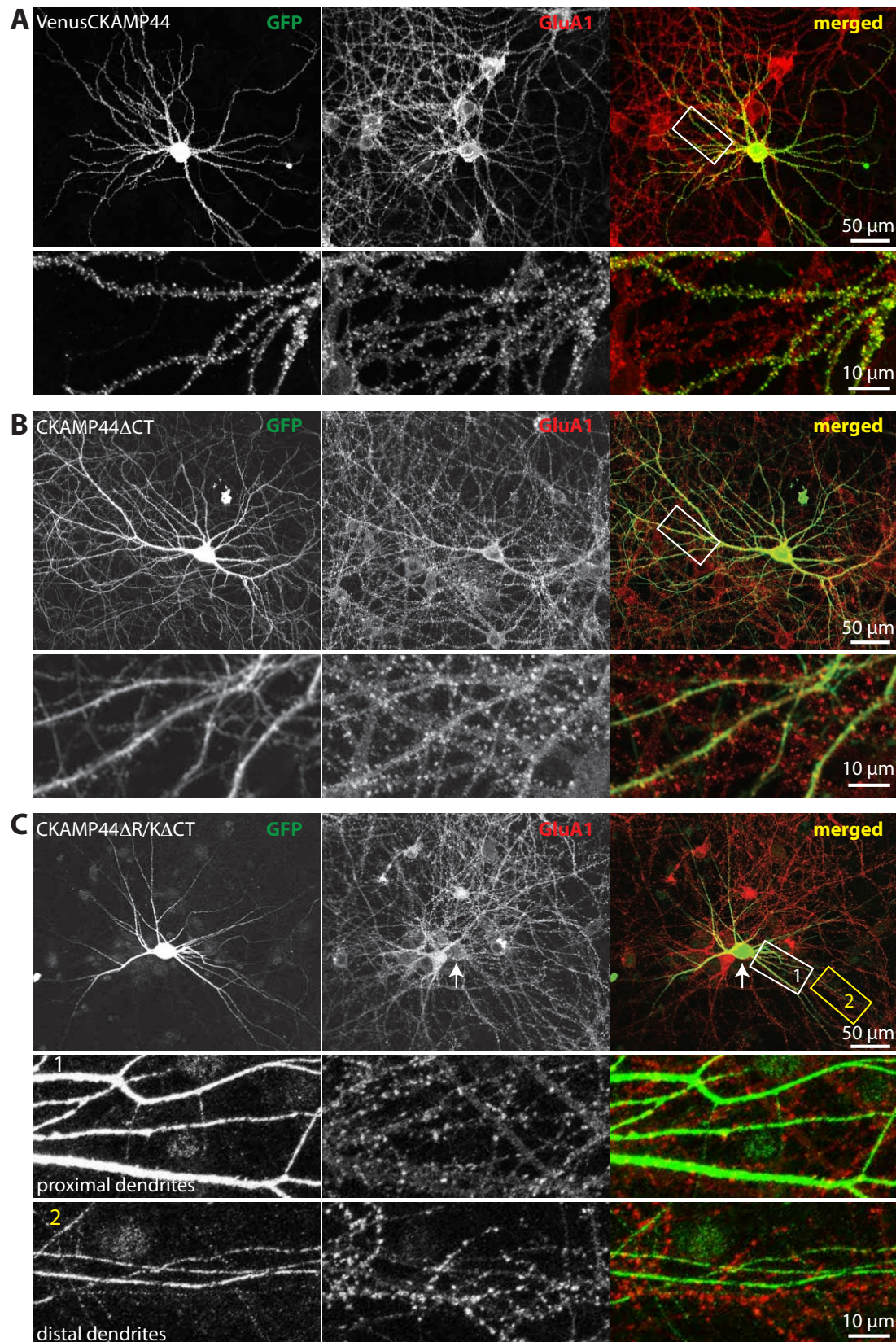
Fig. 15. Dominant negative effect of CKAMP44ΔR/KΔCT on AMPAR expression in transfected rat hippocampal neurons. (A and B) Co-immunostaining of GFP (green) and GluA1 (red) in VenusCKAMP44 (for A) and CKAMP44ΔCT (for B) overexpressed hippocampal neurons. Upper panels represent neuron overview and lower panels show

enlarged dendritic segments of the boxed areas in upper panels, demonstrating that GluA1 expression was normal in GFP positive neurons. **(C)** Co-immunostaining of GFP and GluA1 in CKAMP44ΔR/KΔCT overexpressed hippocampal neurons, demonstrating that the GluA1 expression was greatly diminished in GFP positive neurons (pointed by arrows) compared to neighboring neurons. 1 and 2 are higher magnification images of the boxed areas in the upper panel, showing proximal and distal dendrites. It seems that inefficient CKAMP44ΔR/KΔCT and GluA1 expression is more sever in distal dendrites than in proximal dendrites.

What is worth mentioning is that CKAMP44ΔR/KΔCT had a dominant negative effect on the AMPAR expression in both somata and dendrites, as seen by the week GluA1 signal compared to the one from neighboring neurons (Fig. 15C). This phenomenon became more severe in distal dendrites than in proximal dendrites. This dominant negative effect might be related to the AMPAR/CKAMP44 interaction, since similar effect could not be found by the overexpression of VenusCKAMP44 or CKAMP44ΔCT which maintain AMPAR binding ability (Fig. 15A and 15B). We hypothesized that CKAMP44/AMPAR interaction can be involved in the dendritic stabilization of the AMPARs, which cannot be achieved when the CKAMP44/AMPAR interaction is disturbed by negative competitors like CKAMP44ΔR/KΔCT.
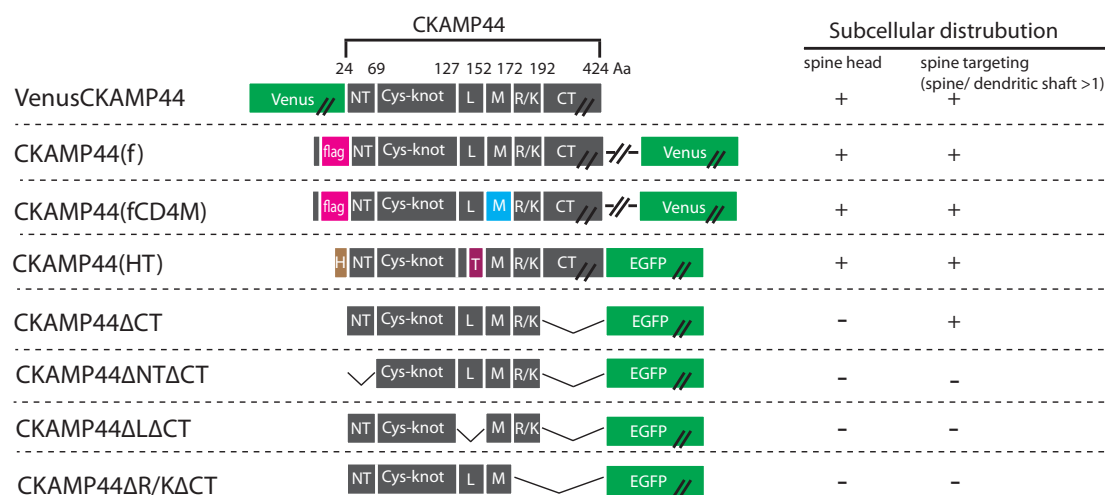
Fig. 16. Summary of subcellular distribution of different CKAMP44 variants in primary neuron culture. Spine head localization was evaluated by observing the overlay of Venus or EGFP and GluA1 signal at spine heads. Spine targeting was evaluated by the green signal intensity in spines over that in dendritic shafts. The C-terminal domain is required for CKAMP44 localization in spine heads, while the NT, L and R/K domain are involved in efficient spine targeting of CKAMP44.

In summary (Fig.16), the subcellular distribution of different CKAMP44 deletion mutants in primary neurons suggests that (i) the TM domain is not important

for the subcellular localization, (ii) the C-terminal domain is required for spine enrichment and spine head expression and (iii) the extracellular and intracellular R/K domain are necessary for CKAMP44 expression in spines. The R/K domain deletion has a dominant negative effect on AMPAR expression, especially in distal dendrites.

2.2.3. rAAV-mediated CKAMP44 variants overexpression *in vivo*

To investigate different CKAMP44 domain functions in CKAMP44 subcellular distribution and AMPAR modulation *in vivo*, all different CKAMP44 variants were overexpressed in hippocampi of $Ckamp44^{-/-}$ mice by rAAV mediated gene transfer at P0 and post-mortem analyzed at P26-40 by immunohistochemistry and electrophysiological recordings.

2.2.3.1. CKAMP44 variants overexpression *in vivo*

Our immunohistological studies showed that all CKAMP44 variants provided comparable expression pattern in mouse hippocampi. GFP or Venus signal could be observed in somatic layers of CA1, CA3 and DG, and also in stratum oriens, stratum radiatum, stratum lacunosum moleculare and DG molecular layers (shown for VenusCKAMP44 in Fig. 17). In sharp contrast, the CKAMP44 with deleted R/K and C-terminal domains (CKAMP44ΔR/KΔCT) exhibited exclusively somatic expression in CA1, CA3 and DG (Fig. 17). CKAMP44ΔR/KΔCT showed more severe deficiency *in vivo* than *in vitro* primary neuron experiments (Fig. 15), which showed that CKAMP44ΔR/KΔCT cannot be targeted to spines, although it is still expressed in dendritic shafts. These data provided further evidence that R/K domain is important for the correct subcellular distribution of CKAMP44.

2.2.3.2. AMPAR modulation of CKAMP44 variants *in vivo*

The rescue of AMPAR modulation by different overexpressed CKAMP44 variants in $Ckamp44^{-/-}$ mice was evaluated in outside-out patches of DG granule cells from acute mouse brain slices by measuring glutamate evoked extrasynaptic AMPAR-mediated excitatory postsynaptic currents (EPSC) by the research group of Dr. J. von Engelhardt.

Electrophysiological recordings showed that the truncation of CKAMP44 C-terminal domain (CKAMP44ΔCT) could still exert CKAMP44 modulatory activity on
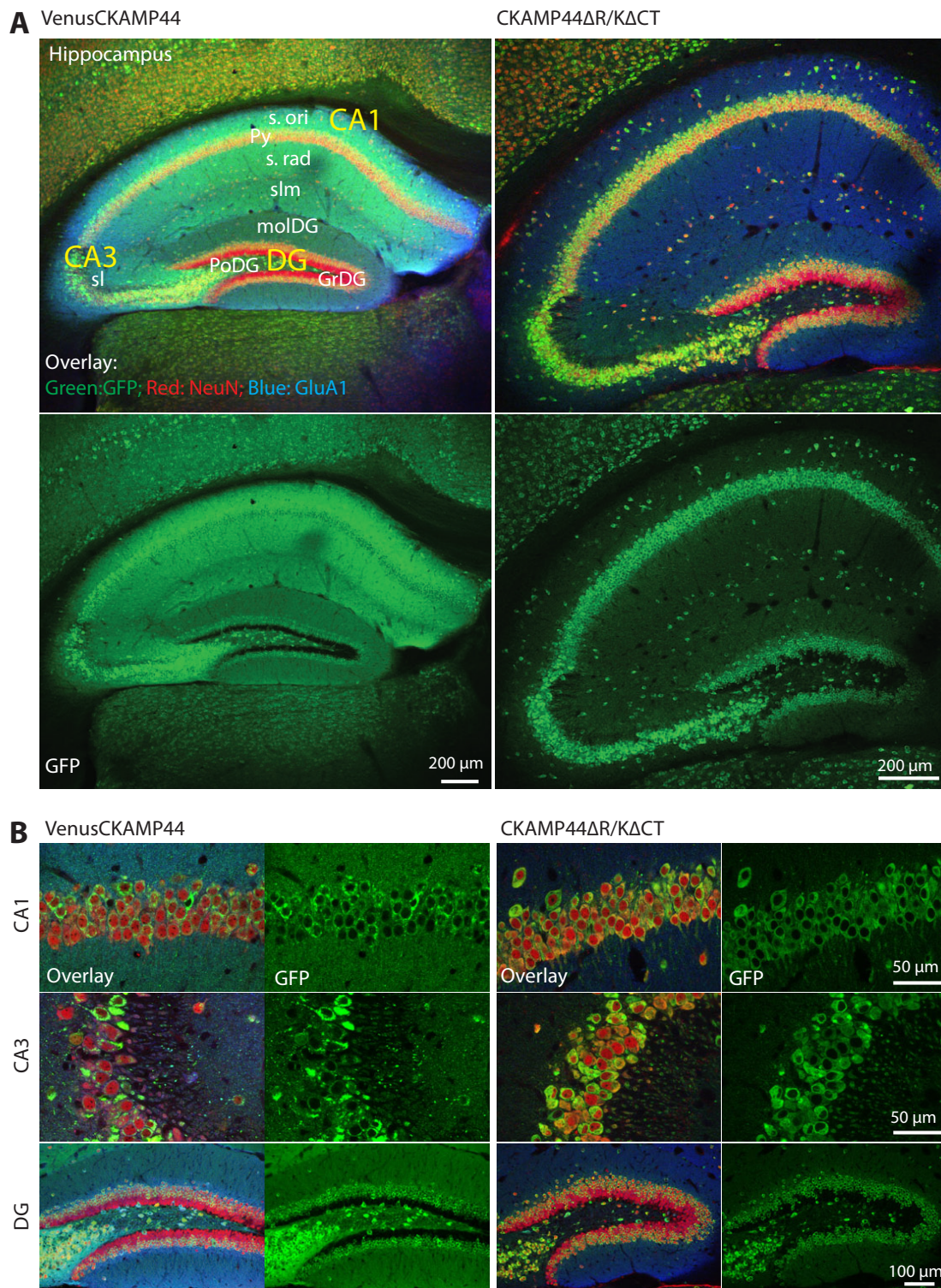
Fig. 17. R/K domain deletion disrupts CKAMP44 dendritic expression *in vivo*. CKAMP44 variants were overexpressed in mouse brain by rAAV-mediated gene delivery at P0, and the injected mice were analyzed post-mortem by immunohistochemistry. Example images are given for VenusCKAMP44 (left) and CKAMP44ΔR/KΔCT (right) overexpressed mouse brain, demonstrating that full-length CKAMP44 (VenusCKAMP44) exhibited efficient expression in both somata and dendritic areas, while CKAMP44ΔR/KΔCT showed exclusively somatic expression. **(A)** Hippocampal areas of horizontal mouse brain sections, stained by α-GFP (green), α-NeuN (red) and α-GluA1 (blue) antibodies. Upper panels are the

merged images of three mentioned immunosignals, and the lower panels represent GFP signal alone. CA1, CA3 and DG areas are indicated. VenusCKAMP44 showed expression throughout the hippocampus, both in somata and in areas outside of somata. However, CKAMP44ΔR/KΔCT was only localized in somata. The somata of neurons are aligned in pyramidal cell layers (Py) of CA1 and CA3 and granule cell layer of the dentate gyrus (GrDG). The dendritic layers, including striatum oriens (s. ori), striatum radiatum (s. rad), stratum lacunosum moleculare (slm), stratum lucidum (sl) of CA3, molecular layer of dentate gyrus (molDG) are indicated. molDG, polymorphic DG layer. **(B)** Higher magnification of the subregion images of the hippocampi shown in A, including CA1, CA3 and DG. Overlay images represent merging signal of GFP, NeuN and GluA1.

AMPAR-mediated currents (Fig. 18), as it could increase peak amplitude and deactivation time constant, and could slow the recovery of AMPARs from desensitization, similar to full-length CKAMP44 (von Engelhardt *et al.*, 2010). But further deletion of R/K domain (CKAMP44ΔR/KΔCT) completely abolished the CKAMP44 modulation of AMPAR properties (Fig. 19). Since R/K domain is involved in AMAPR association as shown by Co-IP (Fig. 12 and 13), the failure in AMPAR modulation for CKAMP44ΔR/KΔCT might only be because the CKAMP44/AMPAR association is disrupted. Thus, one cannot conclude from these experiments that the R/K domain is important for AMPAR modulation.

Except for the central Cys-knot domain (cysteine mutation analysis done by our collaborators, see discussion), two non-cysteine containing regions franking Cys-knot are also essential for CKAMP44 function, since deletion of either N-terminal (ΔNTΔCT) or C-terminal (ΔLΔCT) part of extracellular domain was correlated with a loss of AMPAR current modulation (Fig. 19), although CKAMP44ΔNTΔCT and CKAMP44ΔLΔCT could still interact with AMPARs by our Co-IP result.

Sequence replacement of C-terminal part of extracellular domain by thrombin recognition site (CKAMP44(HT)) still kept CKAMP44 modulatory activity on the gating properties of AMPARs (Fig. 20), suggesting that it is important to keep a certain length between central Cys-knot and TM region.

A peak current

B 20-80% rise time

C τ_{deact}

D τ_{des}

E steady state current

F Recovery from desensitization

■ *Ckamp44*$^{-/-}$
■ *Ckamp44*$^{-/-}$ + CKAMP44ΔCT
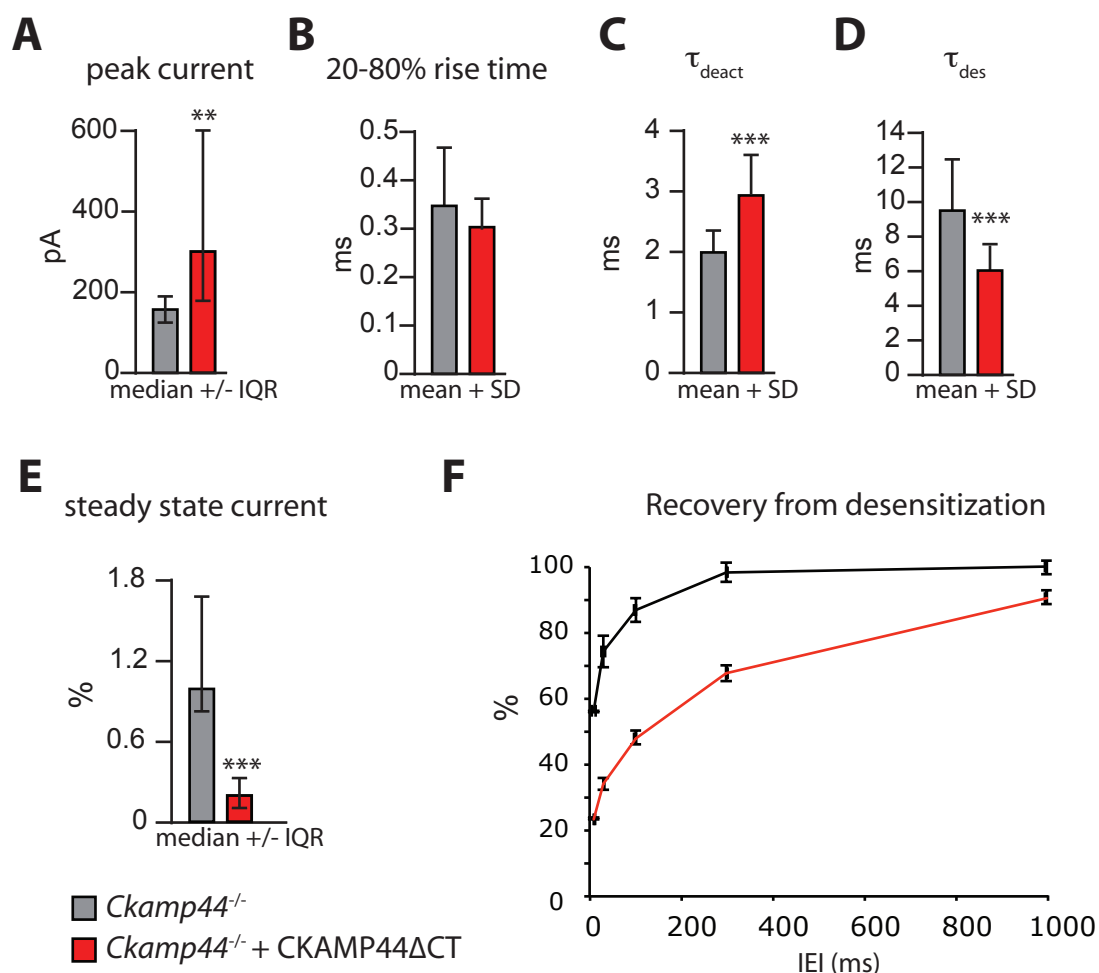
Fig. 18. Overexpression of CKAMP44ΔCT rescues AMPAR-mediated current in dentate gyrus granule cells of *Ckamp*44$^{-/-}$ mice, measured by outside-out patches. CKAMP44ΔCT increases peak current (A) and deactivation time course (C), while decreases desensitization time constant as well as steady state current (E) and slows the recovery from desensitization (F). Error bar representations are depicted for each diagram. Analysis was done by t-test. **P<0.01, ***P<0.001. ms, milliseconds; IEI, interevent interval. The data were provided by Dr. J. von Engelhardt.

Taken together, our CKAMP44 domain mapping *in vivo* indicated that (i) the C-terminal domain is not required for CKAMP44 modulation of AMPAR-mediated extrasynaptic currents, (ii) the extracellular domain is important for modulatory activity of CKAMP44, (iii) the R/K domain of CKAMP44 is important for the dendritic CKAMP44 distribution when overexpressed *in vivo*, (iv) the R/K domain truncation abolished AMPAR modulatory activity of CKAMP44, possibly due to the loss of CKAMP44/AMPAR interaction and (v) the L domain is more length rather than sequence sensitive for the AMPAR modulation of CKAM44.
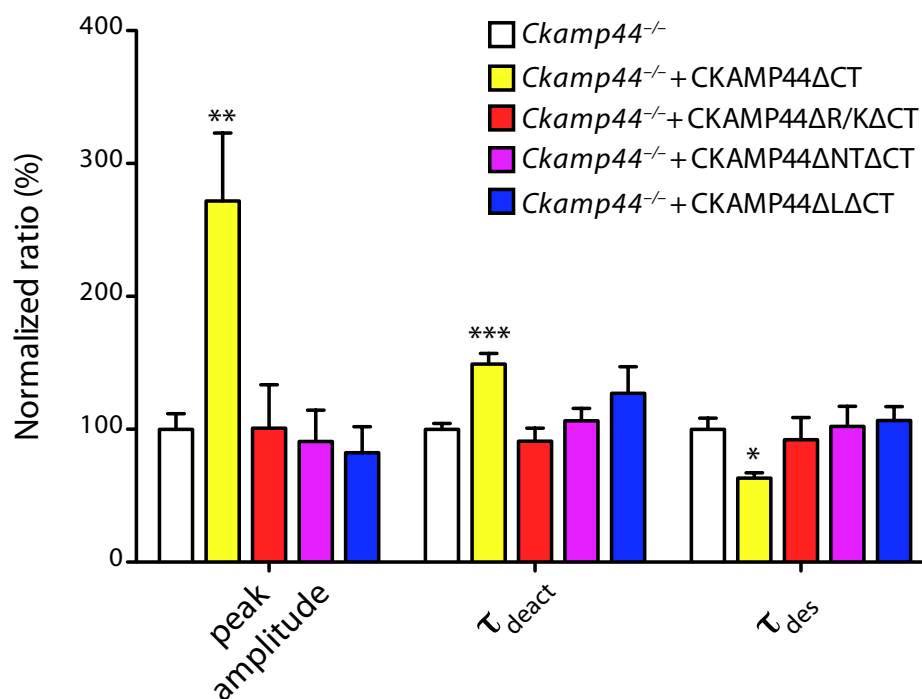
Fig. 19. Collective electrophysiological results obtained from CKAMP44 variant overexpressions in *Ckamp*44[-/-] mice. Only peak amplitude, deactivation (τ_{deact}) and desensitization (τ_{des}) kinetics are shown here (mean ± SEM) for four CKAMP44 variants. All values are normalized to that outside-out patches from neighboring *Ckamp*44[-/-] control neurons. Statistic analysis was performed by one-way ANOVA followed by Bonferroni's post-hoc comparison test. *P<0.05, **P<0.01, ***P<0.001. The original data were provided by Dr. J. von Engelhardt.
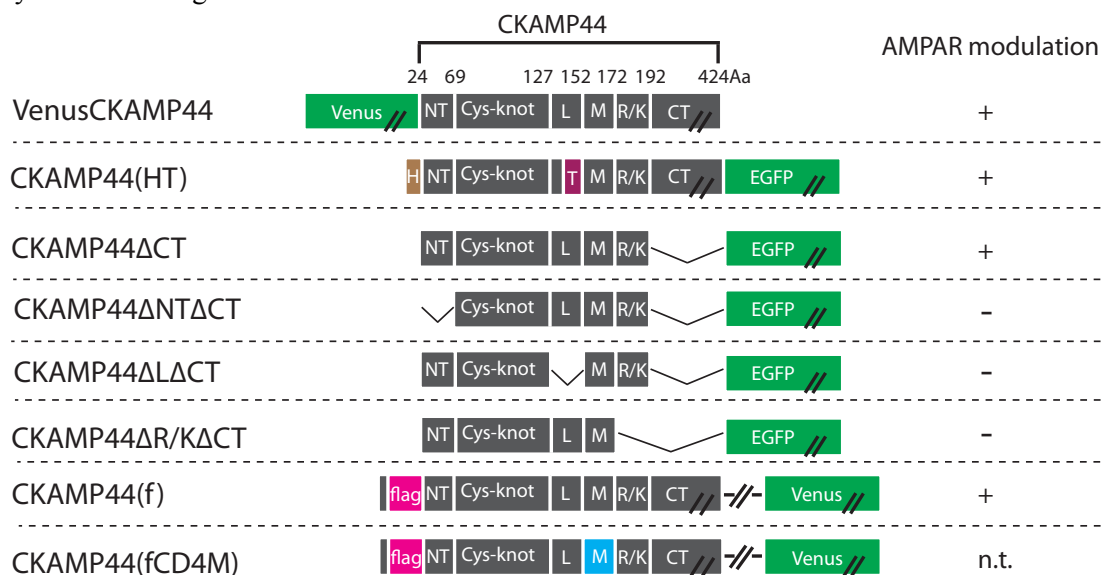
Fig. 20. Summary of AMPAR modulatory activity of different CKAMP44 variants *in vivo*. Extracellular domain is critically involved in AMPAR modulation. '+' and '−' represent positive and negative modulation of AMPARs, respectively, as demonstrated in electrophysiological recordings in acute brain slices of rAAV transduced DG granule cells of *Ckamp*44[-/-] mice. Symbols and constructs are given as in Fig. 11; n.t: not tested.

2.3. CKAMP44 disruption and AMPAR expression

2.3.1. AMPAR expression in the total membrane fraction

According to the electrophysiological data recently obtained by our collaborators (private communication with Dr. J. von Engelhardt, unpublished), CKAMP44 overexpression increases, while CKAMP44 depletion decreases functional synaptic and extrasynaptic AMPAR expression. To analyze whether the same result can be obtained at the molecular level, AMPAR expression level in the total membrane fractions was compared between $Ckamp44^{-/-}$ and wild-type mice by western blots, with four animals for each group. Surprisingly, the results showed that, compared to wild-type mice, $Ckamp44^{-/-}$ mice showed a 1.7 fold increase in GluA2 expression, and a trend in increased GluA1 levels, although not significantly (Fig. 21A). This result is unexpected and not consistent with the electrophysiological data. Possible explanations are that the overexpressed AMPARs are immature or non-functional or not efficiently targeted to the postsynaptic plasma membrane.

2.3.2. AMPAR maturation

In order to analyze whether the genetic disruption of CKAMP44 has an effect on AMPAR maturation, the glycosylation pattern of AMPARs was compared between $Ckamp44^{-/-}$ and wild-type mice using Endoglycosidase H (Endo H) digestion. It is known that AMPARs are N-glycosylated at their extracellular domains, and the degree of complexity of this posttranslational modification, as reflected by differential resistance against glycosidase digestion, is frequently used as an indicator for protein maturation (Hollmann *et al.*, 1994; Sans *et al.*, 2001). Like many other glycoproteins, intermediate immature AMPARs often contain higher degree of N-linked high-mannose carbohydrates, which are sensitive to Endo H (Sans *et al.*, 2001). Among all subunits, GluA2 is the most prominent one in Endo H sensitivity (Sans *et al.*, 2001). It has been reported that two other types of AMPAR modulatory proteins TARPs and CNIHs could change the glycosylation pattern of AMPARs (Herring *et al.*, 2013; Rouach *et al.*, 2005; Sumioka *et al.*, 2011; Tomita *et al.*, 2003). To find out if CKAMP44 has similar function in AMPAR glycosylation, we treated hippocampal homogenates from $Ckamp44^{-/-}$ and wild-type mice with Endo H, and PNGase F, which removes all N-type glycosylations, and can serve as a control for Endo H

sensitive glycoproteins. But no significant difference in the ratio of Endo H resistant to Endo H sensitive GluA2 was found between the two genotypes (Fig. 21B).
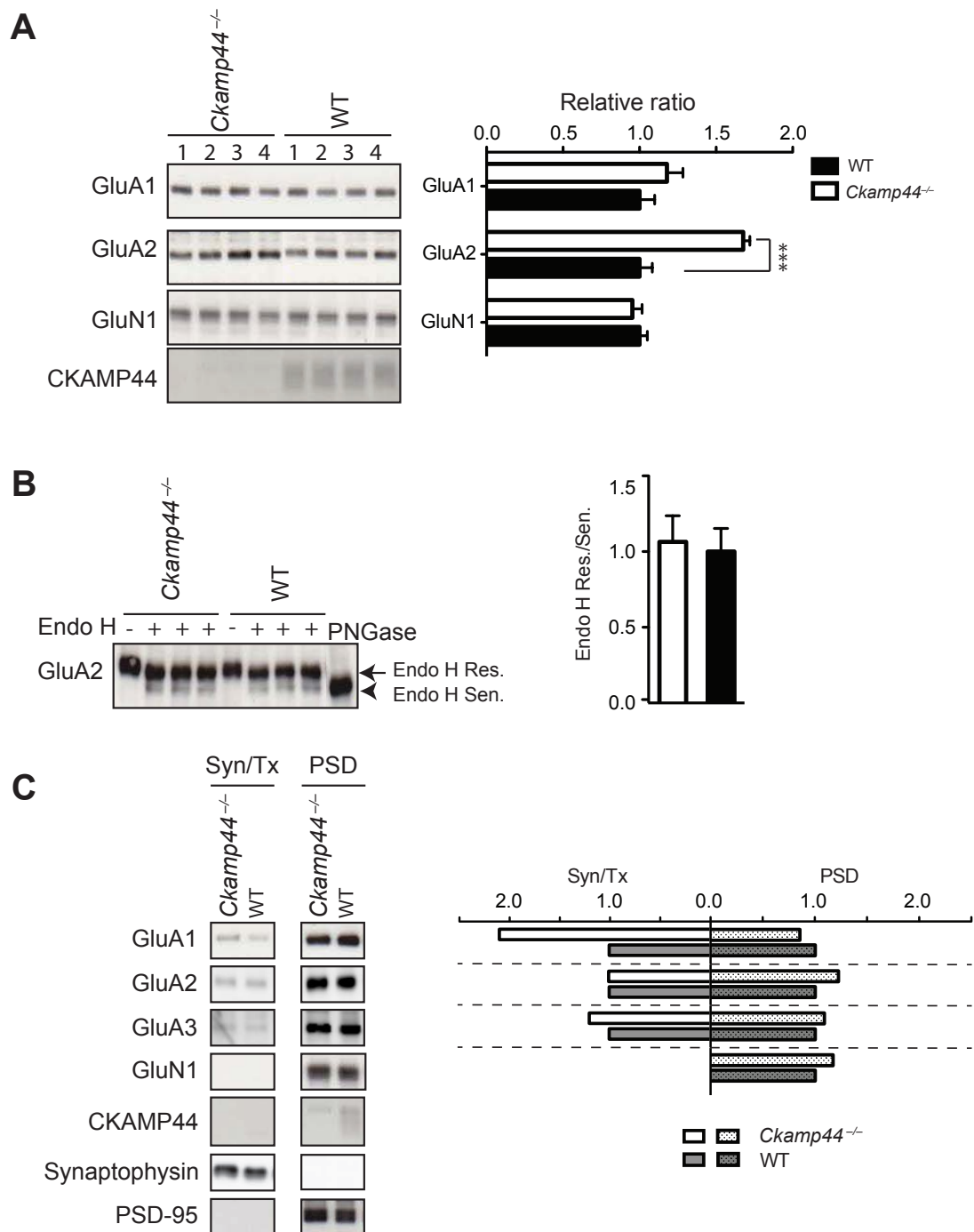
Fig. 21. CKAMP44 depletion increases AMPAR expression. (A) Immunoblot analysis of total hippocampal membrane fractions from four *Ckamp44*$^{-/-}$ and four wild-type mice, comparing the expression of AMPAR subunits GluA1 and GluA2 as well as NMDAR subunit GluN1. CKAMP44 antibody detection confirms the absence of CKAMP44 in *Ckamp44*$^{-/-}$ mice. Bar graph to the right represents the average expression of GluA1, GluA2 and GluN1 in *Ckamp44*$^{-/-}$ mice normalized to wild-type mice, showing a significant increase of GluA2 in *Ckamp44*$^{-/-}$ mice. **(B)** Enzymatic deglycosylation analysis of GluA2 in *Ckamp44*$^{-/-}$ and wild-type mice by Endo H treatment. Glycosylation is removed by unspecific N-glycosidase

PNGase F, shown in the last lane on the right for wild-type mice. Endo H resistant (Res.) and Endo H sensitive (Sen.) GluA2 are indicated by arrow and arrowhead, respectively. Statistic analysis on the right shows that there is no significant difference in the ratio of Endo H Res. to Endo H Sen. GluA2 between *Ckamp44*$^{-/-}$ and wild-type mice **(C)** Subcellular fractionation analysis of Triton-solubilized synaptosome (Syn/Tx) and postsynaptic density (PSD), representing extrasynaptic and synaptic fraction, respectively. An increase in the extrasynatic GluA1 was found in *Ckamp44*$^{-/-}$ mice, but no significant difference in the synaptic fraction was observed. Synatophysin serves as a control for extrasynaptic fraction, while PSD95 for PSD fraction. Syn/Trx: TritonX-100 solubilized synaptosome. PSD: postsynaptic density. Error bars represent SEM. ***P<0.001.

2.3.3. Extrasynaptic and synaptic expression of AMPARs

To investigate whether CKAMP44 has a differential effect on extrasynaptic and synaptic distribution of AMPARs like TARP γ-8 does (Rouach *et al.*, 2005), subcellular fractionation using sucrose gradient was performed for both *Ckamp44*$^{-/-}$ and wild-type mice. GluA1, GluA2, GluA3 and GluN1 were analyzed, and synaptophysin which is a synaptic vesicle glycoprotein specifically localized in presynapse was used as a TritonX-100 solubilized extrasynaptic marker (Syn/Tx). PSD-95 served as a specific postsynaptic marker. Our results showed that GluA1 in the Syn/Tx fraction in *Ckamp44*$^{-/-}$ mice was two-fold higher than that in wild-type mice, but no significant difference was observed in the PSD fraction (Fig. 21C).

In conclusion, western blot analysis of the total AMPAR expression showed that GluA2 was increased in *Ckamp44*$^{-/-}$ mice, which cannot be explained by a bigger pool of immature GluA2. There was a stronger increase in extrasynaptic than in synaptic GluA1. The western blot analysis represents AMPARs from both surface and intracellular AMPARs pool, and the electrophysiolgical observation was only from functional AMPARs expressed on the cell surface, which might explain the discrepancy between the two different methods. Surface AMPAR labeling using biotinylation assay on mouse hippocampal slices is required for analyzing CKAMP44 effect on surface AMPAR expression. Several trials were made for biotinylation, but failed to give any result due to technical problems.

2.4. CKAMP44 expression modulates neuronal morphogenesis

2.4.1. CKAMP44 studies in primary rat hippocampal neurons

Previous reports showed that many postsynaptic proteins are actively involved in regulating neuronal morphology, such as PSD95 (El-Husseini *et al.*, 2000), SHANK2 (Berkel *et al.*, 2012), SPAR (Pak *et al.*, 2001), etc. In the spine targeting analysis, I observed that the overexpression of VenusCKAMP44 increased spine density in rat primary neurons (see Fig. 14). Since CKAMP44 is preferentially expressed in spines, VenusCKAMP44 will also label spines above or below the dendritic shaft, which are not visible in control neurons with Venus overexpression. Therefore, to investigate whether CKAMP44 exerts any effect on neuronal morphology and spine morphogenesis, CKAMP44-IRES-Venus was used for CKAMP44 overexpression (10 DIV to 20 DIV by lipofectamine transfection). The green fluorescence protein Venus is able to outline neurons as well as label spines. Thus CKAMP44-IRES-Venus allows us to overexpress CKAMP44 and to visualize cells using soluble Venus.

Sholl analysis was employed to analyze dendritic branching, by placing the centroid of a soma in the centroid of series concentric circles and counting the number of dendrite intersections for concentric circles (Fig. 22A). The analysis of eight CKAMP44-IRES-Venus and ten Venus overexpressing neurons showed that the number of total intersections as well as dendritic branches 50 to 175 μm away from soma was significantly decreased by CKAMP44 overexpression compared to Venus control (Fig. 22B and 22C), demonstrating the role of CKAMP44 in regulating dendritic arborization.

To analyze spine volume and spine density, high resolution z-stack images of secondary or tertiary dendritic segments longer than 50 μm were taken, and were converted to single image by z-projection with maximum intensity. Spine volume was calculated by measuring green immunofluorescence intensity in spines over mean intensity in dendritic segments, and normalized to Venus expressed neurons. Spine density was calculated by manually counting the number of spines in dendritic segments with known length (Fig. 22A). The analysis of 10 dendritic segments and 930 spines from CKAMP44 overexpressing neurons as well as 23 dendritic segments and 2339 spines from Venus overexpressing neurons showed that CKAMP44 overexpression could significantly reduce spine volume by 16.8% (0.832 ± 0.011) and

increase spine density by 48.6% (11.87 ± 0.438 per 10 μm), when compared to Venus overexpressed control neurons (spine volume 1 ± 0.009, and spine density 7.989 ± 0.179 per 10 μm) (Fig. 22C).
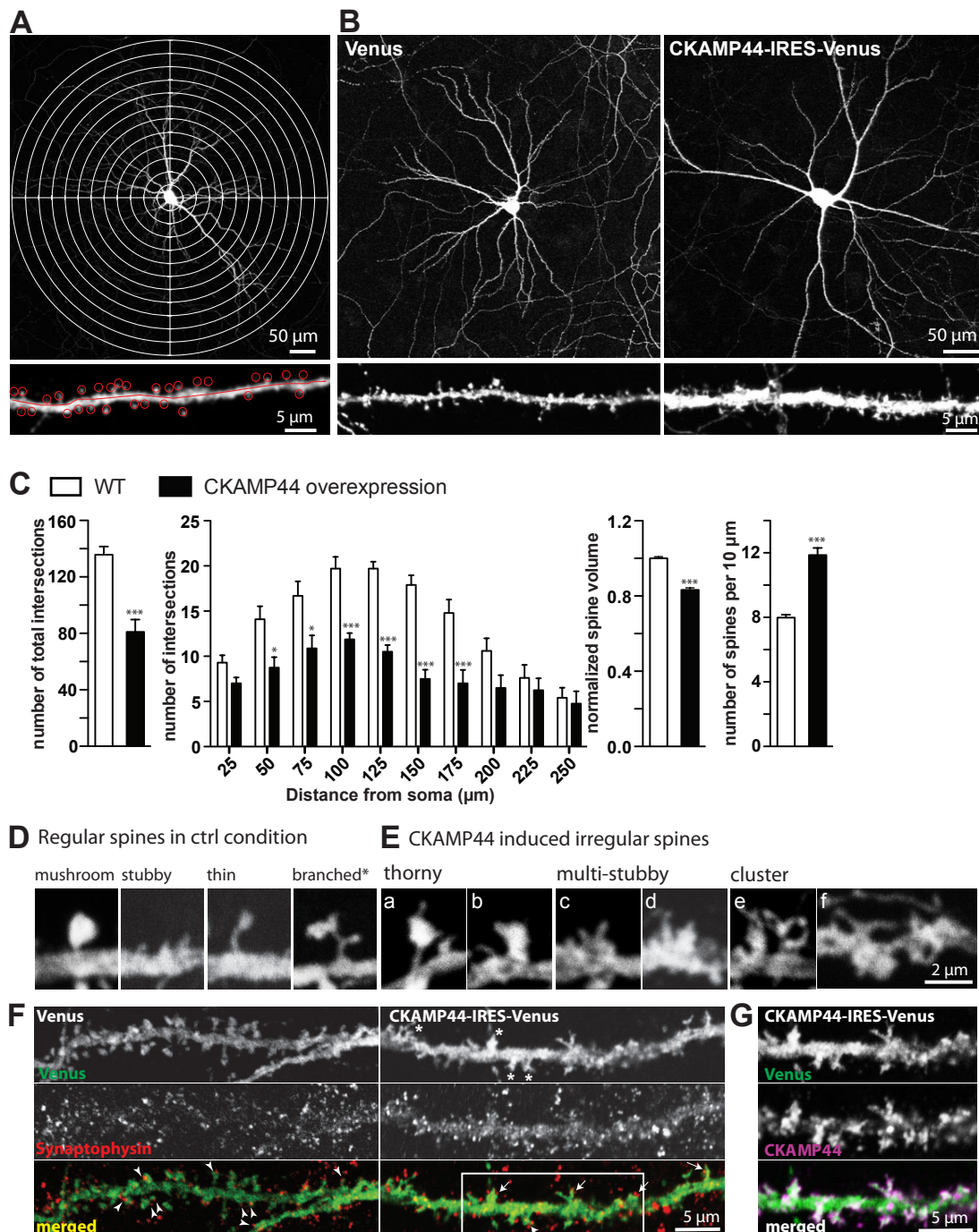
Fig. 22. CKAMP44 overexpression in rat primary neurons decreases dendritic arborization and spine volume and increases spine density. (A) Upper panel, example image of a primary neuron and superimposed ten concentric circles used for sholl analysis. The radius interval between circles is 25 μm per step; lower panel, example dendritic segment showing that spine density was calculated by counting spines (red circles) in a dendritic segment with known length (red line). **(B)** Representative rat neurons (upper panel) and dendritic segments (lower panel) transfected with Venus or CKAMP44-IRES-Venus

demonstrating that CKAMP44 overexpression could decrease dendritic arborization and increase spine density. Note that CKAMP44 also increases the total length as well as the thickness of dendritic branches. **(C)** Left to right, quantification of total dendritic arborization, dendritic distribution, spine density, and relative spine volume. The CKAMP44 overexpression group is compared with the wild-type group. (n=2; 8 neurons, 10 dendritic segments and 930 spines for CKAMP44-IRES-Venus overexpressing condition; 10 neurons, 23 dendritic segments and 2339 spines for Venus overexpressing condition). Total intersections, spine density and spine volume were analyzed by t-test. Dendritic arborizations were analyzed by two-way ANOVA followed by Bonferroni posttest. All values are shown as mean ± SEM. **P<0.01, ***P<0.001. **(D)** Example spines in control neurons transfected with Venus, including mushroom, stubby, thin and branched spines. *, the branched spine is having a mushroom spine on its leftside. **(E)** Example irregular spines induced by CKAMP44-IRES-Venus overexpression, such as thorny spine (a and b), multi-stubby spine (c and d) and cluster spine (e and f). **(F)** Dendrites from neurons transfected with Venus (left) and CKAMP44-IRES-Venus (right), doubled-stained for Venus (green) and presynaptic marker synaptophysin (red). Arrowheads in left images indicate spines contacting with single synaptophysin cluster, and arrows in right images point out spines opposing to multiple distinct synaptophysin clusters. Asterisks (*) in right images label irregular spines. **(G)** Co-immunostaining of GFP (green) and CKAMP44 (purple) of the dendritic area boxed in white in the merged image of F, demonstrating that CKAMP44 is localized in spines. Co-localized signal in merged image is in white.

In addition to spine volume and density, some changes in spine morphology in CKAMP44 overexpression neurons were also observed. In general, there are four types of commonly recognized spine types, including mushroom, thin, stubby and branched spines (Fig. 22D). In matured neuron culture, most of the spines are mushroom shaped with thin necks and well-defined spine heads, smooth in contour and globular in shape. Instead, spines in CKAMP44-IRES-Venus overexpressed neurons are not regular in shape and not smooth in the outline (Figs. 22E, F). Similar irregular spines were also reported before by overexpressing some postsynaptic proteins. For example, overexpressing SPAR, a Rap-specific GTPase-activating protein, could induce "thorny spines" with sharp projections or outgrowth and "multilobed spine" with multiple heads fused together at the top of a single neck (Pak et al., 2001). And overexpression of kalirin-7, a GDP/GTP exchange factor for Rac1, triggers the generation of spines with divergent morphology, including massive lamellipodia, long and highly branched, short and highly branched small and very densely placed (Penzes et al., 2001). By referring to the above mentioned reports, I generalize those irregular spines to three major groups, "thorny spines" with sharp projections (Fig. 22Ea, Eb), "multi-stubby spines" with several stubby spines on top of lamellipodia like structure (Figs. 22Ec, Ed), and "cluster spines" crowed with

several spines that are not well separated from each other (Fig. 22Ee, Ef). Immunostaining of CKAMP44-IRES-Venus transfected neurons showed that CKAMP44 was primarily expressed in spines (Fig. 22F and G). Moreover, many of the spines were in contact with multiple synaptophysin clusters, indicating that overexpression of CKAMP44 induced the formation of multiple synapses on individual dendritic spines (arrows in Fig. 22F).

Therefore, our studies in primary rat hippocampal neurons showed that CKAMP44 overexpression could significantly decrease dendritic arborization and spine volume, increase spine density and change spine morphology.

2.4.2. CKAMP44 studies in primary mouse hippocampal neurons

The rat primary hippocampal neuron studies indicate that CKAMP44 overexpression could modulate neuronal morphogenesis. We next asked whether CKAMP44 knock-out also has an effect on neuron morphology. Therefore, primary mouse hippocampal neurons from *Ckamp44*$^{-/-}$ and wild-type mice (WT) were prepared and Venus transfections were performed for cell labeling. To bidirectional investigate the correlation between neuronal morphology and CKAMP44 expression, CKAMP44-IRES-Venus was overexpressed in WT primary neurons by lipofectamine transfections.

The mouse primary neuron culture was very healthy after plating, but they appeared to be quite vulnerable for long time exogenous gene expression between 10 to 20 days in vitro (DIV). Therefore, the transfection of mouse primary neurons was performed at DIV18, and the neurons were analyzed already two days after the transfection at DIV20.

Quantitative analysis of the structure of dendritic arbor using Sholl analysis from seven *Ckamp44*$^{-/-}$ neurons (*Ckamp44*$^{-/-}$ + Venus), fifteen wild-type neurons (WT + Venus) and eleven CKAMP44 overexpressing neurons (WT + CKAMP44-IRES-Venus) demonstrated that *Ckamp44*$^{-/-}$ neurons exhibited an overall increase in the number of total intersections, and showed more dendritic intersections between 75 and 150 μm away from soma when compared to neurons of wild-type mice (Fig. 23). CKAMP44 overexpressing neurons, on the other hand, didn't show any significant difference in dendritic arborization compared to wild-type neurons.

For the quantification of spine volume, 515, 1945 and 650 spines were analyzed for CKAMP44 KO, wildtype and CKAMP44 overexpression neurons, respectively. For the assessment of spine density, 13, 19 and 9 dendritic segments were analyzed for CKAMP44 KO, wildtype and CKAMP44 overexpression neurons, respectively. The result indicated that CKAMP44 KO resulted in 126% increase in spine volume (2.26 ± 0.15) and 18% decrease in spine density (7.32 ± 0.28 per 10 μm) when compared to wild-type neurons (1 ± 0.04 relative spine volume and 8.91 ± 0.38 per 10 μm spine density). Although a trend towards an increase of spine density in CKAMP44 overexpressing neurons (9.71 ± 0.24 per 10 μm) was observed, the difference was not significant. No difference was observed for CKAMP44 overexpression neurons in spine volume (1.03 ± 0.03) (Fig. 23). Thus, compared to neurons of wild-type mice, the depletion of CKAMP44 was correlated with a decrease in spine density and an increase in spine volume, while CKAMP44 overexpression, on the other hand, did not exert a strong effect on spine density and spine volume.

Taken together, the mouse primary hippocampal neuron studies revealed that deletion of CKAMP44 increases dendritic arborization and spine volume and decreases spine density.

Overexpressing CKAMP44 in mouse neurons failed to have significant effect on neuronal morphology as it was observed in primary hippocampal neurons of rats. This was most likely due to the different time windows used for the transfection of mouse and rat primary neurons (DIV18-20 and DIV10-20 for mouse and rat neurons, respectively). There are two explanations possible, one is that the overexpression of CKAMP44 was not long enough to exert CKAMP44 function, and the other reason might be that neurons have already finished their differentiation at DIV18, and CKAMP44 cannot modulate the morphology of adult neurons.

In conclusion, results from the primary neuron culture studies suggested that, in addition to AMPAR modulation, CKAMP44 modulates dendritic arborization, spine number and spine morphology.
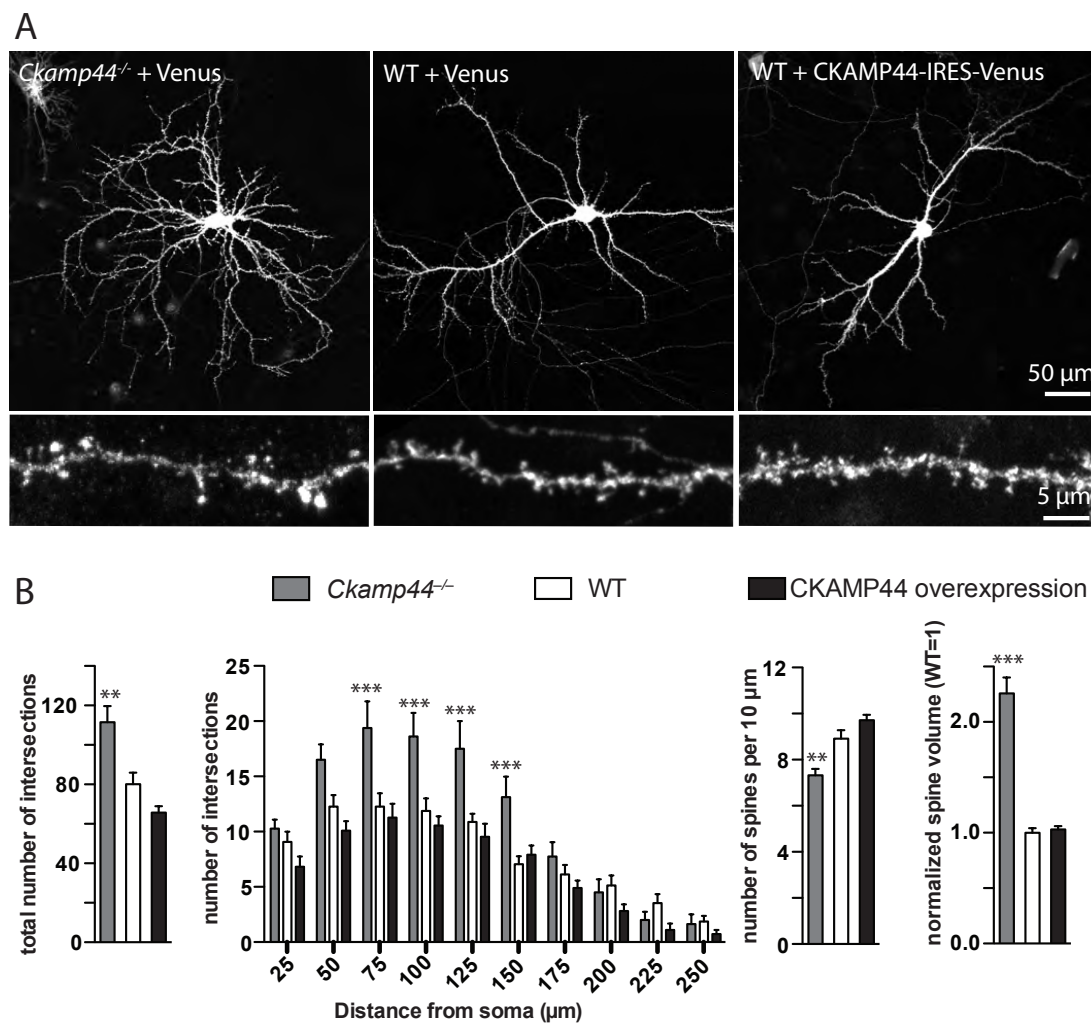
Fig. 23. CKAMP44 depletion in mouse primary hippocampal neurons increases dendritic arborization and spine volume, but decreases spine density. (A) Representative Venus transfected neurons (upper panel) and dendritic segments (lower panel) demonstrating that the loss of CKAMP44 (*Ckamp44*−/−+Venus) increases the complexity of the dendritic arbor, increases spine volume and decreases spine density. The overexpression of CKAMP44 (WT+CKAMP44-IRES-Venus), however, does not change those neuronal features, but can induce irregular spine shape. **(B)** Left to right, quantification analysis of the total number of intersections, dendritic distributions, spine volume and spine density, by using one-way ANOVA and two-way ANOVA (for dendritic distribution). *Ckamp44*−/−+Venus and WT+CKAMP44-IRES-Venus neurons were compared to WT+Venus neurons. All values are shown as mean ± SEM. **$P<0.01$, ***$P<0.001$. (n=2; 7 neurons, 13 dendritic segments and 515 spines for *Ckamp44*−/−+Venus condition; 15 neurons, 19 dendritic segments and 1945 spines for WT+Venus condition; 11 neurons, 9 dendritic segments and 650 spines for WT+CKAMP44-IRES-Venus condition.)

3. Discussion

CKAMP44 is an endogenous AMPAR auxiliary protein which regulates many aspects of AMPAR functions, including AMPAR trafficking and the electrophysiological properties of AMPARs. The previous analysis of CKAMP44 was mainly focused on electrophysiological studies. This study investigated different CKAMP44 domain functions, analyzed AMPAR expression in hippocampal neurons of $Ckamp44^{-/-}$ mice and described new functions of CKAMP44 in neuronal morphogenesis, by using western-blot, co-immunoprecipitation, immunocytochemistry, immunohistochemistry and electrophysiological recordings.

In the presented study, i) specific domains responsible for CKAMP44/AMPAR interaction, AMPAR modulation and subcellular distribution of CKAMP44 were identified, ii) the expression of AMPAR subunits in $Ckamp44^{-/-}$ and wild-type mice was compared and iii) further functions of CKAMP44 in modulating neuronal morphogenesis were described. Our results provide the molecular basis for understanding the biological functions of the postsynaptic protein CKAMP44 and give novel insights into the native AMPAR complex. We propose that CKAMP44 plays an important role in neuronal function by regulating multiple aspects of synaptic plasticity.

3.1. Domain mapping

In this study, a series domain deletions of CKAMP44 identified CKAMP44 domains involved in CKAMP44/AMPAR interaction, AMPAR modulation, and CKAMP44's subcellular distribution (Fig. 24). Our results showed that the extracellular cysteine-rich domain is essential for AMPAR modulation, the R/K domain is involved in CKAMP44/AMPAR interaction as well as in subcellular distribution of CKAMP44 and the C-terminal domain is required for postsynaptic localization.
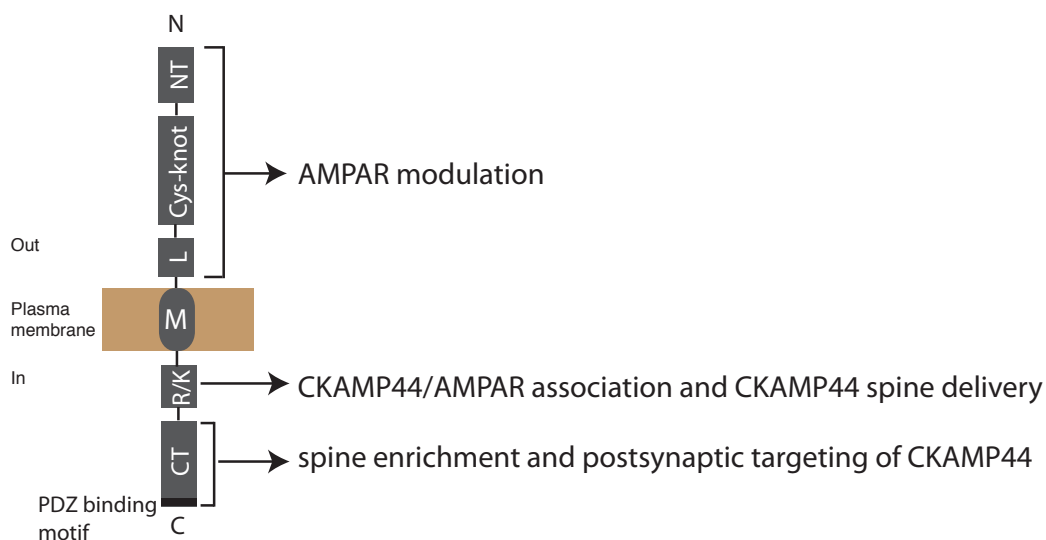
Fig. 24. Schematic representation of different CKAMP44 protein domain functions. By overexpressing a series of recombinant CKAMP44 deletion mutants, the functions of CKAMP44 protein domains were identified. N and C, amino and carboxyl terminal, respectively; NT and CT, N-terminal and C-terminal domain, respectively; Cys-knot, cystine-knot domain; L, linker domain; M, membrane spanning segment; R/K, arginine (R) and lysine (K) rich domain;

3.1.1. Extracellular domain

According to our Co-IP experiments, the extracellular Cys-knot containing domain is not important for the tight CKAMP44/AMPAR association, but it is required for AMPAR modulation as evidenced by electrophysiological recordings, since the removal of the two Cys-knot flanking extracellular segments NT and L didn't influence CKAMP44/AMPAR association, but failed to rescue impaired AMPAR current in *Ckamp44*$^{-/-}$ DG granule neurons. In addition, our collaborators showed that disrupting the disulfide bond formation by three single cysteine mutations disabled the CKAMP44 modulatory activity (Dr. J. von Engelhardt, unpublished), indicating that the Cys-knot is indispensible for CKAMP44 modulation of AMPARs. Similar results are reported for TARPs, which also interact with and modulate AMPARs using the extracellular domain Ex1 (Tomita *et al.*, 2005a; Turetsky *et al.*, 2005).

The CKAMP44 extracellular domain is unique in having eight cysteines (Fig. 11). Many cysteine-rich neurotoxins, e.g. ω-conotoxin (Heinemann and Leipold, 2007) and bungarotoxin (Mebs *et al.*, 1972; Narita *et al.*, 1972), are specific blockers for voltage-gated calcium channels and nicotinic acetylcholine receptors (nAchRs), and contain six and ten cysteines, respectively. Notably, bungarotoxin shares exactly

the same cysteine-pattern and high sequence homology with lynx1, an endogenous GPI-anchored membrane protein in the central nervous system (Ibanez-Tallon *et al.*, 2002; Miwa *et al.*, 1999; Miwa *et al.*, 2006). Lynx1 functions as an nAchRs modulator in a similar manner as bungarotoxin does (Miwa *et al.*, 1999). Therefore, lynx1 is described as an endogenous prototoxin, and gives rise to the initial idea for "tethered toxin" (t-toxin) by anchoring exogenous toxins on the cell surface to achieve specific blocking of ion channels and receptors (Auer *et al.*, 2010; Ibanez-Tallon *et al.*, 2004). In this configuration, the distance between the toxin and the membrane anchor is important for the function of the membrane-tethered neuronal toxins. This model explains our finding that the CKAMP44 L domain is required for AMPAR modulation and that the L domain can be replaced by heterologous amino acid residues without interfering with the function of CKAMP44.

Therefore, CKAMP44 might also function as an endogenous prototoxin. Although no naturally occurring toxins with high sequence similarity are identified, the first six cysteines of CKAMP44 and the six cysteines of ω-conotoxin share a very similar pattern (von Engelhardt *et al.*, 2010). In order to investigate whether the cysteine-rich extracellular domain (CKAMP44-Ex) itself can function as an AMPAR modulator, we expressed the CKAMP44-Ex in *E. coli*. The purified recombinant protein, however, failed to modulate AMPAR-mediated currents. Possible reasons are i) the correct folding of the extracellular domain requires the assistance of other domains; ii) the binding affinity of the extracellular domain to AMPARs is too low. Our following Co-IP result favors the later explanation, since it showed that CKAMP44/AMPAR association is mainly mediated by R/K domain.

In addition to its role in AMPAR modulation, the CKAMP44 extracellular domain seems to be involved in CKAMP44 spine targeting, since the removal of either the NT or the L segment dramatically impaired the ability of CKAMP44 to be expressed in spines of transfected primary neurons. This finding is distracting the idea that the AMPAR interaction via the R/K domain is sufficient for CKAMP44 spine targeting (see below). It indicates that several discontinuous domains are involved in CKAMP44 expression in spines. However, further experiments are required to confirm the function of the extracellular domain in CKAMP44 spine targeting.

3.1.2. R/K domain

3.1.2.1. R/K domain function in AMPAR binding

The finding that R/K domain is important for CKAMP44/AMPAR association is surprising, since this domain is short, and does not have a well-defined secondary structure according to the modeling using the HMM-based protein structure prediction, SAM-T08 (data not shown). As described in the result section 2.2, the R/K domain is a 20 residue stretch after the membrane-spanning domain, and is enriched in positively charged amino acids R and K. Similar R/K domain is also found in other Shisa family members, and thought to help determine the topology of Shisa proteins based on the "positive inside" rule (Pei and Grishin, 2012; von Heijne, 1989). However, in CKAMPs, the R/K domain is extended and more pronounced than that in Shisa 1-5 (Fig. 4), indicating that the R/K domain in CKAMPs has additional function.

A R/K rich region seems also to be involved in the TARP/AMPAR interaction (Tomita *et al.*, 2004). It can be found in C-terminal cytosolic domain of type I TARPs (γ-2, γ-3, γ-4 and γ-8) but not in type II TARPs (γ-5 and γ-7, which selectively modulate certain subgroups of AMPARs) or non-TARPs (γ1 and γ6). This provides further support to the finding that the R/K rich region is a specific motif that directly mediates the physical interaction of AMPARs to TARPs and CKAMP44.

3.1.2.2. R/K domain function in CKAMP44 subcellular expression

CKAMP44 is postsynaptically localized together with AMPARs and PSD95 (von Engelhardt *et al.*, 2010). The presented data shows that in transfected primary neurons, the removal of R/K domain abolished CKAMP44 spine targeting, and had a dominant negative effect on the expression of GluA1. In mouse hippocampi, the R/K domain deleted CKAMP44 (CKAMP44ΔNTΔCT) showed somatic expression and a loss in dendrite expression, suggesting that the R/K domain is critically involved in correct subcellular distribution of CKAMP44 both *in vitro* and *in vivo*.

3.1.3. Intracellular C-terminal (CT) domain

The CT domain is not important for AMPAR binding or for AMPAR modulation, but we found that the CT domain is necessary for the localization of CKAMP44 at spine heads since the CT truncated CKAMP44 could not colocalize with GluA1 at spine

heads, and showed an even distribution in dendritic shafts and spines. The CT domain has a PDZ type II ligand motif at its C-terminus, which might mediate CKAMP44-PSD95 interaction, and enable clustering of CKAMP44 at the postsynaptic density. Therefore, the failure in spine head targeting of CKAMP44ΔCT is most likely due to the loss of the PDZ binding motif at the C-terminus.

3.2. AMPAR expression in the hippocampi of *Ckamp44*$^{-/-}$ mice

In this study, our comparative immunoblot analysis showed that the expression level of GluA2, but not GluA1 or GluN1, was altered in the hippocampi of *Ckamp44*$^{-/-}$ mice. This is in contrast to the results obtained from other AMPAR auxiliary protein knockout experiments, which frequently showed reduced levels of both GluA1 and GluA2. For example, genetic disruption of γ-8 in hippocampus substantially reduced GluA1 and GluA2/3 by 85% (Rouach *et al.*, 2005), and CNIH2 knock-out mice exhibited mild decrease of GluA1 and GluA2 (15% reduction) in hippocampus (Herring *et al.*, 2013).

However, similar to *Ckamp44*$^{-/-}$ mice, TARP γ-2$^{-/-}$ stargazer mice have a mild disruption in total AMPAR level, but show a strong reduction of functional AMPARs at the cell surface (Hashimoto *et al.*, 1999), indicating the importance of TARP γ-2 in regulating AMPAR trafficking. Similarly, CNIH2 knock-out mice (*NexCnih2*$^{-/-}$) also exhibit increased immature AMPARs presumably retained in the ER in the absence of CNIH2 (Herring *et al.*, 2013). We therefore examined AMPAR maturation in *Ckamp44*$^{-/-}$ mice. Surface biotinylation assay in mouse hippocampal slices can directly detect the proportion of functional AMPARs on the cell surface. Several trails carried out for surface biotinylation of AMPARs ended up with either insufficient surface labeling or contamination from cytosolic proteins. So we used the glycosylation of AMPAR subunits to analyze the maturation of AMPARs. The result showed that the glycosylation of GluA2 in *Ckamp44*$^{-/-}$ and wild-type mice is similar, indicating the maturation of AMPARs is comparable between *Ckamp44*$^{-/-}$ and wild-type mice.

After the induction of synaptic plasticity, perisynaptic AMPARs are thought to diffuse into postsynaptic membrane, contributing to the enhancement of synaptic transmission. It was reported that TARP γ-8 preferentially regulates extrasynaptic

AMPARs (Rouach *et al.*, 2005). To find out if CKAMP44 also differentially modulates perisynaptic and postsynaptic AMPARs, subcellular fractionation was performed with brain extracts from *Ckamp44*$^{-/-}$ and wild-type mice. First, in extrasynaptic (Syn/Trx) fractions, increased GluA1 expression in *Ckamp44*$^{-/-}$ mice was observed. Second, in the postsynaptic density (PSD) fraction, no obvious differences were found for GluA1, GluA2, GluA3 and GluN1 between *Ckamp44*$^{-/-}$ and wild-type mice. However, for the subcellular fractionation experiments, the n number is low (four pooled brains of each genotype), which might lead to high experimental error. But at least our experiments can exclude a massive reduction of either extrasyanptic or synaptic AMPARs expression in the hippocampi of *Ckamp44*$^{-/-}$ mice. Instead, our analysis of AMPAR subunit expression in *Ckamp44*$^{-/-}$ mice suggested that CKAMP44 removal leads to increased expression of GluA2 and enhanced level of extrasynaptic GluA1, but has no influence on AMPAR maturation.

Thus, as indicated by *Ckamp44*$^{-/-}$ mice, CKAMP44 seems not to be essential for the normal expression and maturation of AMPAR subunits, compared to other AMPAR auxiliary proteins (Chen *et al.*, 2000; Herring *et al.*, 2013; Rouach *et al.*, 2005). However, compensation mechanisms by other CKAMP family members or other AMPAR auxiliary proteins in *Ckamp44*$^{-/-}$ mice cannot be excluded.

3.3. CKAMP44 modulates neuronal morphology

In addition to AMPAR modulation, we observed that CKAMP44 also modulates neuronal morphogenesis. Our data showed that overexpression of CKAMP44 in rat primary neurons decreased dendritic arborization and spine volume, and increased spine density. CKAMP44 downregulation showed the opposite effect. Moreover, overexpression of CKAMP44 was correlated with irregular spine shapes with more complex morphology and multiple synapses at single spines.

The currently proposed model for dendritic and spine morphogenesis is the dynamic regulation of the cytoskeleton (Matsuzaki *et al.*, 2004; Nagerl *et al.*, 2004; Okamoto *et al.*, 2004). Dendritic trees and spines are undergoing dynamic cytoskeleton-dependent changes in size and shape in response to neuronal activities (Fischer *et al.*, 1998; Matsuzaki *et al.*, 2004; Nagerl *et al.*, 2004), and are believed to be regulated by an interplay between an intrinsic genetic program, extrinsic factors,

and neuronal activity (Parrish *et al.*, 2007). What are the signaling pathways that link CKAMP44 to the regulation of cytoskeleton?

3.3.1. AMPAR and spine morphogenesis

As mentioned before, CKAMP44 modulates AMPAR gating properties, and recently our collaborators showed that CKAMP44 promotes AMPAR surface expression (Dr. J. von Engelhardt, unpublished). Therefore, we asked: "whether CKAMP44 modulation in neuronal morphology is indirectly mediated by increased AMPAR expression which triggers downstream pathways related to cytoskeleton regulation?" It was reported that overexpression of GluA2 subunit could increase spine density as well as spine size, and GluA2 downregulation could inhibit spine morphogenesis, possibly through NTD domain interaction with N-cadherin, but with unknown downstream signaling pathway (Passafaro *et al.*, 2003). Additionally, GluA1 subunit was also implicated in spine morphogenesis, since mutant GluA1 with deficiency in phosphorylation at one functionally-relevant site does not enter synapses in response to LTP stimuli, and blocks LTP-induced spine enlargement (Kopec *et al.*, 2007). The same study also showed that C-terminal domain of GluA1 alone is driven to spines during LTP induction, and is sufficient to induce spine enlargement, indicating that GluA1 could directly interact with intracellular signaling to induce appropriate cytoskeleton changes.

However, the detailed signaling pathway that link AMPAR and spine morphogenesis is poorly understood. A big step that might solve this puzzle is the report that guanine nucleotide exchange factor (GEF) kalirin-7 (Kal7) binds to AMPAR, enhances AMPAR-mediated synaptic transmission and promotes spine growth by activating small GTPase Rac1, which in turn regulates the actin cytoskeleton (Xie *et al.*, 2007). However, this report suggests that Kal7 regulates AMPAR trafficking and stabilization at spines, rather than AMPARs regulates Kal7, and AMPAR enrichment is a parallel event with spine enlargement. Although other AMPAR interacting partners such as 4.1N and SAP97 which promote AMPAR surface expression and AMPAR synaptic trafficking were reported to play a role in modulating spine morphogenesis (Li *et al.*, 2007; Rumbaugh *et al.*, 2003), there is no evidence showing a direct link between AMPAR trafficking and spine morphogenesis via these two proteins.

Therefore, it still remains to be resolved whether enhanced AMPAR surface expression and AMPAR synaptic trafficking is responsible for spine morphogenesis or whether these two events are both consequences of two different intracellular signal transductions. Similarly, it is difficult to predict whether CKAMP44 modulation of AMPARs and spine morphogenesis are in an upstream and downstream relationship or whether they are two different outputs of the same or different pathways.

Interestingly, Kal7 triggers irregular spine morphology, such as massive lamellipodia, small and very densely placed spines (Penzes *et al.*, 2001), very similar to what can be observed by CKAMP44 overexpression. As mentioned above, Kal7 also modulate AMPAR synaptic trafficking and stabilization (Xie *et al.*, 2007). Kal7 is also postsynaptically localized, providing the chance to physically interact with CKAMP44 (Peitz *et al.*, 2002). It seems like Kal7 builds a bridge between spine morphogenesis and AMPAR modulation observed for CKAMP44. Therefore, Kal7 is one possible candidate that transmits CKAMP44 signal, and induces the regulation of spine morphogenesis as well as AMPAR surface expression.

3.3.2. Does CKAMP44 preserve the function of Shisa1/2?

CKAMP44 belongs to the Shisa family (Pei and Grishin, 2012), and several Shisa family members were described as antagonists for Wnt and FGF signaling by retaining Fz and FGFR in the ER and preventing the maturation of these two receptors, and knock-down of Shisa1 inhibits head formation (Shisa1) and depletion of Shisa2 disrupts segmental patterning during development (Furushima *et al.*, 2007; Nagano *et al.*, 2006; Yamamoto *et al.*, 2005). On the other hand, Wnt signaling was also reported to play a key role in the formation and regulation of neuronal circuits, by controlling neuronal differentiation (Hall *et al.*, 2000; Packard *et al.*, 2002), axon outgrowth and guidance (Hall *et al.*, 2000), dendrite development (Rosso *et al.*, 2005), synapse formation (Ahmad-Annuar *et al.*, 2006), and neuronal plasticity (Chen *et al.*, 2006; Lim *et al.*, 2010). There are three major branches of Wnt signaling (Rosso and Inestrosa, 2013), including canonical pathway by activating β-catenin and initiating gene tanscription, planar cell polarity pathway (PCP) by activating Rho-GTPases and JNK and triggering cytoskeleton remodeling, as well as Ca^{2+} pathway through the activation of CaMKII and PKC for gene transcription. Interestingly, Kal7 regulates spine morphogenesis through Rac1 signaling, which is one of the Rho-

GTPase family members (Penzes *et al.*, 2001). Therefore, it is possible that CKAMP44 retains the conserved function of Shisa1 and 2 by regulating Wnt signaling, in particular the PCP pathway, and thus achieves the modulation of dendritic arborization and spine morphogenesis.

3.4. Outlook

The study of CKAMP44, one of the AMPAR auxiliary proteins, has a putative relevance for the therapeutic pharmacology. It was reported that the dysfunction of AMPARs are related to neurological and psychiatric disorders (Rogers *et al.*, 1994; Soundarapandian *et al.*, 2005; Talos *et al.*, 2006a; Talos *et al.*, 2006b; Wu *et al.*, 2007). Thus, the CKAMP44-AMPAR interaction can be a potential therapeutic target for AMPAR-related diseases. The identification of different CKAMP44 domains involved in AMPAR binding and regulation, thus, provides the molecular basis for the regulation of CKAMP44-AMPAR interaction in the future.

The finding that CKAMP44 modulates neuronal morphogenesis opens a new perspective concerning the function of CKAMP44 in the plasticity of the central nervous system. Therefore, it might be of interest to determine which intracellular signaling pathways mediate CKAMP44 induced neuronal morphogenesis, and whether this modulation is AMPAR dependent. In particular, the Kal7 activated small GTPase Rac1 signaling pathways are promising candidates for further analysis in CKAMP44 deficient and overexpressing mice.

4. Materials and methods

4.1. Basic molecular biology

4.1.1. Molecular cloning

All standard molecular cloning methods, including PCR techniques, Restriction digestion, ligation, transformation of competent *E. coli* cells, bacteria culture, and plasmid preparation, were derived from classical published protocols (Ausubel *et al.*, 2000; Sambrook *et al.*, 2001). All pET plasmids for expressing various fluorescent proteins and CKAMPs Cysknot protein were modified from pET C6His KanR-SFGFP. The genes were first amplified from existing plasmids containing the corresponding genes and then inserted as NdeI-BamHI fragments into pET C6His KanR-SFGFP. All pET32a plasmids for expressing CKAMPs Ex were generated by inserting target genes into the multiple cloning sites of pET32a vector using NcoI and XhoI. For CKAMP44 domain mapping studies in eukaryotic system, plasmids expressing CKAMP44 truncations were modified from pAAV-syn-CKAMP44ΔCT-EGFP (Dr. V. Mack) by replacing CKAMP44ΔCT gene with the genes expressing other CKAMP44 truncations. To generate pAAV-syn-CKAMP44(fCD4M)-IRES-Venus, a StuI site was introduced into the C terminal of CKAMP44 in pAAV-syn-CKAMP44-IRES-Venus construct (von Engelhardt *et al.*, 2010), and synthesized CKAMP44N-CD4M (Genscript, USA) gene fragment was inserted into mutated pAAV-syn-CKAMP44-IRES-Venus plasmid by BamHI and StuI. All plasmid constructs were confirmed by DNA sequencing in GATC Biotech (Konstanz).

4.1.2. Western-blot

Protein samples were loaded on SDS-PAGE, and then transferred to 0.45 μm nitrocellulose membranes in blotting buffer (25 mM Tris, 200 mM Glycine, 20% Methanol in H_2O) at 120 V and 400 mA at RT for 1.5 h with icebox or at 30 V and 90 mA for overnight. Membrane was later blocked with blocking buffer (5% BSA in TBST) at RT for 1 h, probed by primary antibody at RT for 2 h or 4 °C for overnight, and incubated in HRP-conjugated secondary antibody at RT for 1 h and 4 to 6 times wash in TBST. Western-blots were developed by ECL kit (GE healthcare) and chemiluminescence was detected either by CCD camera equipped in Fuji-Las-3000 system or by imaging film (GE Healthcare) in dark room.

4.1.3. Immunocytochemistry and immunohistochemistry

Transfected neurons were first fixed by 4% paraformaldehyde (PFA)/PBS, pH 7.5 at 37 °C for 10 min, and subsequently washed by PBS for 3 times. Vibratome-sectioned brain slices were selected and placed in 24 well plate with one slice per well. Staining protocol is similar for cultured neurons and brain slices. Cells or brain slices were blocked and permeabilized by blocking buffer (1% BSA, 5% NGS, 0.5% Triton X-100, PBS, pH 7.5) at room temperature for 1 h, followed by incubation in appropriate primary antibodies (prepared in blocking buffer) for overnight at 4 °C for cultured neurons and at room temperature for brain slices. The next day, cells or brain slices were washed by PBS for four times, and then stained by fluorescence-coupled secondary antibodies for 1 h at room temperature, followed by four times PBS and one time 10 mM Tris buffer (pH 7.5) wash. Coverslips bearing neuron cells or glass slides with brain sections on top were dehydrated on tissue paper and mounted afterwards using Vectorshield H1000. Primary antibodies and their dilution used in this study are listed as follows: rabbit α-GluA1 (Millipore) 1:1,000, mouse α-NeuN (Chemicon) 1:1,000, mouse α-FLAG (Sigma-Aldrich) 1:500, rabbit α-CKAMP44 1:1,000, mouse α-synaptophysin 1:4,000, mouse α-PSD95 1:5,000, chicken α-GFP 1:4,000. Secondary fluorescence antibodies used in this study are FITC, Cy3 or Cy5 conjugated anti-chicken, anti-mouse or anti-rabbit (1:400 dilution) (Jackson Immuno Research).

4.2. Prokaryotic protein expression, purification and characterization

4.2.1. HTNCre expression and purification from *E. coli*

HTNCre expression plasmid (Plasmid 13763: pTriEx-HTNC from Addgene) was retransformed into BL21(DE3)placI *E. coli* strain (Novagen), and the protein expression was performed as previously described (Peitz *et al.*, 2002). Briefly, single colonies were picked and inoculated in 3 ml LB medium supplemented with 0.5% glucose (v/v) with shaking (140 rpm) for overnight at 37 °C. The next day, the densely grown overnight culture was transferred to fresh TB medium plus 0.5% glucose using 1:50 ratio, and let grow in the same condition till OD_{600} reached 1.5. IPTG was then added to the *E. coli* culture to a final concentration of 0.5 mM, which was kept in culturing for another 1 h. Subsequently, the cells were harvested by

centrifugation at 5,000 rpm for 10 min at 4 °C, and the resulting pellet was resuspended in Lysis buffer (50 mM Na_2HPO_4, 5 mM Tris-HCl, pH 7.8) supplemented with lysozyme (1 mg/ml) and later with benzonase (25 U/ml). After incubation at RT for 30 min, the cell lysate was subjected to sonication, followed by tartaric salt buffer (50 mM NaH_2PO_4, 5 mM Tris-HCl, pH 7.82, 2 M L-Tartaric acid, disodium salt, and 20 mM Imidazol) addition, and 5 min incubation on ice. The supernatant of total lysate was loaded to pre-equilibrated Ni^{2+} column, and HTNCre was eluted by gradient increase of imidazole. HTNCre sample was further concentrated by dialyzing against Gylcerol Buffer (50% glycerol, 500 mM NaCl, 20 mM HEPES, pH 7.4) for twice at 4 °C. The concentrated HTNCre Glycerol stock was kept at -20 °C till use.

4.2.2. Functional test for HTNCre *in vitro*

To test HTNCre recombination activity at DNA level, linearized dsDNA bearing two parallel loxP sites was first generated by restriction digestion of pLoxPNeo-1 (Dr. R. Sprengel) and purified by gel separation and recovery. Linearized dsDNA was then incubated with HTNCre in Cre working buffer (500 mM Tris-HCl pH 7.5, 100 mM $MgCl_2$, 1 mg/ml DNAse-free BSA, 10 mM PMSF) at 37 °C for 30 min, and loaded into DNA gel electrophoresis for evaluation. To test HTNCre recombination activity at cellular level, Cre reported cell line CV1/lacZ was plated onto 24 well plate, treated with different concentration of HTNCre on the next day, fixed by 4% PFA/PBS and stained by lacZ staining (50 ml staining buffer: 0.5 ml $K_3[Fe(CN)_6]$, 0.5 ml $K_4[Fe(CN)_6]\cdot 3H_2O$, 0.5 ml 0.2 M $MgCl_2$, 5 ml X-gal (20 mg/ml), 43.5 ml PBS) on the fourth day. Eosin Y was used for counterstaining for imaging under microscope.

4.2.3. Fluorescent protein and CKAMPs-Ex expression and purification from *E. coli*

Plasmids were retransformed into *E. coli* expression host strains, including Tuner $(DE)_3$ pLysS for fluorescent proteins and CKAMPs-Ex and Rosseta-gami B (DE3) pLysS for Trx-CKAMP44-Ex. Single colony was picked and cultured in 3 ml ST-1 medium at 37 °C, 140 rpm for overnight. The culture was then transferred to fresh 200 ml ST-1 medium in a ratio of 1:50, and let grow at 37 °C, 140 rpm for 3-4 h till OD_{600} reached 0.8. IPTG stock was subsequently added to the culture to the final concentration of 1 mM, and the cells were continuously cultured at 37 °C, 140 rpm

for another 4 h. The *E. coli* cells were harvested by centrifugation (6,000 rpm at 4 °C for 10 min), resuspended in Ni^{2+} column binding buffer (20 mM sodium Phosphate, 0.5 M NaCl, 20 mM imidazole, pH 7.5) and lysed by lysozyme treatment (0.5 mg/ml) on ice for 1 h. Cell lysate was further centrifuged at 10,000 rpm for 20 min, and supernatant was loaded to immobilized metal-ion affinity chromatography (Ni^{2+} column) and the protein of interest was eluted by gradient increase of imidazole concentration.

4.2.3.1. Cleaving off Trx-tag using Enterokinase and Thrombin protease digestion

For Enterokinase (2 unit/µl, Roche) digestion, 1 µg Trx-CKAMP44-Ex was incubated with 3 units Enterokinase in working solution (20 mM Tris-HCl pH 7.4, 50 mM NaCl, 2 mM $CaCl_2$) at RT for 16 h. For Thrombin digestion (Sigma-Aldrich), and prepared as 0.2 unit/µl in thrombin storage buffer: 50 mM sodium citrate pH 6.5, 200 mM NaCl, 0.1% PEG-8000, 50% Glycerol), 50 µg Trx-CKAMP44-Ex was used for 1 unit thrombin digestion at RT for 2 h. Thrombin working solution: 20 mM Tris-HCl pH 8.4, 150 mM NaCl, 2.5 mM $CaCl_2$.

4.2.3.2. Separation of Trx-tag and CKAMP44-Ex

To isolate CKAMP44-Ex from Trx-tag, the thrombin treated protein sample was loaded either to Ni^{2+} column or to anion Q ion-exchange column. For Ni^{2+} column reloading, the protein solution was directly loaded to Ni^{2+} column, and the flowthrough was collected as CKAMP44-Ex protein sample. For anion Q column loading, the sample solution was first exchanged to Q column starting buffer (20 mM Tris-HCl, pH 7.6) by desalting column, and then loaded to Q column. Proteins were eluted by gradient increase of NaCl concentration.

4.3. HEK293 cell culture

4.3.1. HEK293 cell culture and transient transfection

HEK293 cells were cultured in minimum essential medium (MEM, Invitrogen) with 10% FCS (fetal calf serum), 1 x Penicillin/ Streptomycin, and 2 mM L-Glutamine, at 37 °C incubator supplied with 5% CO_2. HEK293 cells were seeded at a density of 4.0 x 10^6 per 10 cm dish 24 h prior to transfection. The next day, HEK293 cells were

transfected with 20 µl DNA per well using classical calcium-phoshphate precipitation method (Chen and Okayama, 1987). On the third day, the HEK293 cell culture was subjected to competent MEM medium exchange, and was left grown for 48 h until further analysis.

4.3.2 Co-Immunoprecipition (Co-IP) of CKAMP44 variants with GluA1 from HEK293 cell lysate

HEK293 cells co-transfected with different CKAMP44 variants and GluA1 expression plasmids were harvested by lysis buffer (50 mM Tris HCl, pH 7.4, with 150 mM NaCl, 1 mM EDTA, and 1% Triton X-100). In general, 800 µg total cell lysate was incubated with settled 10 µl α-GFP Agarose beads (MBL) or 20 µl α-FLAG beads (Sigma-Aldrich) pre-equilibrated in lysis buffer at 4 °C for overnight. The next day, the beads were pelleted down by short spin followed by 2 min settle down and the supernatant was kept as flow-through, while beads were washed 4 times by TBS (50 mM Tris HCl, with 150 mM NaCl, pH 7.4). Precipitated protein complex was eluted by 50 µl protein loading buffer at 99 °C for 10 min, and detected by western blot using mouse α-GFP and rabbit α-GluA1 antibodies.

4.4. Primary hippocampal neuron culture

4.4.1. Coating of cover slips by poly-L-lysine

Before neuron culture preparation, 24 well plates (normally with coverslips in each well for future immunocytochemistry analysis) used for neuron culture need to be coated with poly-L-lysine to ensure better cell attachment and growth. Coverslips with 13 mm diameter were autoclaved, put individually into 24 well plates, followed by incubation with 300 µl poly-L-lysine solution (0.1 mg/ml in 100 mM Boric-Acid, pH 8.5) at 37 °C for 30 min to overnight and 3 times PBS wash afterwards. poly-L-lysine treated 24 well plates were supplied with 500 µl plating medium, and placed at 37 °C for at least 30 min before use.

4.4.2. Primary hippocampal neuron preparation

Primary neuron culture from either rat or mice was prepared using previously described protocol. In brief, hippocampi of embryos at E18 were dissected out in cold PBS/Glucose/Hepes buffer and treated with Trypsin at 37 °C for 10 min, followed by

repeated manually pipetting up and down with a fire-polished Pasteur pipette to achieve single cell isolation. After counting and resuspension in plating medium (Minimum Essential Medium supplemented with Fetal Bovine Serum, Glucose, Sodium pyruvate, Penicillin/Streptomycin and L-Glutamate), cells were plated at a density of 5 x 10^4 cells/well in 24 well plates pretreated with poly-L-lysine and incubated at 37 °C supplied with 5% CO_2. The next day, the medium was changed to growth medium (Neurobasal Medium with B27 Supplement, L-Glutamine and Penicillin/Streptomycin), and the primary neuron culture was left grown till use.

4.4.3. Transfection of primary hippocampal neurons

Primary neurons were transfected by lipofectamine 2000 (Invitrogen) at day 10 *in vitro* (DIV10) for rat neurons or at DIV18 for mouse neurons in 24 well plates according to the manufacturer's instruction, and was used for immunostaining at DIV20. In brief, for each well reaction, 2 µl lipofectamine was mixed with 100 µl growth medium and incubated at RT for 5 min. 600 ng DNA plasmid (100 ng for pAAV-syn-Venus to achieve relevant expression level as the other constructs) was added into the medium containing lipofectamine, mixed and incubated at RT for 20 min. In the last 5 min of incubation time, the competent medium of the neuron culture was taken out, and kept in 37 °C incubator. The neuron culture was subsequently washed once by prewarmed fresh neurobasal medium (NBM) to get rid of residual BSA. Meanwhile, 200 µl prewarmed NBM was added into the 100 µl DNA-lipofectamine-medium mixture, and the 300 µl resulting mixture was added to each well. After 4 h incubation at 37 °C, the lipofectamine containing medium was taken out and changed to the competent growth medium. The transfected neuron culture was left grown till further analysis.

4.4.4. Infection of primary hippocampal neurons

Primary hippocampal neurons were used to check the infectivity of purified rAAVs. A series of rAAV dilution ranging from 0.1 µl to 5 µl per well was applied directly to the culture medium at DIV4 and the green fluorescence expressed by the transduced neurons was observed at DIV18 by fluorescence microscope. For good virus preparation, 0.1 µl/well infection was normally enough to give fluorescent protein expression.

4.5. Production and characterization of rAAVs

4.5.1. Large scale rAAV production and purification

rAAVs of Serotype S1/2 was produced by transient co-transfection of HEK293 cells using a pAAV vector expressing gene of interest together with a helper plasmid carrying helper gene pF6Δ and serotype 1 and 2 plasmids bearing corresponding *rep* and *cap* genes pH21 and pRV1. In general, ten 10 cm HEK293 dish culture were used for one virus production. Virus purification was performed as previously described (Smith *et al.*, 2009). Briefly, HEK293 cells were harvested and lysed in TNT buffer (20 mM Tris, 150 mM NaCl, 1% TritonX-100, 10 mM $MgCl_2$, pH 7.5) 72 h after transfection at RT for 10 min. Cell lysate was treated with Benzynase (Sigma-Aldrich) at 37 °C for 1 h to get rid of unpackaged DNA, and centrifugated at 4,000 rpm for 10 min at 4 °C. Supernatant together with harvested cell medium were combined and filtered through 0.22 μm. Filtered crude virus solution was then loaded into AVB sepharose high performance affinity column (GE Healthcare) and virus was subsequently eluted by 50 mM Glycine, pH 2.7, washed 3 times by PBS and concentrated into small volume (100-200 μl) using Amincon Ultra-4 centrifugal filters 100K (Millipore). Purified virus was sterilized by filtering through a 0.22 μm syringe filter (0.22 μm Millex Filter Units, Millipore), aliquoted and stored at -80 °C till use.

4.5.2. rAAV analysis

Purified rAAVs were analyzed for capsid protein, purity, genomic titer, packing efficiency and infection efficiency by Bradford assay, SDS-PAGE, quantitative real-time PCR, transmission electron microscope imaging and infection in primary hippocampal neuron culture. In general, 10 μl virus solution was used for protein determination using Bradford assay. Afterwards, virus with 500 ng relevant protein was used for SDS-PAGE (10% resolving gel) and stained by coomassie blue solution to check the purity.

4.5.3. Genomic titration of rAAVs

Genomic titers of rAAVs were determined by RT-PCR (7500 Real-Time PCR System, Applied Biosystems) using primers against the WPRE element. Primers and probe sequences: WPRE forward primer 5'-CTA TGT TGC TCC TTT TAC GCT ATG-3'; WPRE reverse primer 5'-TCA TAA AGA GAC AGC AAC CAG GAT-3';

TaqMan® probe 6-FAM-CCT TTG TAT CAT GCT ATT GCT TCC-MGB. Reaction mix: 10 µl 2x TaqMan Fast Universal PCR Mastermix, 0.5 µl 20x WPRE primer/probe mix, 1 µl plasmid standard (six standards ranging from 10 ng to 0.0001 ng) or virus sample and 8.5 µl ultrapure water. Real-time PCR cycling conditions: (a) polymerase activation and predenaturation at 50 °C for 2 min and at 95 °C for 10 min; (b) 35 cycles of denaturation at 95 °C for 20 s and annealing/extension at 60 °C for 1 min.

4.5.4. Transmission electron microscopical analysis of rAAV particles

The titration of virus particle to evaluate the rate of DNA filled rAAV was carried out by transmission electron microscopy. rAAV vectors were applied to carbon-coated grids, negatively stained with 1% uranyl acetate, and examined by transmission electron microscopy at 63,000x magnification (Zeiss 912 Omega Transmission Electron Microscope). Empty capsids were stained with uranyl acetate in the capsid core and exhibit a ring-like architecture, while filled rAAV particles were impermeable to uranyl acetate and showed no staining in the middle. Thus the rAAV filling rate could be calculated by manually counting the filled rAAV particles over the total number of rAAV particles.

4.6. Animals

4.6.1. Legal aspects and Animal housing

All animal handling and experimental procedures were performed according to the animal welfare guidelines of the Max Planck Societey, and under the license at the Regierungspräsidium Karlsruhe 35-915.81/G-71/10.

Ckamp44$^{-/-}$ mouse line was maintained in an animal facility (Interfaculty Biomedical Research facility, IBF, University of Heidelberg and Max Planck Institute for Medical Research), and kept individually or in groups of two to four animals at RT between 21 and 23 °C and at a humidity of 90%. A circadian rhythm of 12 h/12 h was maintained with light phase starting at 7 or 8 a.m. All experimental procedures were performed during the light phase. Food and water were provided *ad libitum*.

4.6.2. Protein extraction from mouse brain

To compare AMPAR expression level between *Ckamp44*^{−/−} and wild-type mice, hippocampi were dissected out from the brains of deeply anaesthetized mice, placed into a tissue grinder prefilled with chilled HEPES-buffer sucrose (4 mM HEPES pH 7.4, 0.32 M Sucrose, complete protease inhibitor cocktail), and mechanically homogenized with 10 strokes. *Total protein extraction:* The brain lysate was subjected to low speed centrifugation (1,600 rpm for 10 min at 4 °C) to get rid of DNA debris and big particles (P1), and the supernatant (S1) was kept as total protein extraction. *Total membrane fraction:* The total protein extraction was further centrifuged at high speed at 10,000 g for 20 min. The resulting pellet (P2) was resuspended in TritonX-100 containing buffer (25 mM Hepes buffer pH 7.4, 150 mM NaCl, 1% Triton X-100 plus protease inhibitor), incubated on ice for 30 min, and used as total membrane fraction. *Subcellular fractionation:* Subcellular fractions were prepared as previously described with some modifications (von Engelhardt *et al.*, 2010). Initial steps were the same as described above, except that the P2 was washed once by HEPES-buffered Sucrose and pelleted again to obtain crude synaptosomal fraction (P2'). P2' was hypoosmotic shock by ice-cold H_2O supplemented with protease/phosphatase inhibitors in homogenizer, mixed constantly for complete lysis, and centrifuged again at 25,000 g for 20 min to yield P3 pellet (lysed synaptosomal membrane fraction). The resuspended P3 pellet was loaded onto discontinuous sucrose gradient (0.8/1.0/1.2 M), and ultracentrifuged at ~150,000 g for 2 h. The synaptic plasma membrane (SPM) was recovered in the layer between 1.0 and 1.2 M sucrose. To obtain postsynaptic density (PSD) fraction, 0.5% Triton X-100 was added into the SPM, mixed and centrifuged at 32,000 g for 20 min. The supernatant was kept as Triton X-100 soluble synaptosome (Syn/Trx), and the pellet was PSD-1T pellet. The PSD-1T pellet was resuspended in 50 mM HEPES pH 7.4, 0.5% Triton X-100, 2 mM EDTA plus protease/phosphatase inhibitors, mixed and ultracentrifuged at 200,000 g for 20 min to obtain PSD-2T pellet. The PSD-2T was then resuspended in 50 mM HEPES pH 7.4, 2 mM EDTA buffer with 0.2% SDS, heated at 65 °C for 5 min, and the resulting solution was used as the final PSD fraction.

4.6.3. Delivery of rAAV into brains of newborn mice

To investigate the rescue effect of different CKAMP44 variants on AMPAR activity in *Ckamp44*^{−/−} mice, rAAVs carrying correspondingCKAMP44 variant genes were

stereotaxically injected into bilateral lateral ventricles and hippocampi of neonatal *Ckamp44$^{-/-}$* mouse brains using following coordinates relative to lambda: for lateral ventricle, rostral 2 mm, lateral 0.7 mm and ventral 1.5 mm; for hippocampus, rostral 1 mm, lateral 1 mm and ventral 1.5 mm. In brief, newborn pups were separated from mother and anesthetized on ice with the cover of wet tissue paper for 3-4 min till immobilized. The rAAV was injected through a 33-gauge beveled needle connected to a 100 µl preloaded syringe. The injection was controlled by a microprocessor-controlled WPI (World Precision Instruments) infusion-pump at a speed of 1 µl/min. Following electrophysiology and immunohistochemistry were carried out one month after the injection.

4.6.4. Vibratome sectioning of mouse brains

Mice were anaesthetized by isoflurane and perfused intracardially with warm PBS and 4% paraformaldehyde (PFA) in PBS prior to decapitation. Brains were taken out and fixed in 4% PFA for 2 h or overnight (in case of bad perfusion) at 4 °C. After embedded in 2.5% agarose/PBS, the brains were coronally sliced on a vibratome into 70 µm sections, starting from rostral to caudal. Sectioned brain slices were stored in PBS with 0.02% sodium azide at or cryoprotected and stored at -20 °C.

4.6.5. Electrophysiological recording

Outside-put patches were carried out as previously described (von Engelhardt *et al.*, 2010). Briefly, mouse brains were dissected out from deeply anaesthetized (isoflurane) P16-P30 mice, and cut into 250 µm thin slices in ice-cold dissection buffer containing (in mM): 125 NaCl, 25 NaHCO$_3$, 1.25 NaH$_2$PO$_4$, 2.5 KCl, 2 CaCl$_2$, 1 MgCl$_2$, 25 glucose, saturated with 95% O$_2$/5% CO$_2$ (pH 7.4). Slices were then gently transferred to ACSF buffer (25 mM NaCl, 25 mM NaHCO$_3$, 1.25 mM NaH$_2$PO$_4$, 2.5 mM KCl, 2 mM CaCl$_2$, 1 mM MgCl$_2$, 25 mM glucose, pH 7.4, bubbled with 95% O$_2$/5% CO$_2$) for at least 1 h prior to recording. Borosillicate glass recording pipettes (5-7 MΩ) were filled with solution containing (in mM) 120 (Cs)gluconate, 8 KCl, 10 CsCl, 0.2 EGTA (pH 7.3), 10 HEPES, 2 (Mg)ATP, 0.3 (Na$_3$)GTP, 10 (Na$_2$)phosphocreatine. Fast application of glutamate onto outside-out was performed using theta glass tubing mounted on a piezo translator. Application pipettes were tested by perfusing solutions with different salt concentrations through the two barrels onto open patch pipettes and recording current changes with 1 and 100 ms moves of

the application pipette. Only application pipettes with current change 20-80% rise times below 100 μs and with a reasonable symmetrical on- and offset were used. The application solution contained (in mM): 135 NaCl, 10 HEPES, 5.4 KCl, 1.8 $CaCl_2$, 1 $MgCl_2$, 5 glucose (pH 7.2).

4.7. Imaging

Confocal images were acquired using Leica TCS confocal microscope (SP2) equipped with 543 nm HeNe and 450-530 nm Argon lasers and 10x, 20x, 63x glycerol lens. Images were analyzed by ImageJ. For spine density and spine volume studies, high-resolution 7 z-stack images of dendrites with 350 nm step interval were acquired by using 63x glycerol objective and 2x optical zoom. In a typical experiment, secondary dendrites longer than 50 μm with evenly distributed spines were selected for counting. Other images were taken with 16 times scanning of single focal plane.

4.8. Imaging analysis

To describe the amount and distribution of dendrites, the center of a neuron soma was placed in the centroid of 10 series concentric circles with the same radius interval representing 25 μm. The intersections between neuron dendrites and each circle were manually counted. For spine density and spine volume studies, z-stack images of dendrites were reconstituted to a single image by doing Z projection with maximum intensity in ImageJ. Spine density was obtained by counting the number of spines over a known dendritic length. To obtain spine volume, the mean fluorescence intensity of individual spines in a fixed circle area and total dendrites traced by perimeter was measured, and the average spine/dendrite intensity value was calculated as spine volume. To quantify the spine targeting efficiency, the ratio of pixel intensity of each spine and the mean pixel intensity of dendritic area was calculated.

4.9. Materials

4.9.1. Plasmid list

Plasmid name	Source / Reference
pET-C6His KanR-SFGFP	Dr. R. Sprengel, MPI for Medical Research, Heidelberg
pET-C6His KanR-CYPet	generated in this thesis
pET-C6His KanR-Pet	generated in this thesis
pET-C6His KanR-mOrange	generated in this thesis
pET-C6His KanR-Tag RFPT	generated in this thesis
pET-C6His KanR-keima-Red	generated in this thesis
pET-C6His KanR-TFP	generated in this thesis
pET-C6His KanR-Venus	generated in this thesis
pET-C6His KanR-hGFP	generated in this thesis
pET C6HIS KanR-CKAMP39 Ex	generated in this thesis
pET C6HIS KanR-CKAMP44 Ex	generated in this thesis
pET C6HIS KanR-CKAMP52 Ex	generated in this thesis
pET C6HIS KanR-CKAMP59 Ex	generated in this thesis
pET32a-Trx-CKAMP44 Ex	generated in this thesis
pET32a-Trx-CKAMP39 Ex	generated in this thesis
pET32a-Trx-CKAMP52 Ex	generated in this thesis
pAAV-Syn-CKAMP44-IRES-Venus	Dr. J. von Engelhardt
pAAV-Syn-CKAMP44(flag)-IRES-Venus	Dr. J. von Engelhardt
pAAV-Syn-CKAMP44(flag,hCD4TM)-IRES-Venus	generated in this thesis
pAAV-Syn-VenusCKAMP44	Anja Groß, Bachelor thesis (2011)
pAAV-Syn-CKAMP44ΔCT-EGFP	Dr. V. Mack, Evotec AG Hamburg, Germany
pAAV-Syn-CKAMP44ΔNTΔCT-EGFP	generated in this thesis
pAAV-Syn-CKAMP44ΔLΔCT-EGFP	generated in this thesis
pAAV-Syn-CKAMP39ΔCT-EGFP	generated in this thesis
pAAV-Syn-CKAMP44ΔR/KΔCT-EGFP	generated in this thesis
pAAV-Syn-CKAMP44N-hCD4TM-Venus	generated in this thesis
pRK-CKAMP44(HT)-EGFP	generated in this thesis

4.9.2. Antibodies

Antibody	Specifications		
Primary antibody	Species	Dilution	Manufacturer
α-GFP	mouse	1:10,000 (WB), 1:4,000(ICC/IHC)	Clontech
α-GFP	chicken	1:4,000 (ICC/IHC)	Abcam
α-Flag	mouse	1:500 (WB/ICC/IHC)	Sigma-Aldrich
α-NeuN	mouse	1:1000 (IHC)	Chemicon
α-GluA1	rabbit	1: 2,000 (WB) 1:1,000 (ICC/IHC)	Millipore
α-CKAMP44	rabbit	1:1,000 (WB/ICC/IHC)	Covance
α-2A	rabbit	1:2,000 (WB) 1:1,000 (ICC/IHC)	Millipore
α-PSD95	mouse	1:8,000 (WB) 1:4,000 (ICC/IHC)	Thermo
α-synaptophysin	mouse	1:8,000 (WB) 1:4,000 (ICC/IHC)	Sigma-Aldrich
α-GAPDH	mouse	1: 10,000 (WB)	Abcam
α-βActin	mouse	1:5,000 (WB)	Sigma-Aldrich
Secondary antibody	Species	Dilution	Manufacturer
FITC-labeled α-chicken	donkey	1:600 (ICC/IHC)	Jackson Immuno Research
Cy3-labeled α-mouse	goat	1:600(ICC/IHC)	Jackson Immuno Research
Cy5-labeled α-rabbit	goat	1:600(ICC/IHC)	Jackson Immuno Research
Peroxidase-coupled α-mouse	goat	1:15,000 (WB)	Vector Laboratories
Peroxidase-coupled α-rabbit	goat	1:15,000 (WB)	Vector Laboratories

5. References

Ahmad-Annuar, A., Ciani, L., Simeonidis, I., Herreros, J., Fredj, N.B., Rosso, S.B., Hall, A., Brickley, S., and Salinas, P.C. (2006). Signaling across the synapse: a role for Wnt and Dishevelled in presynaptic assembly and neurotransmitter release. *J Cell Biol* 174: 127-139.

Auer, S., Sturzebecher, A.S., Juttner, R., Santos-Torres, J., Hanack, C., Frahm, S., Liehl, B., and Ibanez-Tallon, I. (2010). Silencing neurotransmission with membrane-tethered toxins. *Nat Methods* 7: 229-236.

Ausubel, F.M., Brent, R., Kingston, R.E., Moore, D.D., Seidman, J.G., Smith, J.A., and Struhl, K. (2000). *Current protocols in molecular biology*.

Bats, C., Groc, L., and Choquet, D. (2007). The interaction between Stargazin and PSD-95 regulates AMPA receptor surface trafficking. *Neuron* 53: 719-734.

Berkel, S., Tang, W., Trevino, M., Vogt, M., Obenhaus, H.A., Gass, P., Scherer, S.W., Sprengel, R., Schratt, G., and Rappold, G.A. (2012). Inherited and de novo SHANK2 variants associated with autism spectrum disorder impair neuronal morphogenesis and physiology. *Hum Mol Genet* 21: 344-357.

Bokel, C., Dass, S., Wilsch-Brauninger, M., and Roth, S. (2006). Drosophila Cornichon acts as cargo receptor for ER export of the TGFalpha-like growth factor Gurken. *Development* 133: 459-470.

Boulter, J., Hollmann, M., O'Shea-Greenfield, A., Hartley, M., Deneris, E., Maron, C., and Heinemann, S. (1990). Molecular cloning and functional expression of glutamate receptor subunit genes. *Science* 249: 1033-1037.

Brusa, R., Zimmermann, F., Koh, D.S., Feldmeyer, D., Gass, P., Seeburg, P.H., and Sprengel, R. (1995). Early-onset epilepsy and postnatal lethality associated with an editing-deficient GluR-B allele in mice. *Science* 270: 1677-1680.

Burnashev, N., Khodorova, A., Jonas, P., Helm, P.J., Wisden, W., Monyer, H., Seeburg, P.H., and Sakmann, B. (1992). Calcium-permeable AMPA-kainate receptors in fusiform cerebellar glial cells. *Science* 256: 1566-1570.

Castillon, G.A., Watanabe, R., Taylor, M., Schwabe, T.M., and Riezman, H. (2009). Concentration of GPI-anchored proteins upon ER exit in yeast. *Traffic* 10: 186-200.

Chen, C., and Okayama, H. (1987). High-efficiency transformation of mammalian cells by plasmid DNA. *Mol Cell Biol* 7: 2745-2752.

Chen, J., Park, C.S., and Tang, S.J. (2006). Activity-dependent synaptic Wnt release regulates hippocampal long term potentiation. *J Biol Chem* 281: 11910-11916.

Chen, L., Bao, S., Qiao, X., and Thompson, R.F. (1999). Impaired cerebellar synapse maturation in waggler, a mutant mouse with a disrupted neuronal calcium channel gamma subunit. *Proc Natl Acad Sci U S A* 96: 12132-12137.

Chen, L., Chetkovich, D.M., Petralia, R.S., Sweeney, N.T., Kawasaki, Y., Wenthold, R.J., Bredt, D.S., and Nicoll, R.A. (2000). Stargazin regulates synaptic targeting of AMPA receptors by two distinct mechanisms. *Nature* 408: 936-943.

Chen, L., El-Husseini, A., Tomita, S., Bredt, D.S., and Nicoll, R.A. (2003). Stargazin differentially controls the trafficking of alpha-amino-3-hydroxyl-5-methyl-4-isoxazolepropionate and kainate receptors. *Mol Pharmacol* 64: 703-706.

Cho, C.H., St-Gelais, F., Zhang, W., Tomita, S., and Howe, J.R. (2007). Two families of TARP isoforms that have distinct effects on the kinetic properties of AMPA receptors and synaptic currents. *Neuron* 55: 890-904.

Colquhoun, D., Jonas, P., and Sakmann, B. (1992). Action of brief pulses of glutamate on AMPA/kainate receptors in patches from different neurones of rat hippocampal slices. *J Physiol* 458: 261-287.

Cuadra, A.E., Kuo, S.H., Kawasaki, Y., Bredt, D.S., and Chetkovich, D.M. (2004). AMPA receptor synaptic targeting regulated by stargazin interactions with the Golgi-resident PDZ protein nPIST. *J Neurosci* 24: 7491-7502.

Dakoji, S., Tomita, S., Karimzadegan, S., Nicoll, R.A., and Bredt, D.S. (2003). Interaction of transmembrane AMPA receptor regulatory proteins with multiple membrane associated guanylate kinases. *Neuropharmacology* 45: 849-856.

El-Husseini, A.E., Schnell, E., Chetkovich, D.M., Nicoll, R.A., and Bredt, D.S. (2000). PSD-95 involvement in maturation of excitatory synapses. *Science* 290: 1364-1368.

Elias, G.M., Funke, L., Stein, V., Grant, S.G., Bredt, D.S., and Nicoll, R.A. (2006). Synapse-specific and developmentally regulated targeting of AMPA receptors by a family of MAGUK scaffolding proteins. *Neuron* 52: 307-320.

Fischer, M., Kaech, S., Knutti, D., and Matus, A. (1998). Rapid actin-based plasticity in dendritic spines. *Neuron* 20: 847-854.

Fukaya, M., Yamazaki, M., Sakimura, K., and Watanabe, M. (2005). Spatial diversity in gene expression for VDCCgamma subunit family in developing and adult mouse brains. *Neurosci Res* 53: 376-383.

Furushima, K., Yamamoto, A., Nagano, T., Shibata, M., Miyachi, H., Abe, T., Ohshima, N., Kiyonari, H., and Aizawa, S. (2007). Mouse homologues of Shisa antagonistic to Wnt and Fgf signalings. *Dev Biol* 306: 480-492.

Geiger, J.R., Melcher, T., Koh, D.S., Sakmann, B., Seeburg, P.H., Jonas, P., and Monyer, H. (1995). Relative abundance of subunit mRNAs determines gating and Ca^{2+} permeability of AMPA receptors in principal neurons and interneurons in rat CNS. *Neuron* 15: 193-204.

Green, P.J., Warre, R., Hayes, P.D., McNaughton, N.C., Medhurst, A.D., Pangalos, M., Duckworth, D.M., and Randall, A.D. (2001). Kinetic modification of the alpha(1I) subunit-mediated T-type Ca(2+) channel by a human neuronal Ca(2+) channel gamma subunit. *J Physiol* 533: 467-478.

Greger, I.H., Khatri, L., Kong, X., and Ziff, E.B. (2003). AMPA receptor tetramerization is mediated by Q/R editing. *Neuron* 40: 763-774.

Greger, I.H., Khatri, L., and Ziff, E.B. (2002). RNA editing at arg607 controls AMPA receptor exit from the endoplasmic reticulum. *Neuron* 34: 759-772.

Hall, A.C., Lucas, F.R., and Salinas, P.C. (2000). Axonal remodeling and synaptic differentiation in the cerebellum is regulated by WNT-7a signaling. *Cell* 100: 525-535.

Harmel, N., Cokic, B., Zolles, G., Berkefeld, H., Mauric, V., Fakler, B., Stein, V., and Klocker, N. (2012). AMPA receptors commandeer an ancient cargo exporter for use as an auxiliary subunit for signaling. *PloS one* 7: e30681.

Hashimoto, K., Fukaya, M., Qiao, X., Sakimura, K., Watanabe, M., and Kano, M. (1999). Impairment of AMPA receptor function in cerebellar granule cells of ataxic mutant mouse stargazer. *J Neurosci* 19: 6027-6036.

Hayashi, Y., Shi, S.H., Esteban, J.A., Piccini, A., Poncer, J.C., and Malinow, R. (2000). Driving AMPA receptors into synapses by LTP and CaMKII: requirement for GluR1 and PDZ domain interaction. *Science* 287: 2262-2267.

Heinemann, S.H., and Leipold, E. (2007). Conotoxins of the O-superfamily affecting voltage-gated sodium channels. *Cell Mol Life Sci* 64: 1329-1340.

Herring, B.E., Shi, Y., Suh, Y.H., Zheng, C.Y., Blankenship, S.M., Roche, K.W., and Nicoll, R.A. (2013). Cornichon proteins determine the subunit composition of synaptic AMPA receptors. *Neuron* 77: 1083-1096.

Higuchi, M., Maas, S., Single, F.N., Hartner, J., Rozov, A., Burnashev, N., Feldmeyer, D., Sprengel, R., and Seeburg, P.H. (2000). Point mutation in an AMPA receptor gene rescues lethality in mice deficient in the RNA-editing enzyme ADAR2. *Nature* 406: 78-81.

Higuchi, M., Single, F.N., Kohler, M., Sommer, B., Sprengel, R., and Seeburg, P.H. (1993). RNA editing of AMPA receptor subunit GluR-B: a base-paired intron-exon structure determines position and efficiency. *Cell* 75: 1361-1370.

Hollmann, M., Hartley, M., and Heinemann, S. (1991). Ca^{2+} permeability of KA-AMPA--gated glutamate receptor channels depends on subunit composition. *Science* 252: 851-853.

Hollmann, M., and Heinemann, S. (1994). Cloned glutamate receptors. *Annu Rev Neurosci* 17: 31-108.

Hollmann, M., Maron, C., and Heinemann, S. (1994). N-glycosylation site tagging suggests a three transmembrane domain topology for the glutamate receptor GluR1. *Neuron* 13: 1331-1343.

Hollmann, M., Rogers, S.W., O'Shea-Greenfield, A., Deneris, E.S., Hughes, T.E., Gasic, G.P., and Heinemann, S. (1990). Glutamate receptor GluR-K1: structure, function, and expression in the brain. *Cold Spring Harb Symp Quant Biol* 55: 41-55.

Hoshino, H., Uchida, T., Otsuki, T., Kawamoto, S., Okubo, K., Takeichi, M., and Chisaka, O. (2007). Cornichon-like protein facilitates secretion of HB-EGF and regulates proper development of cranial nerves. *Mol Biol Cell* 18: 1143-1152.

Ibanez-Tallon, I., Miwa, J.M., Wang, H.L., Adams, N.C., Crabtree, G.W., Sine, S.M., and Heintz, N. (2002). Novel modulation of neuronal nicotinic acetylcholine receptors by association with the endogenous prototoxin lynx1. *Neuron* 33: 893-903.

Ibanez-Tallon, I., Wen, H., Miwa, J.M., Xing, J., Tekinay, A.B., Ono, F., Brehm, P., and Heintz, N. (2004). Tethering naturally occurring peptide toxins for cell-autonomous modulation of ion channels and receptors in vivo. *Neuron* 43: 305-311.

Kato, A.S., Gill, M.B., Ho, M.T., Yu, H., Tu, Y., Siuda, E.R., Wang, H., Qian, Y.W., Nisenbaum, E.S., Tomita, S., and Bredt, D.S. (2010). Hippocampal AMPA receptor gating controlled by both TARP and cornichon proteins. *Neuron* 68: 1082-1096.

Kato, A.S., Siuda, E.R., Nisenbaum, E.S., and Bredt, D.S. (2008). AMPA receptor subunit-specific regulation by a distinct family of type II TARPs. *Neuron* 59: 986-996.

Kato, A.S., Zhou, W., Milstein, A.D., Knierman, M.D., Siuda, E.R., Dotzlaf, J.E., Yu, H., Hale, J.E., Nisenbaum, E.S., Nicoll, R.A., and Bredt, D.S. (2007). New transmembrane AMPA receptor regulatory protein isoform, gamma-7, differentially regulates AMPA receptors. *J Neurosci* 27: 4969-4977.

Keinanen, K., Wisden, W., Sommer, B., Werner, P., Herb, A., Verdoorn, T.A., Sakmann, B., and Seeburg, P.H. (1990). A family of AMPA-selective glutamate receptors. *Science* 249: 556-560.

Klugbauer, N., Dai, S., Specht, V., Lacinova, L., Marais, E., Bohn, G., and Hofmann, F. (2000). A family of gamma-like calcium channel subunits. *FEBS Lett* 470: 189-197.

Kopec, C.D., Real, E., Kessels, H.W., and Malinow, R. (2007). GluR1 links structural and functional plasticity at excitatory synapses. *J Neurosci* 27: 13706-13718.

Korber, C., Werner, M., Hoffmann, J., Sager, C., Tietze, M., Schmid, S.M., Kott, S., and Hollmann, M. (2007). Stargazin interaction with alpha-amino-3-hydroxy-5-methyl-4-isoxazole propionate (AMPA) receptors is critically dependent on the amino acid at the narrow constriction of the ion channel. *J Biol Chem* 282: 18758-18766.

Kott, S., Werner, M., Korber, C., and Hollmann, M. (2007). Electrophysiological properties of AMPA receptors are differentially modulated depending on the associated member of the TARP family. *J Neurosci* 27: 3780-3789.

Letts, V.A., Felix, R., Biddlecome, G.H., Arikkath, J., Mahaffey, C.L., Valenzuela, A., Bartlett, F.S., 2nd, Mori, Y., Campbell, K.P., and Frankel, W.N. (1998). The mouse stargazer gene encodes a neuronal Ca^{2+}-channel gamma subunit. *Nat Genet* 19: 340-347.

Li, H., Khirug, S., Cai, C., Ludwig, A., Blaesse, P., Kolikova, J., Afzalov, R., Coleman, S.K., Lauri, S., Airaksinen, M.S.*, et al.* (2007). KCC2 interacts with the dendritic cytoskeleton to promote spine development. *Neuron* 56: 1019-1033.

Lim, B.K., Cho, S.J., Sumbre, G., and Poo, M.M. (2010). Region-specific contribution of ephrin-B and Wnt signaling to receptive field plasticity in developing optic tectum. *Neuron* 65: 899-911.

Lomeli, H., Mosbacher, J., Melcher, T., Hoger, T., Geiger, J.R., Kuner, T., Monyer, H., Higuchi, M., Bach, A., and Seeburg, P.H. (1994). Control of kinetic properties of AMPA receptor channels by nuclear RNA editing. *Science* 266: 1709-1713.

Ludwig, D.L., and Stringer, J.R. (1994). Spontaneous and induced homologous recombination between lacZ chromosomal direct repeats in CV-1 cells. *Somat Cell Mol Genet* 20: 11-25.

Matsuzaki, M., Honkura, N., Ellis-Davies, G.C., and Kasai, H. (2004). Structural basis of long-term potentiation in single dendritic spines. *Nature* 429: 761-766.

Mebs, D., Narita, K., Iwanaga, S., Samejima, Y., and Lee, C.Y. (1972). Purification, properties and amino acid sequence of -bungarotoxin from the venom of Bungarus multicinctus. *Hoppe Seylers Z Physiol Chem* 353: 243-262.

Menuz, K., Kerchner, G.A., O'Brien, J.L., and Nicoll, R.A. (2009). Critical role for TARPs in early development despite broad functional redundancy. *Neuropharmacology* 56: 22-29.

Menuz, K., O'Brien, J.L., Karmizadegan, S., Bredt, D.S., and Nicoll, R.A. (2008). TARP redundancy is critical for maintaining AMPA receptor function. *J Neurosci* 28: 8740-8746.

Milstein, A.D., Zhou, W., Karimzadegan, S., Bredt, D.S., and Nicoll, R.A. (2007). TARP subtypes differentially and dose-dependently control synaptic AMPA receptor gating. *Neuron* 55: 905-918.

Miwa, J.M., Ibanez-Tallon, I., Crabtree, G.W., Sanchez, R., Sali, A., Role, L.W., and Heintz, N. (1999). lynx1, an endogenous toxin-like modulator of nicotinic acetylcholine receptors in the mammalian CNS. *Neuron* 23: 105-114.

Miwa, J.M., Stevens, T.R., King, S.L., Caldarone, B.J., Ibanez-Tallon, I., Xiao, C., Fitzsimonds, R.M., Pavlides, C., Lester, H.A., Picciotto, M.R., and Heintz, N. (2006). The prototoxin lynx1 acts on nicotinic acetylcholine receptors to balance neuronal activity and survival in vivo. *Neuron* 51: 587-600.

Monyer, H., Seeburg, P.H., and Wisden, W. (1991). Glutamate-operated channels: developmentally early and mature forms arise by alternative splicing. *Neuron* 6: 799-810.

Morris, R.G., Anderson, E., Lynch, G.S., and Baudry, M. (1986). Selective impairment of learning and blockade of long-term potentiation by an N-methyl-D-aspartate receptor antagonist, AP5. *Nature* 319: 774-776.

Mosbacher, J., Schoepfer, R., Monyer, H., Burnashev, N., Seeburg, P.H., and Ruppersberg, J.P. (1994). A molecular determinant for submillisecond desensitization in glutamate receptors. *Science* 266: 1059-1062.

Nagano, T., Takehara, S., Takahashi, M., Aizawa, S., and Yamamoto, A. (2006). Shisa2 promotes the maturation of somitic precursors and transition to the segmental fate in Xenopus embryos. *Development* 133: 4643-4654.

Nagerl, U.V., Eberhorn, N., Cambridge, S.B., and Bonhoeffer, T. (2004). Bidirectional activity-dependent morphological plasticity in hippocampal neurons. *Neuron* 44: 759-767.

Nakagawa, T., Cheng, Y., Ramm, E., Sheng, M., and Walz, T. (2005). Structure and different conformational states of native AMPA receptor complexes. *Nature* 433: 545-549.

Narita, K., Mebs, D., Iwanaga, S., Samejima, Y., and Lee, C.Y. (1972). Primary structure of -bungarotoxin from Bungarus multicinctus venom. *Taiwan Yi Xue Hui Za Zhi* 71: 336-343.

Niedworok, C.J., Schwarz, I., Ledderose, J., Giese, G., Conzelmann, K.K., and Schwarz, M.K. (2012). Charting monosynaptic connectivity maps by two-color light-sheet fluorescence microscopy. *Cell Rep* 2: 1375-1386.

Noebels, J.L., Qiao, X., Bronson, R.T., Spencer, C., and Davisson, M.T. (1990). Stargazer: a new neurological mutant on chromosome 15 in the mouse with prolonged cortical seizures. *Epilepsy Res* 7: 129-135.

Nolden, L., Edenhofer, F., Haupt, S., Koch, P., Wunderlich, F.T., Siemen, H., and Brustle, O. (2006). Site-specific recombination in human embryonic stem cells induced by cell-permeant Cre recombinase. *Nat Methods* 3: 461-467.

Okamoto, K., Nagai, T., Miyawaki, A., and Hayashi, Y. (2004). Rapid and persistent modulation of actin dynamics regulates postsynaptic reorganization underlying bidirectional plasticity. *Nat Neurosci* 7: 1104-1112.

Osten, P., and Stern-Bach, Y. (2006). Learning from stargazin: the mouse, the phenotype and the unexpected. *Curr Opin Neurobiol* 16: 275-280.

Packard, M., Koo, E.S., Gorczyca, M., Sharpe, J., Cumberledge, S., and Budnik, V. (2002). The Drosophila Wnt, wingless, provides an essential signal for pre- and postsynaptic differentiation. *Cell* 111: 319-330.

Pak, D.T., Yang, S., Rudolph-Correia, S., Kim, E., and Sheng, M. (2001). Regulation of dendritic spine morphology by SPAR, a PSD-95-associated RapGAP. *Neuron* 31: 289-303.

Parrish, J.Z., Emoto, K., Kim, M.D., and Jan, Y.N. (2007). Mechanisms that regulate establishment, maintenance, and remodeling of dendritic fields. *Annu Rev Neurosci* 30: 399-423.

Passafaro, M., Nakagawa, T., Sala, C., and Sheng, M. (2003). Induction of dendritic spines by an extracellular domain of AMPA receptor subunit GluR2. *Nature* 424: 677-681.

Pei, J., and Grishin, N.V. (2012). Unexpected diversity in Shisa-like proteins suggests the importance of their roles as transmembrane adaptors. *Cell Signal* 24: 758-769.

Peitz, M., Pfannkuche, K., Rajewsky, K., and Edenhofer, F. (2002). Ability of the hydrophobic FGF and basic TAT peptides to promote cellular uptake of recombinant Cre recombinase: a tool for efficient genetic engineering of mammalian genomes. *Proc Natl Acad Sci U S A* 99: 4489-4494.

Penzes, P., Johnson, R.C., Sattler, R., Zhang, X., Huganir, R.L., Kambampati, V., Mains, R.E., and Eipper, B.A. (2001). The neuronal Rho-GEF Kalirin-7 interacts with PDZ domain-containing proteins and regulates dendritic morphogenesis. *Neuron* 29: 229-242.

Priel, A., Kolleker, A., Ayalon, G., Gillor, M., Osten, P., and Stern-Bach, Y. (2005). Stargazin reduces desensitization and slows deactivation of the AMPA-type glutamate receptors. *J Neurosci* 25: 2682-2686.

Reisel, D., Bannerman, D.M., Schmitt, W.B., Deacon, R.M., Flint, J., Borchardt, T., Seeburg, P.H., and Rawlins, J.N. (2002). Spatial memory dissociations in mice lacking GluR1. *Nat Neurosci* 5: 868-873.

Rogers, S.W., Andrews, P.I., Gahring, L.C., Whisenand, T., Cauley, K., Crain, B., Hughes, T.E., Heinemann, S.F., and McNamara, J.O. (1994). Autoantibodies to glutamate receptor GluR3 in Rasmussen's encephalitis. *Science* 265: 648-651.

Rosenmund, C., Stern-Bach, Y., and Stevens, C.F. (1998). The tetrameric structure of a glutamate receptor channel. *Science* 280: 1596-1599.

Rosso, S.B., and Inestrosa, N.C. (2013). WNT signaling in neuronal maturation and synaptogenesis. *Front Cell Neurosci* 7: 103.

Rosso, S.B., Sussman, D., Wynshaw-Boris, A., and Salinas, P.C. (2005). Wnt signaling through Dishevelled, Rac and JNK regulates dendritic development. *Nat Neurosci* 8: 34-42.

Rouach, N., Byrd, K., Petralia, R.S., Elias, G.M., Adesnik, H., Tomita, S., Karimzadegan, S., Kealey, C., Bredt, D.S., and Nicoll, R.A. (2005). TARP gamma-8 controls hippocampal AMPA receptor number, distribution and synaptic plasticity. *Nat Neurosci* 8: 1525-1533.

Rousset, M., Cens, T., Restituito, S., Barrere, C., Black, J.L., 3rd, McEnery, M.W., and Charnet, P. (2001). Functional roles of gamma2, gamma3 and gamma4, three new Ca^{2+} channel subunits, in P/Q-type Ca^{2+} channel expressed in Xenopus oocytes. *J Physiol* 532: 583-593.

Rumbaugh, G., Sia, G.M., Garner, C.C., and Huganir, R.L. (2003). Synapse-associated protein-97 isoform-specific regulation of surface AMPA receptors and synaptic function in cultured neurons. *J Neurosci* 23: 4567-4576.

Sambrook, J., Fritsch, E.F., Maniatis, T., and Russell, D.W. (2001). *Molecular cloning*, 3rd edn (Cold Spring Harbor, NY: Cold Spring Harbor Laboratory Press).

Sans, N., Racca, C., Petralia, R.S., Wang, Y.X., McCallum, J., and Wenthold, R.J. (2001). Synapse-associated protein 97 selectively associates with a subset of AMPA receptors early in their biosynthetic pathway. *J Neurosci* 21: 7506-7516.

Schnell, E., Sizemore, M., Karimzadegan, S., Chen, L., Bredt, D.S., and Nicoll, R.A. (2002). Direct interactions between PSD-95 and stargazin control synaptic AMPA receptor number. *Proc Natl Acad Sci U S A* 99: 13902-13907.

Schober, D.A., Gill, M.B., Yu, H., Gernert, D.L., Jeffries, M.W., Ornstein, P.L., Kato, A.S., Felder, C.C., and Bredt, D.S. (2011). Transmembrane AMPA receptor regulatory proteins and cornichon-2 allosterically regulate AMPA receptor antagonists and potentiators. *J Biol Chem* 286: 13134-13142.

Schwenk, J., Harmel, N., Zolles, G., Bildl, W., Kulik, A., Heimrich, B., Chisaka, O., Jonas, P., Schulte, U., Fakler, B., and Klocker, N. (2009). Functional proteomics identify cornichon proteins as auxiliary subunits of AMPA receptors. *Science* 323: 1313-1319.

Shi, Y., Suh, Y.H., Milstein, A.D., Isozaki, K., Schmid, S.M., Roche, K.W., and Nicoll, R.A. (2010). Functional comparison of the effects of TARPs and cornichons on AMPA receptor trafficking and gating. *Proc Natl Acad Sci U S A* 107: 16315-16319.

Shimshek, D.R., Kim, J., Hubner, M.R., Spergel, D.J., Buchholz, F., Casanova, E., Stewart, A.F., Seeburg, P.H., and Sprengel, R. (2002). Codon-improved Cre recombinase (iCre) expression in the mouse. *Genesis* 32: 19-26.

Smith, R.H., Levy, J.R., and Kotin, R.M. (2009). A simplified baculovirus-AAV expression vector system coupled with one-step affinity purification yields high-titer rAAV stocks from insect cells. *Mol Ther* 17: 1888-1896.

Sobolevsky, A.I., Rosconi, M.P., and Gouaux, E. (2009). X-ray structure, symmetry and mechanism of an AMPA-subtype glutamate receptor. *Nature* 462: 745-756.

Sommer, B., Keinanen, K., Verdoorn, T.A., Wisden, W., Burnashev, N., Herb, A., Kohler, M., Takagi, T., Sakmann, B., and Seeburg, P.H. (1990). Flip and flop: a cell-specific functional switch in glutamate-operated channels of the CNS. *Science* 249: 1580-1585.

Sommer, B., Kohler, M., Sprengel, R., and Seeburg, P.H. (1991). RNA editing in brain controls a determinant of ion flow in glutamate-gated channels. *Cell* 67: 11-19.

Soto, D., Coombs, I.D., Kelly, L., Farrant, M., and Cull-Candy, S.G. (2007). Stargazin attenuates intracellular polyamine block of calcium-permeable AMPA receptors. *Nat Neurosci* 10: 1260-1267.

Soundarapandian, M.M., Tu, W.H., Peng, P.L., Zervos, A.S., and Lu, Y. (2005). AMPA receptor subunit GluR2 gates injurious signals in ischemic stroke. *Mol Neurobiol* 32: 145-155.

Sprengel, R. (2006). Role of AMPA receptors in synaptic plasticity. *Cell Tissue Res* 326: 447-455.

Sprengel, R. (2013). *Ionotropic Glutamate Receptors*. In Neuroscience in the 21st Century, D.W. Pfaff, ed. (Springer New York), pp. 59-80.

Sprengel, R., Honek, J., Voigt, A., Mack, V., von Engelhardt, J., Layer, L., Seeburg, P.H., and Monyer, H. (2009). Endogenous modulators of AMPA receptors. *Neuroscience Meeting Planner, Chicago* Abstract:: 512.516.

Sumioka, A., Brown, T.E., Kato, A.S., Bredt, D.S., Kauer, J.A., and Tomita, S. (2011). PDZ binding of TARPgamma-8 controls synaptic transmission but not synaptic plasticity. *Nat Neurosci* 14: 1410-1412.

Talos, D.M., Fishman, R.E., Park, H., Folkerth, R.D., Follett, P.L., Volpe, J.J., and Jensen, F.E. (2006a). Developmental regulation of alpha-amino-3-hydroxy-5-methyl-4-isoxazole-propionic acid receptor subunit expression in forebrain and relationship to regional susceptibility to hypoxic/ischemic injury. I. Rodent cerebral white matter and cortex. *J Comp Neurol* 497: 42-60.

Talos, D.M., Follett, P.L., Folkerth, R.D., Fishman, R.E., Trachtenberg, F.L., Volpe, J.J., and Jensen, F.E. (2006b). Developmental regulation of alpha-amino-3-hydroxy-5-methyl-4-isoxazole-propionic acid receptor subunit expression in forebrain and relationship to regional susceptibility to hypoxic/ischemic injury. II. Human cerebral white matter and cortex. *J Comp Neurol* 497: 61-77.

Tomita, S., Adesnik, H., Sekiguchi, M., Zhang, W., Wada, K., Howe, J.R., Nicoll, R.A., and Bredt, D.S. (2005a). Stargazin modulates AMPA receptor gating and trafficking by distinct domains. *Nature* 435: 1052-1058.

Tomita, S., Byrd, R.K., Rouach, N., Bellone, C., Venegas, A., O'Brien, J.L., Kim, K.S., Olsen, O., Nicoll, R.A., and Bredt, D.S. (2007). AMPA receptors and stargazin-like transmembrane AMPA receptor-regulatory proteins mediate hippocampal kainate neurotoxicity. *Proc Natl Acad Sci U S A* 104: 18784-18788.

Tomita, S., Chen, L., Kawasaki, Y., Petralia, R.S., Wenthold, R.J., Nicoll, R.A., and Bredt, D.S. (2003). Functional studies and distribution define a family of transmembrane AMPA receptor regulatory proteins. *J Cell Biol* 161: 805-816.

Tomita, S., Fukata, M., Nicoll, R.A., and Bredt, D.S. (2004). Dynamic interaction of stargazin-like TARPs with cycling AMPA receptors at synapses. *Science* 303: 1508-1511.

Tomita, S., Sekiguchi, M., Wada, K., Nicoll, R.A., and Bredt, D.S. (2006). Stargazin controls the pharmacology of AMPA receptor potentiators. *Proc Natl Acad Sci U S A* 103: 10064-10067.

Tomita, S., Stein, V., Stocker, T.J., Nicoll, R.A., and Bredt, D.S. (2005b). Bidirectional synaptic plasticity regulated by phosphorylation of stargazin-like TARPs. *Neuron* 45: 269-277.

Tsien, J.Z., Huerta, P.T., and Tonegawa, S. (1996). The essential role of hippocampal CA1 NMDA receptor-dependent synaptic plasticity in spatial memory. *Cell* 87: 1327-1338.

Turetsky, D., Garringer, E., and Patneau, D.K. (2005). Stargazin modulates native AMPA receptor functional properties by two distinct mechanisms. *J Neurosci* 25: 7438-7448.

Vandenberghe, W., Nicoll, R.A., and Bredt, D.S. (2005a). Interaction with the unfolded protein response reveals a role for stargazin in biosynthetic AMPA receptor transport. *J Neurosci* 25: 1095-1102.

Vandenberghe, W., Nicoll, R.A., and Bredt, D.S. (2005b). Stargazin is an AMPA receptor auxiliary subunit. *Proc Natl Acad Sci U S A* 102: 485-490.

von Engelhardt, J., Mack, V., Sprengel, R., Kavenstock, N., Li, K.W., Stern-Bach, Y., Smit, A.B., Seeburg, P.H., and Monyer, H. (2010). CKAMP44: a brain-specific protein attenuating short-term synaptic plasticity in the dentate gyrus. *Science* 327: 1518-1522.

von Heijne, G. (1989). Control of topology and mode of assembly of a polytopic membrane protein by positively charged residues. *Nature* 341: 456-458.

Wenthold, R.J., Petralia, R.S., Blahos J, I.I., and Niedzielski, A.S. (1996). Evidence for multiple AMPA receptor complexes in hippocampal CA1/CA2 neurons. *J Neurosci* 16: 1982-1989.

Wu, Y., Arai, A.C., Rumbaugh, G., Srivastava, A.K., Turner, G., Hayashi, T., Suzuki, E., Jiang, Y., Zhang, L., Rodriguez, J.*, et al.* (2007). Mutations in ionotropic AMPA receptor 3 alter channel properties and are associated with moderate cognitive impairment in humans. *Proc Natl Acad Sci U S A* 104: 18163-18168.

Xie, Z., Srivastava, D.P., Photowala, H., Kai, L., Cahill, M.E., Woolfrey, K.M., Shum, C.Y., Surmeier, D.J., and Penzes, P. (2007). Kalirin-7 controls activity-dependent structural and functional plasticity of dendritic spines. *Neuron* 56: 640-656.

Yamamoto, A., Nagano, T., Takehara, S., Hibi, M., and Aizawa, S. (2005). Shisa promotes head formation through the inhibition of receptor protein maturation for the caudalizing factors, Wnt and FGF. *Cell* 120: 223-235.

Yamazaki, M., Ohno-Shosaku, T., Fukaya, M., Kano, M., Watanabe, M., and Sakimura, K. (2004). A novel action of stargazin as an enhancer of AMPA receptor activity. *Neurosci Res* 50: 369-374.

Zamanillo, D., Sprengel, R., Hvalby, Ø., Jensen, V., Burnashev, N., Rozov, A., Kaiser, K.M., Köster, H.J., Borchardt, T., Worley, P.*, et al.* (1999). Importance of AMPA receptors for hippocampal synaptic plasticity but not for spatial learning. *Science (New York, NY)* 284: 1805-1811.